NTNU

Norwegian University of
Science and Technology

# Initialization, Phase stability and dynamic Simulation of a thermodynamic Control Volume

**Silje Kreken Almeland**

Chemical Engineering
Submission date: July 2011
Supervisor: Tore Haug-Warberg, IKP

Norwegian University of Science and Technology
Department of Chemical Engineering

# Preface

This thesis is written as a final part of my masters degree from the Norwegian University of Science and Technology (NTNU) in 2011, and is performed as part of the development of a new generic interface for thermodynamic equilibrium calculations. This development project has been supported by the main advisor and is still ongoing. The candidate has only held the responsibility of testing the interface and developing the equilibrium algorithms for calculating a concrete non-equilibrium dynamic control volume in a pressure relief program owned by Petrell AS. The paper represents cooperation between NTNU, Petrell AS and SINTEF.

First of all I would like to thank my supervisor professor Tore Haug-Warberg for his support, guidance, and encouragement throughout the project. I also want to thank Petrell AS that allowed me to take part in their project. A special thank is given also to Anders Granskogen Bjørnstad for his guidance and teamwork.

Finally, thanks to my great family for their never-ending love, support, and encouragement. And to my friends that make me laugh.

## Declaration of Compliance

I hereby declare that this is an independent work in compliance with the exam regulations of the Norwegian University of Science and Technology.

Date and signature _____

# Contents

**Abstract** **5**

**1 Introduction** **7**
1.1 Background and Motivation . . . 7
1.2 Historical Review . . . 8
1.3 Scope of Work . . . 9

**2 Theoretical Background** **11**
2.1 Phase Stability . . . 11
2.1.1 Defining the Concept . . . 11
2.1.2 The Pressure-Volume Isotherm . . . 13
2.1.3 Near the Critical Point . . . 14
2.1.4 The Tangent Plane Condition . . . 15
2.2 Initialization . . . 17
2.2.1 Particle Swarm Optimization (PSO) . . . 17
2.2.2 PSO in Phase Equilibrium Calculations . . . 20
2.3 Calculating the Phase Equilibrium . . . 21
2.3.1 The Criterion of Equilibrium . . . 21
2.3.2 Newton-Raphson . . . 23
2.3.3 Equation of State . . . 25

**3 Methodology of Control Volumes** **27**
3.1 VessFire Topologies . . . 27
3.1.1 The Basics of the VessFire Model . . . 27
3.1.2 Dynamics . . . 30
3.1.3 Changing between Topologies . . . 32
3.1.4 Implementation Details . . . 34
3.2 Testing the Model . . . 36
3.2.1 Experimental Details . . . 36
3.2.2 Two Component Case . . . 37
3.2.3 VessFire Case . . . 38
3.2.4 One Component Case . . . 39
3.3 Initialization . . . 39
3.3.1 Implementation of the PSO algorithm . . . 40
3.3.2 Preparing the States for PSO . . . 41
3.4 Testing of PSO . . . 44

**4 Results** **45**
4.1 Testing the Model . . . 45
4.1.1 Two Component Case . . . 45

4.1.2 VessFire Case . . . 48
4.1.3 One Component Case . . . 50
4.1.4 Summary . . . 51
4.2 Preparing the states for PSO . . . 54
4.2.1 The Step Functions . . . 55
4.2.2 Comparison between Hp and Tp . . . 57
4.2.3 Calculation with other Starting Points . . . 60
4.2.4 Investigation of a non convergent Tp-points . . . 64
4.3 Testing PSO-implentation . . . 66

**5 Discussion** **69**
5.1 The VessFire Model . . . 69
5.2 Preparing the states for PSO . . . 71
5.3 PSO . . . 73

**6 Conclusion** **75**
6.1 The VessFire model . . . 75
6.2 Preparation of feasible States . . . 75
6.3 PSO . . . 76

**References** **76**

**A Derivations** **81**
A.1 Equation set for the different topologies . . . 81
A.2 Deviation of mass- and energy balances . . . 82

**B Data from PSO** **85**
B.1 PSO-tables . . . 85

# Abstract

In this master work a thermodynamic model fitted to be used in connection with the flow simulator VessFire has been generated. Based on the behavior of this simulator, the thermodynamic model has to be able to take care of mass- and energy input and output, and that phases existing phases might disappear, and new phases might appear. Based on this fact, mechanisms were developed for these purposes. The starting point for this model was two control volumes, each consisting of a main phase and a utility phase. To exclude phases from the system a norm criterion was applied, whilst the mechanism to introduce a new phase was based on the tangent plane criterion. A main desire was to verify the performance of the model when applied to variable heat– and mass input, as well as to detect its shortcomings.

Three test cases were applied to the model, a two-component case, a one-component-case, and a VessFire case with process data from VessFire as input. The results from the two component case and VessFire case demonstrate that the model responds well to the heat- and mass inputs applied to the system in these cases. For all time steps in these cases the system converges to the expected topologies in a relatively small number (5-10) of iterations. Both the norm criterion for excluding phases and the initialization routine based on the tangent plane criterion, was proved to work. Further on, the testing of the model reveals that a shortcoming exists when the temperature of the mixture approaches the critical temperature. At this point the initialization mechanism based on the tangent plane criterion has no meaning anymore. Then an global initialization routine has to be applied to the system. To develop routines to overcome these shortcomings was the focus of the next part of the work.

In this work the stochastic initialization method Dynamic Multi Swarm — Particle Swarm Optimization (DMS-PSO)(Liang and Suganthan, 2005) have been tested as a relevant initialization method to be applied to the VessFire model. This is a global optimization routine that is based on the concept of swarm intelligence.

The testing of an initialization routine for a vapor—liquid phase equilibrium system, requires feasible one-phase states for the system to start the searches. To be able to perform a systematic and efficient test regime, some knowledge is also needed about the properties of the system. In this connection it is of considerable importance to obtain a knowledge about the stability conditions for the system.

In this work feasible one-phase states to test the initialization routine were obtained by converging one-phase calculations in $Hp$, $UV$, $Tp$, and $pV$-coordinates. The main goal was to generate feasible states to test DMS-PSO, a secondary goal of this part of the work was to investigate which coordinates that would be appropriate for converging the states.

The main discovery of the investigation of the convergence- and stability properties for the different grids, was that the calculated state for a single point in the $Tp$-grid became very different depending on the initialization of the calculations. The results from this work shows that the iteration sequence converges to the closest of the three alternative solutions available on the $pV$-isotherm. The resulting states will differ according to this. This behavior was not present for the $Hp$-scheme. Here the

calculations converge to unique defined states regardless of the initialization point.

Based on the feasible states that were generated, (DMS-PSO) was implemented and tested for the four component system, $N_2$, $CH_4$, $C_2$, $C_3$. The results from this testing revealed that the implemented routine was able to obtain a negative tangent plane distance at locations near the phase envelope. This was true both on the vapor- and the liquid side of the unstable area. To include the trial phases to the system, an $UVn$-flash was applied to calculate the equilibrium composition. For all trial phases introduced to liquid systems, the equilibrium calculations converged to non trivial solutions. Nevertheless, for all trial phases included in the vapor system, the equilibrium calculations failed to converge.

Although the implemented routine was able to find trial phases with negative tangent plane distance for more than half of the metastable points, the current implementation of the routine has some considerable drawbacks. Better solutions could have been found regarding the decisions of the boundaries, as well as to the choice of parameters to estimate.

# Chapter 1

# Introduction

## 1.1 Background and Motivation

This work is part of a project at Petrell AS, where a new thermodynamic package for a process simulator should be developed. The thermodynamic package in current use is a blackbox package by NIST (NIST, 2011), known to give inconsistent results in some cases. To improve the thermodynamic behavior, as well as to get a better control over the thermodynamic calculations, it was decided to build a new package, based on the thermodynamic function library developed by Tore Haug-Warberg and Bjørn Tore Løvfall at NTNU (Lovfall, 2008).

The process simulator in question is called VessFire, and is a product offered by Petrell AS.

> *"VessFire is a simulation program for time-dependent non-linear analysis of thermo-mechanical response during blow-down of process equipment, exposed, and unexposed, to fire. VessFire solves the problem of heat transfer, conduction, thermodynamics, and stress of object contents using a coupled approach. The thermodynamic behavior of object contents is simulated to represent evaporation, condensing, boiling, vapor expansion and the pressure, as the fluid are progressively heated up by the object shell"* (petrell.no, 2011).

The software is able to simulate multi-phase fluids. In this context multi-phase means thermodynamic material phases like e.g. vapor, liquid1, liquid2 etc. In the simulator each phase can be modeled as a single control volume (CV), which means that there is one control volume for each phase [1]. When the process equipment is exposed to external changes, like alterations in temperature or pressure, the containment of the different phases will change. This means that the connected control volumes have to exchange mass. One way to achieve this is by thermodynamic equilibrium calculations. Another way is to conduct mass transfer calculations based on diffusion, convection and turbulence.

To perform the thermodynamic calculations, the program has first to detect whether the phase is unstable. This is done by a stability check at each time step. If the phase do not pass the stability check, it means that it is unstable. The program then calls for the thermodynamic package, which performs an equilibrium calculation, and returns the correct state of the control volumes to the simulator. The calculation procedure is quite complex, however.

A thermodynamic package used in connection with this simulator have to be modeled from the same basis as VessFire. Also the thermodynamic model has to be able to take care of mass- and energy

[1] A fluid mechanical CV is not equal to a thermodynamic CV. In a thermodynamic CV each phase is considered as a single single CV. A fluid mechanical CV can include more than one thermodynamic phases

input and output, which leads to alternations in physical variables like temperature and pressure, which again results in that phases are formed, disappear and are reintroduced. To be able to model this dynamic behavior, the model must support the appearance and disappearance of phases. This lead to the discussion of stability analysis, and initialization, which are the main foci of this thesis.

## 1.2 Historical Review

Mathematical models play a vital role in process system engineering. Nearly every area of application contain some form of mathematical representation of the system behavior. Over the last 50 years, there has been a widespread use of models for predicting both steady state and dynamic behavior of processes (Hangos and Cameron, c2001). Phase behavior is essential to the modeling of all chemical processes both land-based and offshore. Hence the task of phase equilibrium calculations enters into the picture. Many applications in the fields of petroleum reservoir simulation and process simulation require a considerable number of phase equilibrium calculations.

The problem of solving phase equilibria in multicomponent thermodynamic systems is usually composed of three independent subproblems: Initialization, solving the equations, and checking whether the calculated phase is stable (Ghiorso, 1994). Historically, the second of these subproblems, solving the numerical problem, has received the greatest attention (Ghiorso, 1994). The traditional way of solving the phase equilibrium problem has been based on solving the Rachford-Rice equation. Successive substitution in combination with Newton's method is used to solve the Rachford-Rice equation (Michael L. Michelsen, 2004). An advantage of this method is that the computing time grows as a linear function of the components in the system. Nevertheless, the convergence order of this method is only linear, and convergence becomes slower as it approaches the critical point of the mixture. Orbach and Crowe (1975) introduced the Dominant eigenvalue method. This method was a method to accelerate the convergence of a computation sequence by transforming the sequence into a new sequence with higher convergence order.

Besides the successive substitution method, there are methods based on the Newton scheme. These methods can be divided into the two subclasses. The first subclasses consists of methods based on the Newton-Raphson method. The Newton-Raphson method solves simultaneously the whole set of descriptive equations in terms of all the problem unknowns (Ammar and Renon, 1987). The second subclass consists of methods based on the minimization of Gibbs free energy. In these methods the equilibrium problem is solved as a general optimization problem, minimizing the Gibbs energy of the system (Michael L. Michelsen, 2004). A main advantage of the methods based on the Newton scheme is that a second order convergence is obtained, as the iteration sequence approaches the solution. Nevertheless, for these methods, calculation of the Hessian matrix of the energy function is needed, which is associated with a large computing load (Nocedal and Wright, 2006). Also these methods are more sensitive to initialization values (Ammar and Renon, 1987). Another drawback of the Newton based methods is that the Hessian matrix approaches singularity near bubble points and critical points (Trangenstein, 1987). Nevertheless, as the concept of stability analysis entered into this area of science during the 1980's, the second order convergence methods tend to gain popularity (Michael L. Michelsen, 2004).

The most difficult and time-consuming part of the entire calculation can be the initialization part/to establish a good initial guess. Michael L. Michelsen (2004) claims that by competent selection of initial estimates, based on stability analysis, combined with Newton-Raphson's method, all two-phase equilibrium problems could be solved (Michael L. Michelsen, 2004). Although this statement might have been somewhat optimistic, stability analysis can be an advantageous tool associated with equilibrium calculations. Stability analysis can be used both during the initialization phase, as well as to

verify the stability of the different phases resulting from a calculated an equilibrium calculation, or in checking the stability of an existing phase, to reveal if a new phase should be introduced (Ghiorso, 1994).

In the equilibrium state, an energy function is minimized. Which energy function that is minimized depends on the physical conditions. An energy function is minimized in its extensive canonical variables, whilst the intensive canonical variable is constant. During the numerical this minimum is searched. A main challenge associated with stability analyses of phase equilibrium, is to decide whether the calculated minimum is a local or a global minimum. Several researches have presented work within the area of phase stability and initialization (Michelsen, 1982; Stateva and Tsvetkov, 1991; Ghiorso, 1994; Radzyminski and Whiting, 1987; Hua et al., 1998). Stability analysis as discussed by Michelsen (1982) involves applying the Gibbs' tangent plane criterion in studying the energy surface. The concept of this method is to detect whether a given solution is a global solution, based on testing the tangent plane equations for different locations in the search space (Michael L. Michelsen, 2004). This concept has served as a starting point for much research in the area.

The Tunneling method presented by Levy and Montalvo in 1977 (Boggs et al., 1985), was designed to find the global optimum of a general non-convex smooth function (Nichita et al., 2004). The concept of this approach is to minimize the tangent plane distance, using a modified tunneling function. The Tunneling function is constructed to escape from local minima, and ending up at the global minimum. This approach has been applied to different kind of phase equilibrium problems (Nichita et al., 2004). Another branch of routines that have gained popularity in chemical engineering recently are the stochastic global optimization routines. Their recent popularity is due to the fact that they provide robust solution with relatively little computational effort (Srinivas and Rangaiah, 2007). Some of these are routines based on the concept of swarm intelligence. A class of algorithms within this branch are based on the Particle Swarm Optimization (PSO) routine developed by Kennedy and Eberhart (1995). In PSO, a number of simple entities are placed in the search space of some problem or function. Each of these entities evaluate the objective function at its current location. Each particle then determines its movement through the search space by combining its own history and the history of the entire swarm (Kennedy and Eberhart, 1995). Whilst PSO is based on the flock behavior of birds, another class of minimization methods within this branch are based on the behavior of ants. These methods were first introduced by the *Ant Colony Optimization* algorithm presented by Marco Dorigo in 1992 (Li et al., 2009).

## 1.3 Scope of Work

The aim of this master project was to develop a thermodynamic model for equilibrium calculations to be used in a process simulator. This was done in collaboration with Anders Granskogen Bjørnstad at Petrell AS. This model should be able to model phase behavior for a system exposed to alterations in heat and mass input. To perform the equilibrium calculations, the Newton-Raphson method was used. The partial derivatives of the energy function was supplied by a function library developed by Tore Haug-Warberg et al at NTNU (Lovfall, 2008). Some important aspects associated with the model was to generate mechanisms to reveal the occasions when a new phase should be formed, as well as the occasions when an existing phase should be omitted from the system. To find solutions to these challenges the attention had to be directed into the area of phase stability and initialization.

In this work a rigorous analysis on the stability of the system $N_2$, $CH_4$, $C_2$, $C_3$ was done. Concerning initialization, the focus of this work has been on the tangent plane function and the probabilistic initialization routine, Particle Swarm Optimization (PSO).

As the aim of this work was to develop a thermodynamic package to be used in a process simulator,

the first half of the time period for this master work was invested in the generation, as well as implementation, of a suitable model. The generated model was proved to respond well for heat- and mass input for some real value cases supplied by VessFire, which was the process simulator in question. As the model succeeds to function for the process data, the focus of the work was changed from modeling and implementation, to the question of developing/finding a suitable routine for initializing the phase equilibrium calculations. Initialization methods like the Tunneling Method and the Particle Swarm Optimization was studied (litt usikker på om eg skal ha med denne setninga, blir nesten ei forteljing dette). It was chosen to implement and test the Particle Swarm Optimization method for the four component system $N_2$, $CH_4$, $C_2$, $C_3$. This seemed to be an exiting method owing to the fact that it is a relatively new method, and it does not appear to be used in any particular extent in this area of science. The aim was to be able to make a statement whether a probabilistic routine like PSO could be effectively used in the area of phase equilibrium calculations. To be able to test the routine, starting states was generated from one-phase convergence of the system, and an rigorous analysis on the stability of the system $N_2$, $CH_4$, $C_2$, $C_3$ was done.

# Chapter 2

# Theoretical Background

## 2.1 Phase Stability

The determination of phase stability, whether a given phase will split into multiple phases, is a key step in phase equilibrium calculations, and thus in the simulation and design of a wide variety of processes in chemical process engineering (Hua et al., 1998). The resulting assemblage from an equilibrium calculation must be evaluated for potential metastability, which means that the derived phase compositions must fall outside the unphysical regions, and phases not included in the system must be less stable than those currently in the equilibrium assemblage (Ghiorso, 1994). Also the system has to be examined for whether or not the trivial solution is obtained. Then the thermodynamic stability problem can be viewed as a complex problem, which aims to identify a multicomponent system under given thermodynamic conditions as either stable unstable or metastable (Stateva and Tsvetkov, 1991). This problem of determining the phase stability conditions for a system has been (and is?) an important area of research (Stateva and Tsvetkov, 1991). Baker et al and Michelsen have shown the advantage of studying the free energy area for this purpose (Radzyminski and Whiting, 1987). The phase stability problem is frequently formulated in terms of the tangent plane, based on the approach by the danish researcher Michelsen L. Michelsen, who has performed a main piece of work in this area. Nevertheless, to be able to discuss on the phase stability property of a system, a clear formulation, as well as definitions, of the characteristics of the various stability states are needed. This are given in the following section.

### 2.1.1 Defining the Concept

Considerations of stability lead to some of the most interesting and significant predictions of thermodynamics (Callen, 1985). The criterion of stability is that the thermodynamic potential in question (H,A,G,U) must be a convex function of its extensive parameters, and a concave function of its intensive parameters (Callen, 1985). Figure 2.1 illustrates a possible situation for a thermodynamic potential plotted against one of its extensive variables (for a two phase system?). From Figure 2.1 one can observe two different convex regions, and one concave region.

Mathematically, for the statement of convexity for the energy function as expressed by its extensive parameters, the Hessian matrix with respect to its extensive parameters has to be positive definite, $\frac{\partial^2 F}{\partial X \partial X} > 0$. For this requirement to be satisfied, all the eigenvalues of the Hessian have to be positive (Nocedal and Wright, 2006). The extensive variables associated with the energy functions, $H, A, U, G$ are $S, V, N$. Then the second derivatives of the energy function, $F$, has to be positive definite with respect to $S, V, N$. The inequality, $(\frac{\partial^2 F}{\partial N \partial N})_{X \neq N}$, is known as the limit of diffusional stability

(Radzyminski and Whiting, 1987). This is the most stringent condition, and is therefore said to be the mathematical condition of intrinsic stability (Radzyminski and Whiting, 1987). The condition, $(\frac{\partial^2 F}{\partial V \partial V})_{X \neq V}$, is known as the condition of mechanical stability, this is a less stringent condition for thermodynamic stability (Ghiorso, 1994). Nevertheless, there might be cases where both the thermodynamic stability and the diffusional stability are violated at the same time.

More trivially speaking a system at given thermodynamical conditions is said to be stable if there do not exist a state with lower energy for the given mixture (Stateva and Tsvetkov, 1991). According to this statement, the system at Figure 2.1 is stable in the lowest minima, in this case, corresponding to the largest value of the extensive quantity. Mathematically, this means that the system is stable at its global minimum, and not in its local minima. If the criteria of stability is not satisfied a system breaks up into two or more phases (Callen, 1985). Then for the location of the convex part of Figure 2.1, the system will add another phase. From a fundamental point of view, a stable system is a system which will return to its original state after it has been exposed to external fluctuations (Stateva and Tsvetkov, 1991). An unstable system is classified as a system which turns into another state when such fluctuations ceases. Figure 2.1 at page 12, shows that such conditions for stability holds for both minimum. At these area also the energy potential will be a convex function of the extensive variables. System trapped in such secondary minima, are defined at metastable phases. These phases will be effective in stable equilibrium, as if the deeper minima did not exist (Callen, 1985).

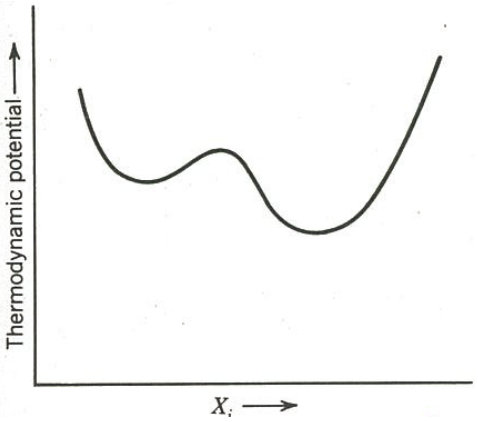


Figure 2.1: Thermodynamic potential with multiple minima (Callen, 1985).

Nevertheless, according to the definition of stability as a state where no other state, at given thermodynamic conditions, have lower energy, the left minima will not be considered as a stable state. Mathematically this minima will qualify as a stable state, as both the diffusional-, as well as the mechanical, stability is satisfied. This makes it hard for a mathematical equation solver to detect whether a system is trapped in a metastable state, or if the global minimum is found.

The form of the curve for the energy potential changes with alterations in some of the thermodynamic parameters (Callen, 1985). At two-phase equilibrium the value for the energy potential will be the same for two distinct local minima, which for these cases both constitutes the global minima. If the point of interest was to move off the coexistence curve in either direction, then one or the other of these minima are becoming the global minima. This is illustrated for Gibbs' energy as function of volume in Figure 2.2.

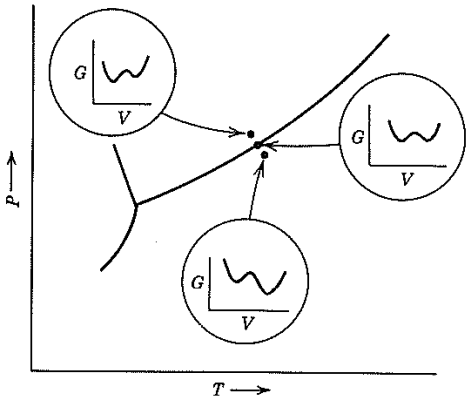


Figure 2.2: Competition of two minima of the Gibbs potential near the coexistence curve (Callen, 1985).

The shift of the equilibrium position from one local minimum to the other is known as a first order phase transition (Callen, 1985). Such an incident is induced by a change in some of the thermodynamic variables (Callen, 1985). Each transition can be viewed as the result of a failure of these stability criteria (Callen, 1985). The two states between which a first-order phase transition occurs are distinct, occuring at separate regions of the thermodynamic configuration space, which mean that they cor-

respond to very different molar volume, molar entropy, and so forth (Callen, 1985). This becomes obvious based on observations from Figure 2.2 and Figure 2.1.

### 2.1.2 The Pressure-Volume Isotherm

The thermodynamical potentials (H, A, U, G) might be the fundamental entities to play with. Nevertheless, a more common description of a thermodynamic system is by its *volume-pressure*-isotherms. For many gases the shape of these isotherms are described by the form of the isotherms predicted by various cubic equation of states, which all have similar shapes, and are derived from the van der Waal equation of state (Callen, 1985). The general shape of the van der Waal isotherm is illustrated in Figure 2.3, and in Figure 2.4a.

The different letters marked in Figure 2.3 corresponds to different pressures representing characteristic fundamental states. At pressure $p_S$ liquid is the only phase that might exist for the given system. Reducing the pressure, whilst the temperature is held constant, this fact will exist until the $p_R$ is reached. At this pressure there exist two possible phases. Continuing to reduce the pressure in the quasi statistical direction, with constant temperature, three states of equal P and T are available for the system. This will be valid until the pressure is reduced below $p_B$. Which state that will constitute the global minimizer of the energy potential for a given pressure, are different dependent on the pressure relatively to the curvature of the isotherm. Nevertheless, it should be observed that the isotherm on Figure 2.3 do not satisfy the conditions of mechanic stability, $(\frac{\partial p}{\partial V})_{T,\mathbf{n}}$, everywhere. This condition is clearly violated in the portion of the isotherm from M to F, which means that this region corresponds to unphysical states (Callen, 1985). At location M and F, $(\frac{\partial p}{\partial V})_{T,n} = 0$. These points can be viewed as limits for mechanical stability, from the liquid side and from the gas side, respectively.

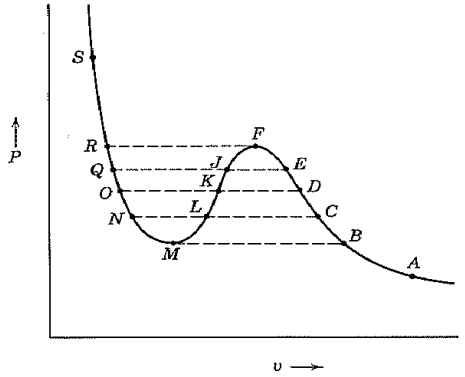


Figure 2.3: The general shape of the pV-isotherms for a cubic equation of state below the critical state (Callen, 1985).

Considering the pressure $p_Q$, at this pressure, the possible states, Q, J, and E, might exist. As already indicated, $p_J$ corresponds to an unstable state. At this particular pressure, the liquid state (Q) will correspond to the global minima-, whilst the gas state (E) will represent the local minima of the energy potential (Callen, 1985). This will be the case for all pressures in the interval $\langle p_R, p_O \rangle$. The points K and D represent the inflection points of the particular isotherm.

Pressure $p_O = p_D$ represent the two-phase equilibrium state, which correspond to the state where the two local minima of the $AV$—isotherm will have the same value for the energy potential. For pressures below $p_O = p_D$, the gas phase volume will have the deepest lowest minima on the $AV$—isotherm, and then represent the true stable state. At these locations a liquid state might exist as a metastable state (Callen, 1985). The opposite is true in the region $\langle p_O, p_R \rangle$. Here the liquid phase constitutes the global minimum, and thus the stable state, whilst a gas phase might exist as a metastable state. Based on the foregoing information, the isotherm in Figure 2.3 can be viewed as the underlying fundamental isotherm, whilst a thermodynamic stable isotherm would be the curve S-O-K-D-A (Callen, 1985).

### 2.1.3 Near the Critical Point

> *"The entired structure of thermodynamics appeared in the middle of the last century to be logically complete, but the structure founded on one ostensibility detail. That "detail" had to do with the properties of the system in the neighborhood of the critical point"*

This quote is cited from Callen (1985), and introduce an important aspect of the behavior of a thermodynamic system. As the critical point is approached, the properties of the gas and liquid phases tend to approach one another, resulting in only one homogeneous phase at the critical point. This phase is defined as a supercritical fluid (Callen, 1985). Figure 2.4b and Figure 2.4a, demonstrate the curvature of the $GV$—isotherm, and $pV$—isotherm as the critical state is approached.

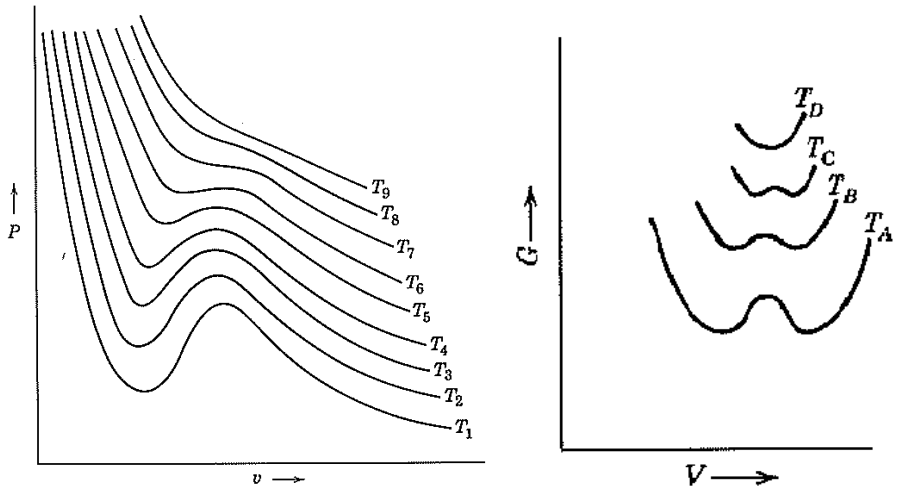


(a) pV-isotherms (b) GV-isotherms

Figure 2.4: The development of the isotherms as the system approaches the critical point

From Figure 2.4b one can observe that the function of the given energy potential becomes flat, which means that only small alterations in some thermodynamic parameters will change which state is the stable, as the state draw near the critical point . At the point where the critical state is reached, the distinction between the to phases totally disappears, this corresponds to that only one minima exist at, and beyond, this point (Callen, 1985). For a $pV$—isotherm the critical temperature can be observed at the point where the isotherm no longer has minimum- or maximum points. In Figure 2.4a this can be observed for isotherm $T_7$. Above the critical temperature a liquid cannot be formed by an increase in pressure, but with enough pressure a solid may be formed.

Summarized, in the near critical regions most probable values, which are the subject of thermodynamic theory, differ from the average values which are measured by experiments (Callen, 1985). Thermodynamic behavior near the critical point are governed by a set of critical exponents (Callen, 1985), and is beyond the scope of this thesis. As the temperature are raised sufficiently far beyond the critical temperature, the minima of the thermodynamic potential get steeper, and the near critical behavior ceases (Callen, 1985). This is illustrated for the $GV$—diagram in Figure 2.5.

**Based on the knowledge** from the previous sections, a foundation for the understanding of the phase stability analysis, frequently performed associated to phase equilibrium calculations in the in the process industry, has been built. Governing approaches to the phase stability analysis in these area of science, have been based on the tangent plane method (sett inn nokre av artiklane som referanse på dette). This method will be outlined in the next subsection.

### 2.1.4 The Tangent Plane Condition

The phase stability problem is frequently formulated in terms of the tangent plane condition (Hua et al., 1998). The practical application of the tangent plane condition in connection with phase equilibrium was demonstrated by Baker et al. in 1982 (Michael L. Michelsen, 2004). The basics of this concept is to introduce a trial phase to the given system, and then minimize the difference in a given energy potential between these two phases. The choice of energy potential, depends on the given working conditions. Traditionally $T$ and $p$ are to be constant in chemical processes, thus the Gibbs' energy function have received the greatest attention in this area of science (ref på dette, termoboka kanskje, evt omformulera). The tangent plane condition, as outlined by Michelsen (Michelsen, 1982), is based on an Taylor expansion of Gibbs' energy. From this approach the following minimization problem are deduced to test the stability of an existing phase:

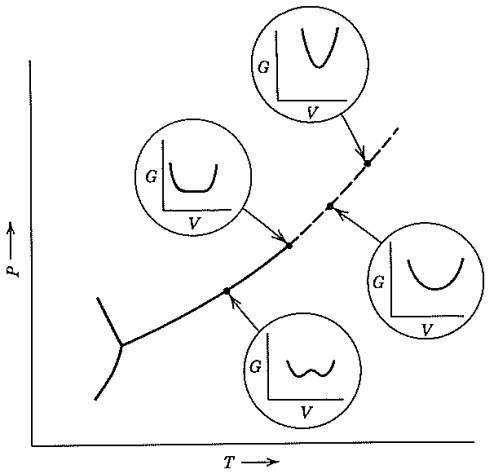

Figure 2.5: Developement of GV beond the critical point

$$\text{Given} \quad x \equiv \frac{n}{e^T n} \quad \text{and} \quad \mu = \mu(x)$$

where

$$n = [n_1, n_2 \ldots, n_n]^T, \quad x = [x_1, x_2, \ldots, x_n]^T, \quad e^T = [1, 1, \ldots, 1]$$

$$\text{Minimize} \quad \delta \equiv x^T(\mu_(x) - \mu^0)$$

$$\text{Subject to} \quad e^T x = 1 \quad \text{and} \quad x \geq 0$$

where $\delta$ represent the tangent plane distance, and $\mu(x)$ and $x$ denotes the chemical potential and mole fraction of the new phase respectively.

If, at the solution $x$ of this problem, $\delta \geq 0$, then the original phase is stable. Contrarily, if $\delta < 0$, the existing state is unstable and the new phase should be introduced (Trangenstein, 1987). Geometrically the $\delta$ is the vertical distance from the tangent hyperplane to the molar Gibbs' energy surface at the original composition, to the energy surface for the two phase system (Michelsen, 1982). This is shown schematically in Figure 2.6.

**The tangent plane test** outlined in the previous section is based on Gibbs' energy, nevertheless the same principals will apply to any other of the thermodynamical functions. In this master thesis the calculations are based on Helmholtz energy. To get a clear picture of the foundations of the tangent plane criteria, a fully derivation based on Helmholtz energy is outlined next.

Consider a multicomponent, single phase, mixture at a given temperature, $T_0$. By Euler integration the Helmholtz energy, A(T,V,n), with canonical veriables T, V, and N, can be expressed as follows (Haug-Warberg, 2006):

$$A = \sum \left(\frac{\partial A}{\partial X_i}\right)_{X_{j\neq i}, \zeta_j} X_i = -pV + \mu^T n \tag{2.1}$$

where vector notation is used.

Assume that a new phase with an infinitesimal mole amount, $\epsilon$, is formed from the original mixture with mole amount $N$. As the new phase is formed, the mole amount of the original phase is represented by, $N-\epsilon$. The change in Helmholtz energy can then by expressed as follows:

$$\Delta A = A_I + A_{II} - A_0 = A(N-\epsilon) + A(\epsilon) - A_0 \tag{2.2}$$

where $A_0$ represent the original energy for the one-phase system.

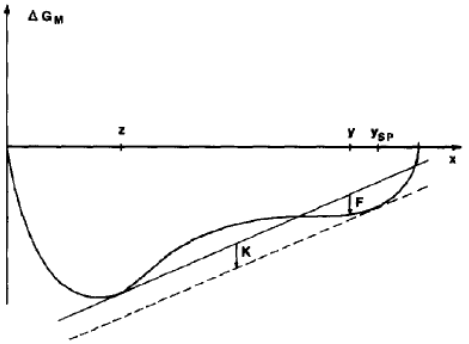


Figure 2.6: Developement of GV beond the critical point

Then do a first order Taylor extension of $A(N-\epsilon)$:

$$A(N-\epsilon) = A_0 + (\nabla A)^T \Delta X \quad \text{, where} \Delta X = -\begin{pmatrix}\delta V \\ \delta N\end{pmatrix} \tag{2.3}$$

Set this expression into equation (2.37):

$$\Delta A = A(\epsilon) + (\nabla A)^T \Delta X \tag{2.4}$$

where,

$$\nabla A = \left(\frac{\partial A}{\partial X}\right)_T = \begin{bmatrix}(\frac{\partial A}{\partial V})_{T,n} \\ (\frac{\partial A}{\partial N})_{T,V}\end{bmatrix} = \begin{bmatrix}-p \\ \mu\end{bmatrix}$$

Then the following expression is obtained for $\Delta A$:

$$\Delta A = A(\epsilon) + p\delta V - \mu\delta N \tag{2.5}$$

From Euler integration Helmholtz energy for the new phase can be expressed as:

$$A(\epsilon) = -pV + \mu N$$

the volume and the mole amount of the new phase will be equal to $\delta V$ and $\delta N$ respectively. The final expression for the alteration in Helmholtz energy by introducing the new phase is then:

$$\Delta A = -(p-p^0)\delta V + (\mu-\mu^0)^T \delta N \tag{2.6}$$

which represent the tangent plane function in a Helmholtz frame. As long as the original phase is the most stable phase, Helmoholtz energy for this phase will be less than for the two-phase system. Then equation (2.6) will give a positive result. Nevertheless, whenever this equation gives a negative value, the original system is unstable or metastable, and the new phase should be introduced (Michelsen, 1982).

In theory, this tangent plane check would be able to determine whether a phase is stable or metastable. The challenge is only to initialize the test with appropriate estimates for the composition of the trial phase. For this problem numerous algorithms have been purposed in the literature (Stateva and Tsvetkov, 1991; Ghiorso, 1994; Nichita et al., 2004). This will be the theme of the following chapter.

## 2.2 Initialization

The thermodynamic model that are to be generated, has to be able to take care of mass- and energy input and output. From time to time this have the outcome that phases are formed, disappear and are reintroduced. To be able to solve this task, the thermodynamic package has to include some kind of stability check to predict whether the existing phase is stable, unstable, or metastable. To detect whether a phase is unstable, are be easily performed by mathematical testing for diffusive- (2.7), and mechanical stability (2.8) conditions,

$$\left(\frac{\partial p}{\partial V}\right)_{T,n} \leq 0 \tag{2.7}$$

$$\left(\frac{\partial F}{\partial N \partial N}\right)_{T,n} \leq 0 \tag{2.8}$$

where $F$ denotes the thermodynamic potential. The distinction between metastable and stable mixtures are more difficult. The metastability is not reflected by the properties of the Hessian matrix of the energy potential F and verification of intrinsically stability requires a global search (Stateva and Tsvetkov, 1991). The manifold of algorithms on this theme is multitudinous in literature, some of them available in (Michelsen, 1982; Stateva and Tsvetkov, 1991; Ghiorso, 1994; Radzyminski and Whiting, 1987; Hua et al., 1998; Ammar and Renon, 1987). Nevertheless, it still seems to be a problem to develope a routine to perform well, sufficiently accurate or within acceptable computation time, for a wide range of cases. Optimization routines based on swarm intelligence constitute a relatively new direction of algorithms used to solve multidimensional minimization problems. These are stochastic methods that are based on the social behavior of various animals. Particle Swarm Optimization (Kennedy and Eberhart, 1995) represents one such routine.

### 2.2.1 Particle Swarm Optimization (PSO)

Particle swarm optimization (PSO) has root in two main component methodologies. The coupling to the behavior of animals, like bird flocking, fish schooling, and swarming theory in particular, might be the most obvious. Nevertheless, it is also related to evolutionary computation, and has ties to both generic algorithms and evolutionary programming (Kennedy and Eberhart, 1995). PSO can be easily implemented and is known to be computational inexpensive, owing to the fact that its memory and speed requirements are low(Jiang et al., 2007). The basic concepts of this algorithm are presented in the following paragraph.

#### The standard algorithm

PSO is a population based optimization tool, where the system is initialized with a population of random particles, searching for optima for an objective function in the search space (Jiang et al., 2007). The PSO algorithm is initialized with a population of random candidate solutions, the particles (Trelea, 2003).

For a multidimensional system of $d$ dimensions, a particle will be a vector of length $n$. For each of these dimensions and upper and lower bound are to be given, this will define the search space (Poli et al., 2007). Each particle is then given a randomized velocity, which is a vector of dimension $n$, and its position is moved through the problem space in an iterative manner. The velocity, which represents the step in the multidimensional space, is determined based on a combination of the best

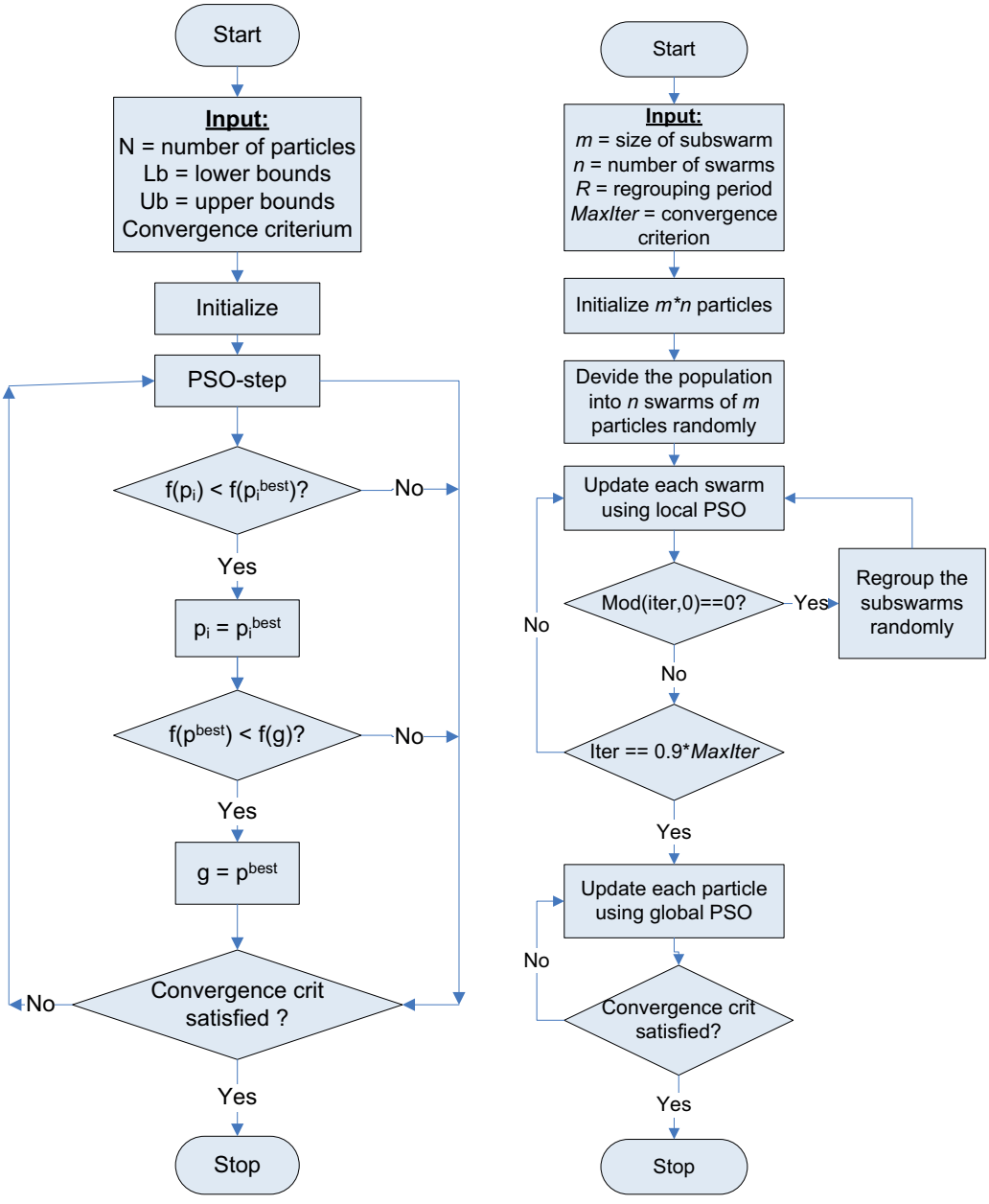


(a) The PSO algorithm (b) Local PSO

Figure 2.7: Flowchart for the PSO-alogoritm.

position obtained by the individual particle and the best position obtained for the whole swarm, up to a given time (Trelea, 2003). The equation used to express this step is given in equation (2.9):

$$V_{k+1} = aV_k + b_1 r_1(p - x_k) + b_2 r_2(g - x_k) \tag{2.9}$$

At iteration $k$, the velocity $v_k$ of a given particle is updated based on its current value affected $a$, which is a factor known as the inertia weight $a$, as well as a term which attract the particle towards its previously best known position, $p$, and the best position known by the entire swarm, $g$ (Trelea, 2003). The strength of attraction against each of these best positions are determined by the ratio $r_1$ to $r_2$. Randomness to achieve the ability to test various regions in the problem space, in order to locate a good optimum, is introduced via the random numbers $r_1$ and $r_2$. These parameters are usually chosen as uniform random numbers in the interval $[0,1]$ (Trelea, 2003; Poli et al., 2007):

$$r_1, r_2 = uniform(0,1) \tag{2.10}$$

Then the particle flies from its current position towards the new position according to equation (2.11).

$$x_{k+1} = x_k + v_{k+1} \tag{2.11}$$

At each iteration of the algorithm, the objective function is evaluated for the current position. If that position is better than any positions that have been found for that particular particle, the current position is considered as the particles' new best position (Poli et al., 2007). A particle by itself has almost no power to solve any problem, progress only occur when particles interact (Poli et al., 2007). Each particle has to execute some form of communication with other particles. Then given that a particular position has been considered as a particles' best position, the objective value of this position is compared with the best value found by the entire swarm. For each iteration the best value both for the entire swarm and for each particle are stored for comparison on later iterations. This iterative process is repeated until a user-defined criterion is reached (Jiang et al., 2007). Figure 2.7a illustrates the steps in the standard PSO-routine.

A main drawback of the method is that premature convergence might be obtained (Trelea, 2003; Jiang et al., 2007). Nevertheless, this limitation can to some extent be prevented by choosing the equation parameters properly (Trelea, 2003). The parameters $b_1$ and $b_2$ are tuning variables for the algorithm. The tuning of this variables will have a great effect on the performance of the algorithm (Trelea, 2003). A main objective for the tuning of these variables is to achieve a good balance between the ability to include the whole search space, to ensure the global optimum has been found, and the ability to concentrate the search around promising candidates. This is known as the exploration-exploitation trade off (Trelea, 2003). Trelea Trelea (2003) shows how the user can do well-informed decisions on tuning these parameters based on dynamic system theory.

As researchers has learned about the routine, new versions have been evolved (Poli et al., 2007). In this world of PSO routines, a partition can be made among global and local versions of PSO (Liang and Suganthan, 2005). The original version can be considered as a global version, where the objective function for each particle is compared with the value for best position in the entire swarm, the globally best value (Liang and Suganthan, 2005). In the local versions the swarm is divided into smaller subswarms. Then the general search routine is performed within each subswarm. The local routines have demonstrated better properties for exploring the search space, but traditionally, the global routines tend to converge faster (Poli et al., 2007). Nevertheless, the development of dynamic routines, where the subswarms are periodically schuffled, seemed to smarten up this drawback of the local routines (Poli et al., 2007; Jiang et al., 2007; Liang and Suganthan, 2005). Dynamic versions of

the local methods have shown to greatly elevate the ability of exploration and exploition (Jiang et al., 2007). The Dynamic Multi-Swarm Particle Swarm Optimizer (Liang and Suganthan, 2005) is such an algorithm. This routine is outlined in the following section.

#### Dynamic Multi-Swarm Particle Swarm Optimizer

The dynamic multi-swarm particle swarm optimizer method (Liang and Suganthan, 2005) is developed based on the local version of PSO. As in other local PSO-methods, the whole population is divided into several small swarms, the sub-swarms. In this approach, a dynamic multi-swarm particle swarm optimizer (DMS-PSO), whose neighborhood is dynamic and randomly chosen, is purposed. The flowchart, which illustrates the step in this algorithm, is given in Figure 2.7.

In order to slow down the population's convergence and increase diversity, the population is divided into small sized swarms. Built on the fact that PSO with small neighborhood performs well on complex problems (Liang and Suganthan, 2005), the size of the sub-swarms in DMS-PSO, are chosen to be small compared to similar versions of PSO. Each swarm uses its own member to search for better area in the search space of that particular sub-swarm. The search within each sub-swarm are performed in an iterative manner, according to the standard PSO-routine, which is illustrated in Figure 2.7a.

**Since** its introduction in 1995, the particle swarm optimization has been used across a wide range of applications where non-linear problems have to be solved(Kennedy and Eberhart, 1995). In an overview article Poli et al. (2007) list applications in 26 categories, based on 1100 publications on particle swarm optimization stored in the IEEE Xplore database at that time (2007). Recently, also the community of chemical engineers have shown interest for these stochastic optimization routines, and PSO has been successfully used for several chemical applications, including thermodynamic calculation (Bonilla-Petriciolet and Segovia-Hernández, 2010). In the next section this area of research will be reviewed shortly.

### 2.2.2 PSO in Phase Equilibrium Calculations

In the way stochastic optimization routines only require calculation of the objective function, many thermodynamic problems that are very difficult to solve by conventional techniques, due to the ill-structure surface of the thermodynamic potential, can be solved by such methods (Bonilla-Petriciolet and Segovia-Hernández, 2010). Recently several stochastic global optimization methods have been applied to solve problems related to phase equilibrium (Bonilla-Petriciolet and Segovia-Hernández, 2010). Based on its simplicity, both in formulation and implementation, PSO has shown to be one of the most promising stochastic methods in this area of science. Ferrari et al. (2009) tested the performance of PSO to estimate the parameters in models describing liquid-liquid phase behavior of binary and multicomponent systems. They reported results in good agreement with experimental data (Ferrari et al., 2009). Rahman et al. (2009) reported a variant of PSO to be able to locate global minimum of tpd for a binary and a ternary three phase equilibrium system (Rahman et al., 2009). A wide ranging study of various PSO variants was performed by (Bonilla-Petriciolet and Segovia-Hernández, 2010). In this study the standard PSO was compared with some of its variants applied to multicomponent system for both non-reactive and reactive phase equilibrium systems (Bonilla-Petriciolet and Segovia-Hernández, 2010). The conclusions of this work indicated that the classical PSO with constant values for the tuning variables $b_1$ and $b_2$, performed best for both non-reactive and reactive systems (Bonilla-Petriciolet and Segovia-Hernández, 2010). Nevertheless, the result indicated that PSO was effective, but not reliable methods to perform the global optimization of the tangent plane distance and the minimum Gibbs' energy (Bonilla-Petriciolet and Segovia-Hernández, 2010).

**Due** to the fact that higher dimensional problems are expected to be more complex and more difficult to solve, an important aspect should be to test PSO for multicomponent systems. Apart from the research of Bonilla-Petriciolet and Segovia-Hernández (2010), the testing of PSO applied to multicomponent systems seem to be restricted in literature. In this work testing of the local dynamic PSO version, DMS-PSO, should be tested on a four component two-phase system. The main goal is to test the performance of DMS-PSO in the metastable area.

## 2.3 Calculating the Phase Equilibrium

Phase equilibrium calculations are of considerable importance within a wide range of chemical processes. Therefore numerous algorithms have been applied for this purpose. Nevertheless, a starting point for every equilibrium calculation is the statement of the thermodynamic criterion of equilibrium.

### 2.3.1 The Criterion of Equilibrium

The second law of thermodynamics for an isolated system (2.12) serves as the starting point for the statement of the condition for thermodynamic equilibrium (Michael L. Michelsen, 2004).

$$(dS)_{U,V,n} \geq 0 \tag{2.12}$$

An isolated system is a system that neither exchanges heat, work or matter with its surroundings (Michael L. Michelsen, 2004). A consequence of (2.12) is that for an isolated system, the entropy will approach equilibrium by increasing its entropy. The equilibrium state of a particular system is obtained when the entropy of the system is maximized. At this point the following characteristics will be true for the entropy:

$$(dS)_{U,V,n} = 0 \tag{2.13}$$

$$(d^2S)_{U,V,n} < 0 \tag{2.14}$$

To make a general statement of the equilibrium conditions for a non-reacting phase equilibrium system, a multicomponent system must be considered. Since an isolated system do not exchange energy, mass or work with its surroundings, these quantities must be conserved within the system, which makes the system subject to the following expressions for the extensive independent properties $U$, $V$, and $n$:

$$\sum_{\pi=\alpha}^{\omega} dU^{\pi} = 0 \tag{2.15}$$

$$\sum_{\pi=\alpha}^{\omega} dV^{\pi} = 0 \tag{2.16}$$

$$\sum_{\pi=\alpha}^{\omega} dn_i^{\pi} = 0, \quad \forall i \in [1,n] \tag{2.17}$$

where $\pi$ denoted the different phases, and $i$ denotes the different components in the system. Since the fundamental equation relates changes taking place between equilibrium states in an isolated system, we can write the condition of equilibrium in the following way:

$$(dS)_{U,V,n} = \sum_{\pi=\alpha}^{\omega} \frac{dU^{\pi}}{T^{\pi}} + \sum_{\pi=\alpha}^{\omega} \frac{dV^{\pi}}{T^{\pi}} + \sum_{\pi=\alpha}^{\omega} \sum_{i=1}^{n} \frac{\mu_i^{\pi}}{T^{\pi}} dn_i = 0 \tag{2.18}$$

where the independent variables are subject to (2.15)- (2.17). From these equations it is possible to isolate $dU^{\omega}$, $dV^{\omega}$, and $dn_i^{\omega}$, $\quad \forall i \in [1,n]$. The following equation emerge by insertion in (2.18):

$$(dS)_{U,V,n} = \sum_{\pi=\alpha}^{\psi} [(\frac{1}{T^{\pi}} - \frac{1}{T^{\omega}})dU^{\pi} + (\frac{p^{\pi}}{T^{\pi}} - \frac{p^{\omega}}{T^{\omega}})dV^{\pi} + \sum_{i=1}^{n} (\frac{\mu_i^{\pi}}{T^{\pi}} - \frac{\mu_i^{\omega}}{T^{\omega}})dn_i^{\pi}] = 0 \tag{2.19}$$

It is assumed to be $\alpha, \beta, \ldots, \psi, \omega$ phases in the system. Near the equilibrium point $dU^{\alpha}, \ldots, dU^{\psi}$, $dV^{\alpha}, \ldots, dV^{\psi}$, and $dn_1^{\alpha}, \ldots, dn_n^{\psi}$ are independent variables. Then to fulfill $dS_{U,V,n} = 0$ the following must be true:

$$T^{\alpha} = T^{\beta} = \cdots = T^{\psi} = T^{\omega} \tag{2.20}$$

$$p^{\alpha} = p^{\beta} = \cdots = p^{\psi} = p^{\omega} \tag{2.21}$$

$$\mu^{\alpha} = \mu^{\beta} = \cdots = \mu^{\psi} = \mu^{\omega} \tag{2.22}$$

where

$$\mu = [\mu_1, \mu_2, \ldots, \mu_n]$$

From Equation (2.20)- (2.22) it is evident that temperature, pressure, and chemical are uniform properties for the system at equilibrium. This serve as the generic criterion for phase equilibrium in thermodynamic systems (litt usikker på om den setninga er korrekt).

In many cases we do not use $U, V, n$ as the independent variables, often it is more desirable to use other variables like $T, p, V$ and $n$ (Michael L. Michelsen, 2004). Then one of the energy potentials has to be considered as the optimizing goal. Whereas the entropy is maximized in its canonical variables at equilibrium, the equilibrium state corresponds to a minimization of the energy potentials in their canonical variables at different conditions. Whether $H, A, U$ or $G$ are to be minimized, depends on which variables that are to be constant for that particular situation (Haug-Warberg, 2006). Due to the fact that an energy potential is minimized subjected to constraints in its canonical variables, $G(T, p, n)$ are the potential to minimize when the pressure and temperature are held constant for a closed system. Correspondingly, $A(T, V, n)$ are minimized at equilibrium, when the temperature and the volume are constant for a closed system, and so forth. These correlations can be easily deduced from the first law of thermodynamics (Michael L. Michelsen, 2004).

Based on the equilibrium criterion outlined in this section, iterative methods can be applied to solve the phase equilibrium problems. In the literature several algorithms have been developed for this purpose. The Newton-Raphson method represents one such method. This method will be the theme of the next section.

### 2.3.2 Newton-Raphson

The generic criterion for thermodynamic equilibrium is given in Equation (2.20)- (2.22), and is that the temperature, pressure and chemical potential are uniform for all phases in the specific system (Haug-Warberg, 2006). For a closed system, also the extensive canonical variables of the energy potential, have to be conserved in the system. The Newton-Raphson algorithm consists in solving simultaneously the whole set of descriptive equations, in terms of all the problem unknowns. The equation set will have the following form:

$$f = b \tag{2.23}$$

If an entropy, $S(U,V,n)$, framework is convenient, the equation matrix for a two-phase system would then be as demonstrated by (2.24):

$$\begin{pmatrix} T^\alpha & - & T^\beta \\ p^\alpha & - & p^\beta \\ \mu^\alpha & - & \mu^\beta \\ U^\alpha & + & U^\beta \\ V^\alpha & + & V^\beta \\ n^\alpha & + & n^\beta \end{pmatrix} = \begin{pmatrix} 0 \\ 0 \\ 0 \\ U_{tot} \\ V_{tot} \\ n_{tot} \end{pmatrix} \tag{2.24}$$

where the left hand side represent $f$ and the right hand side represent $b$. The Newton method solves the equation system based on an first order Taylor expansion of the equation set:

$$f_{k+1} = f_k + J_x \Delta x = b \tag{2.25}$$

which leads to the following iteration step:

$$\delta x = (J_x)^{-1}(b - f) \tag{2.26}$$

where $x$ in (2.25) and (2.26) represent the iteration variables, and will depend on the energy function chosen. The equation for a step in the iteration variables is then as shown by (2.27):

$$x_{k+1} = x_k + \tau \Delta x \tag{2.27}$$

where $\tau \in \langle 0, 1]$ is a step shortener that shortens the step if some physical constraints are broken. This shortener continue to shorten the step until the new state fulfills the given constraints. When iterating on physical phenomena, which is the case in phase equilibrium calculations, some constraint will be set on the iteration step due to physical constraints. The volume, and the mass can not be negative. A phase equilibrium system will also be sensitive for large alterations in temperature and mole fraction. Another possibility to guide the iteration sequence against the solution, is to set constrictions on the objective function (Nocedal and Wright, 2006). Nevertheless, this will place a limitation on the flexibility of the algorithm, and might inhibit the solver to find the global solution (Nocedal and Wright, 2006).

The first three equations in (2.24) represent the generic equilibrium criterion, and will be the same independent of the choice of state function.

A strength for methods based on the Newton solver is that they obtain quadratic convergence (Nocedal and Wright, 2006). It takes normally 3-5 iterations before a second order convergence is reached

(Nocedal and Wright, 2006). Nevertheless, it is a common fact that the Newton method needs to be initiated sufficiently close to the solution (Nocedal and Wright, 2006). Then if the starting point are far from the solution, the Newton method might not find the global solution. This is because the derivative matrix, that decide on the direction, might lead the sequence in a wrong direction as long as the Hessian matrix is not positive definite (Nocedal and Wright, 2006). Whether the the solver is able to find the right solution, as well as a solution at all, depends on the topology of the given energy surface. If the energy surface exists of local minimas the solver might end up finding a local solution.

The successive substitution, which is the method traditionally used for phase equilibrium calculations, has second order convergence. In that way, the local convergence properties of the Newton method are excellent. Nevertheless, the method successive substitution is less addicted to the quality of the start values (Haug-Warberg, 2006). Even though the Newton method might has preferable convergence properties, the computational costs per iteration will be larger than compared to the method of successive substitution (Haug-Warberg, 2006). This is because the Hessian of the state function has to be calculated for methods based on Newton.

### Condition and numeric stability

Applied to (2.24) specifically, and to phase equilibrium calculations based on Newton's method in general, the Jacobian will contain the second derivative of the the state functions. A main reason why these methods have not been able to outperform successive substitution in general, is due to the fact of the poor conditioning of the Hessian of the energy function, near critical points, bubble points and dew points. In these situations the direction obtained by the Hessian will be heavily influenced by the steepest decent. The result will be linear convergence rate, then to a much greater cost per iteration than what would be the case using successive substitution (Trangenstein, 1987).

It is impossible for the particular energy potential to have a local minimum at a point where some component is absent from one of the phases because this would lead to an infinite chemical potential. Whenever one of the phases becomes small, the Hessian of the state function becomes nearly singular (Trangenstein, 1987). The same problem will occur if two phases have nearly the same composition. This is the reasons for the singularity of the Hessian matrix of the energy function as the system approaches the boiling point or the critical point.

Trying to solve the Newton equation when the Jacobian in (2.26) is nearly singular the iteration is susceptible to run into numerical difficulties (Trangenstein, 1987). Most important, the factorization of the second derivative matrix may involve catastrophic cancellation of one of the pivots corresponding to the nearly non-singularity. To satisfy the stability conditions both the diffusive condition $(\frac{\partial \mu}{\partial N}) > 0$ and $(\frac{\partial p}{\partial V}) < 0$. Due to the rounding error that arrives due to the bad conditioning of the matrices, it may be difficult to determine numerically whether a nearly singular matrix is positive definite (Trangenstein, 1987). Then it will be difficult to separate a minima from a saddle point of the energy surface. Also the solution of the linear system may be inaccurate due to the errors in the factorization, and the iterates may bubble around without making progress to the solution (Trangenstein, 1987).

It can be possible to at least partly overcome these problems, and then be able to make reliable determinations of the positive definiteness of the second derivatives near the phase envelope, by numerical efforts. Based on the Householder transformation, which is a method used to solve near singularity problems by numerical, Trangenstein (1987) purposed that a solution can be to compute a transformation to separate the poorly scaled direction from the well-scaled direction. A detailed discussion of this is beyond the scope of this thesis.

Nevertheless to be able to perform the equilibrium calculations, a model for predicting the derivatives of the state function is needed. Then the equations of state enters into the pictures.

### 2.3.3 Equation of State

Although the interpretation of thermodynamics is quite mathematical, the overall foundation of thermodynamics rely on empirical relations (Haug-Warberg, 2006). Especially, this is evident by the use of equations of state as a starting point for calculating thermodynamic properties. Except from a few representations from statistic mechanics, there do not exist models founded on exact formulations. The equations of state mostly in use are semi-empirical expressions based on some empirical and adjustable model parameters (Haug-Warberg, 2006).

An equation of state expresses intensive quantities in terms of independent extensive parameters (Callen, 1985). Based on the fact that the temperature, pressure and chemical potentials are partial derivatives of $S, V, n$, the following expressions will be valid:

$$T = T(S,V,n) \quad p = p(S,V,n) \quad \mu = \mu(S,V,n) \tag{2.28}$$

which constitute the fundamental equations of state. The fundamental equations of state (2.28) is expressed as functions of $S, V, n$, which represent the canonical variables for internal energy $U$. Then intuitively $U$ should be used as the energy function to describe the state. Nevertheless, due to the fact that the expressions in Equation (2.28) only are known as implicit functions, it is more common to use $T, p, n$ or $T, V, n$ as a starting point for the calculations (Haug-Warberg, 2006). Traditionally, $T, p, n$ have received most attention in thermodynamic modeling, probably due to laboratory conditions. Nevertheless, due to the equations of state using volume as independent variable give a consistent description of vapor-liquid equilibrium applied to near critical conditions, $T, V, n$ are preferable for theoretical applications (Haug-Warberg, 2006). The cubic equation of state is based on the Van der Waal equation on the form $p(T, V, n)$. Examples of expressions within this familiy are Redlich-Kwong (RK), Soave-Redlich-Kwong (SRK) and Peng-Robinson. In this work, the calculations of the thermodynamic properties is based on Peng-Robinson equation of state.

#### Peng-Robinson equation of state

The Peng-Robinson equation of state (Peng and Robinson, 1976) was developed in order to improve liquid density predictions as well as the ability to estimate vapor pressures and equilibrium ratios. Also the model should provide reasonable accuracy near the critical point. Another objective was that the parameters should be expressible in terms of the critical properties and the acentric factor, and that the mixing rules should not employ more than a single binary interaction parameter, which should be independent of temperature pressure and composition (Peng and Robinson, 1976). The resulting equation became as follows:

$$p = \frac{RT}{v-b} - \frac{a(T)}{v(v+b)+b(v-b)} \tag{2.29}$$

where $b = \sum x_i b_i$ is the hard core volume. The parameter $a = \sum\sum x_i x_j a_{ij}$ can be regarded as a measure of the intermolecular attraction force. $T_c$ represent the critical temperature. An evaluation of (2.29) at the critical point gives the following expressions for the parameters $a$, $b$ and the compression factor $Z$:

$$a(T_c) = 0.45724 \frac{R^2 T_c^2}{p_c} \tag{2.30}$$

$$b(T_c) = 0.07780 \frac{RT_c}{p_c} \tag{2.31}$$

$$Z_c = 0.307 \tag{2.32}$$

At temperatures different from $T_c$, the following relation yields:

$$a(T) = a(T_c)\alpha(T_r, \omega) \tag{2.33}$$

where $\alpha(T_r, \omega)$ is a dimensionless function of reduced temperature and the acentric factor. This term equals unity at the critical temperature. The hard core volume is not considered to be temperature dependent:

$$b(T) = b(T_c) \tag{2.34}$$

Based on empirical data the following expression was used for $\alpha(T_r, \omega)$:

$$\omega^{\frac{1}{2}} = 1 + \kappa(1 - T_r^{\frac{1}{2}}) \tag{2.35}$$

where $\kappa$ is a constant characteristic of each substance, and expressed by (2.36):

$$\kappa = 0.37464 + 1.54226\omega - 0.26992\omega^2 \tag{2.36}$$

which fulfills the Peng-Robinson expression.

The Peng-Robinson equation is on the form $p(T, V, n)$, and $T, V, n$ constitute the independent variables. In the way thermodynamic calculations are most easily performed using the canonical variables of the energy function in question, Helmholtz energy, $A(T, V, n)$, would be the natural choice for equations of state on the form $p(T, V, n)$.

Using Helmholtz energy as a starting point, Equation (2.37) will serve as the starting point for an expression of Helmholtz energy:

$$(dA)_T = -pdV + \sum_{i=1}^{n} \mu_i dN_i \tag{2.37}$$

this expression can then be integrated as long as expressions for $p(T, V, n)$ as well as $\mu(T, V, n)$ are available. Unfortunately the last of these tend to constitute a very complicated expression when multicomponent systems are present (Haug-Warberg, 2006). A more convenient method is to use an idealized model as a reference and then express the deviate between the real fluid and this hypothetical idealized state, calculating the residual function:

$$A^{rv,eos} = A(T, V, n)^{eos} - A(T, V, n)^{ig} \hat{=} \int_{\infty}^{V} \left( p(T, V, n)^{eos} - p^{ig} \right) dV \tag{2.38}$$

where $p(T, V, n)^{eos}$ is the pressure calculated from a specific equation of state, whilst $p^{ig}$ are the ideal contribution. Then an expression for the residual Helmholtz energy can be obtained by insertion of $p(T, V, n)$ for a given equation of state. Given an expression for $A^{rv}$, its derivatives can be calculated, and other thermodynamical properties can be deduced.

In this work the thermodynamic properties were supplied by a thermodynamic functional library developed by Tore Haug-Warberg and Bjørn Tore Løfall at NTNU (Lovfall, 2008).

# Chapter 3

# Methodology of Control Volumes

In this master work a thermodynamic model fitted to be used in connection with the flow simulator VessFire (see section 1.1) has been generated. Based on the behavior of this simulator, the thermodynamic model has to be able to take care of mass- and energy input and output, and that phases existing phases might disappear, and new phases might appear. The foundation for such a thermodynamic package is to be able to generate a model that captures the physics in a suitable manner.

This method part (as well as the whole master work) exist of two main parts. First a modelling part is present. Here the foundation and the various mechanism of the model, as well as the implementation in Matlab, is given. Then the procedure for some mass- and heat input cases, that were applied to the model to test its performance, are present (litt dårleg setning). These two stages represent the first part of this master work, and are directly connected to the modeling part. Then the focus are directed at initialization techniques and phase stability. Here the implementation of the particle swarm optimization (PSO) method is given. To be able to perform a sufficiently rigorous testing regime for this implementation, some preparations had to be done, these are also outlined. Finally the testing of the PSO algorithm is outlined. First a test for a simple two component case is given, then a rigorous testing regime on a four component mixture in the metastable area for the mixture is outlined. The latter based on an enthalpy-pressure envelope generated by SINTEF, as well as own preparations.

## 3.1 VessFire Topologies

A thermodynamic package to be used in connection with VessFire has to be modeled from the same basis as this simulator. To be able to model the dynamic behavior of heat- and mass input, the model need mechanisms to support appearance and disappearance of phases. Based on these facts Tore Haug-Warberg in cooperation with Petrell AS developed the control volumes given in Figure 3.1 as a starting point for the thermodynamic package.

### 3.1.1 The Basics of the VessFire Model

The system in Figure 3.1 consists of two control volumes, CV1 and CV2, which mainly represent vapor and liquid respectively. To be able to exchange mass and heat between the phases a utility- or transport phase are present in each of the phases. CV1 is then composed of the main vapor phase, V1, as well as a liquid utility phase, L1. The liquid phase L1 then represents condensation that may appear when the system is cooled. In CV2 the liquid phase L2 serves as the main phase, whilst the vapor phase V2 is the utility phase. V2 then represents evaporation that may be formed in the liquid

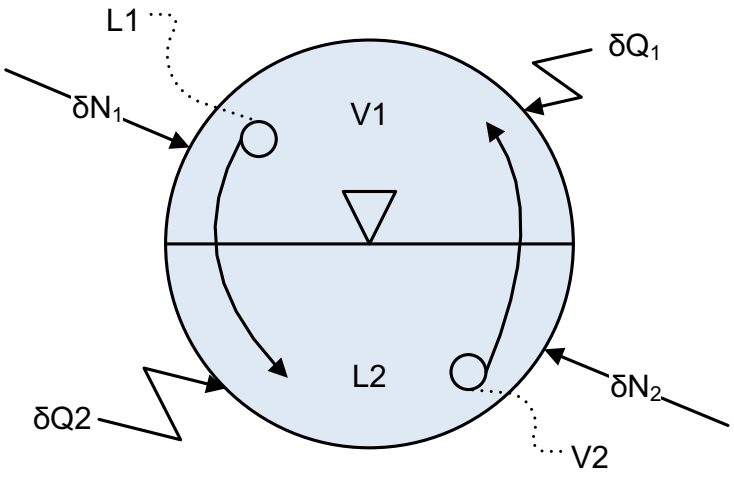


Figure 3.1: The Petrell control volumes. Two control volumes, vapor (CV1) and liquid (CV2), and four phases V1,L1,L2,V2 are present. Also mass- and heat input can be applied to each of the control volumes. $\delta\mathbf{N}_1$, $\delta\mathbf{N}_2$, $\delta Q_1$, $\delta Q_2$ can be poistive (input), or negative (output).

phase when the system is heated. Each control volume is modeled as in an inherent local equilibrium at each time step. This means that the main phase is supposed to be in equilibrium with its precipitation, and the temperature, pressure, and chemical potential are equal between them. Furthermore the pressure is assumed to reach a global equilibrium, which means that the pressures are equal for both phases.

When the system is exposed to external mass- or heat input, the liquid phase may start to vaporize, or the vapor phase may start condensing, then the utility phases will serve as transport mechanisms for mass between the phases. In this way the system can respond to the alternating conditions. For this transport the mass- and energy balances need to be fulfilled for the system. Also the volume of the two main phases are assumed to be constant within the system.

Altogether, this give the following system of equations as a foundation for the thermodynamic model:

$$\begin{pmatrix} T^{V1} & -T^{L1} & & & \\ p^{V1} & -p^{L1} & & & \\ \boldsymbol{\mu}^{V1} & -\boldsymbol{\mu}^{L1} & & & \\ & & T^{L2} & -T^{V2} & \\ & & p^{L2} & -p^{V2} & \\ & & \boldsymbol{\mu}^{L2} & -\boldsymbol{\mu}^{V2} & \\ U^{V1} & +H^{L1} & & -H^{V2} & \\ V^{V1} & & +V^{L2} & & \\ \boldsymbol{n}^{V1} & +\boldsymbol{n}^{L1} & & -\boldsymbol{n}^{V2} & \\ & -H^{L1} & +U^{L2} & +H^{V2} & \\ p^{V1} & & -p^{L2} & & \\ & -\boldsymbol{n}^{L1} & +\boldsymbol{n}^{L2} & +\boldsymbol{n}^{V2} & \end{pmatrix}^{k+1} = \begin{pmatrix} 0 \\ 0 \\ 0 \\ \\ 0 \\ 0 \\ 0 \\ \\ U^{V1}+\delta U^{V1} \\ V^{V1}+V^{L2} \\ \mathbf{n}^{V1}+\delta\mathbf{n}^{1} \\ \\ U^{L2}+\delta U^{L2} \\ 0 \\ \mathbf{n}^{L2}+\delta\mathbf{n}^{L2} \end{pmatrix}^{k} \tag{3.1}$$

The equations for the mass- and energy balances are deduced in appendix A.1. The terms $\delta U^{V1}$, $\delta U^{L2}$, $\delta\mathbf{n}_{V1}$, $\delta\mathbf{n}_{L2}$ in (3.1) equals $\delta Q_1$, $\delta Q_2$, $\delta\mathbf{n}_{V1}$, $\delta\mathbf{n}_{L2}$ in Figure 3.1, and represent the heat- and mass input applied to the system at each time step respectively.

The equation system (3.1) is in the form $f = b$, and is solved by the Newton in an iterative manner.

This solution method is outlined in section 2.3.2.

In this work a function library, based on the Peng-Robinson equation of state, was used to provide the thermodynamic properties for the calculations. The thermodynamic function library in question is developed by Tore Haug-Warberg and Bjørn Tore Løvfall at Department of Chemical Engineering, NTNU (Lovfall, 2008). The models are coded in an in-house language called RGrad supporting automatic gradient calculations, and from there exported to C-code which is compiled into a set of DLL's accessible from Matlab, Octave and Ruby (Lovfall, 2008). In the way Peng-Robinson (outlined in section **??**subsec:eos)) equation is on the form $p(T,V,\mathbf{n})$, the function library are based on Helmholtz energy as the starting point to calculate the thermodynamic properties (see section 2.3.3).

As the equilibrium calculations are based on a Helmholtz, $A(T,V,\mathbf{n})$, framework the iteration variables become $T,V,n$, which represent the canonical variables for the energy function. Nevertheless, in way the intensive canonical variable are to be held constant when minimizing the energy function, only $V$ and $n$ are the true iteration variables for calculations based on a Helmholtz model. To make the model general, for being used for thermodynamical models based on other then Helmholtz energy, all the canonical variables were included in the matrices. Then the expression for a Newton step becomes:

$$\delta \begin{pmatrix} T^{V1} \\ V^{V1} \\ \mathbf{n}^{V1} \\ T^{L1} \\ V^{L1} \\ \mathbf{n}^{L1} \\ T^{L2} \\ V^{L2} \\ \mathbf{n}^{L2} \\ T^{V2} \\ V^{V2} \\ \mathbf{n}^{V2} \end{pmatrix} = J^{-1}_{T,V,\mathbf{n}}\left(b-f\right) \tag{3.2}$$

where $b-f$ are evident from (3.1) and $J^{-1}_{T,V,\mathbf{n}}$ is the Jacobian matrix containing the first derivatives of $f$ with respect to the iteration variables $T,V,\mathbf{n}$ . The next state is then defined by:

$$\begin{pmatrix} T^{V1} \\ V^{V1} \\ \mathbf{n}^{V1} \\ T^{L1} \\ V^{L1} \\ \mathbf{n}^{L1} \\ T^{L2} \\ V^{L2} \\ \mathbf{n}^{L2} \\ T^{V2} \\ V^{V2} \\ \mathbf{n}^{V2} \end{pmatrix}^{k+1} = \begin{pmatrix} T^{V1} \\ V^{V1} \\ \mathbf{n}^{V1} \\ T^{L1} \\ V^{L1} \\ \mathbf{n}^{L1} \\ T^{L2} \\ V^{L2} \\ \mathbf{n}^{L2} \\ T^{V2} \\ V^{V2} \\ \mathbf{n}^{V2} \end{pmatrix}^{k} + \tau J^{-1}_{T,V,\mathbf{n}}\left(b-f\right) \tag{3.3}$$

where $\tau \in \langle 0,1]$ is the step shortener. The solver in this work was set to shorten the step if a call to the function library returned a negative value, and if the total volume for the system became negative,

as well as if the total amount of mole obtained a negative value. The function library will return a negative value if the system representing some unphysical states. For further knowledge about this, the interested reader are guided to the homepage of Tore Haug-Warberg (Lovfall, 2008).

In the way that the flow simulator assume each phase to be in a stable local equilibrium at each time step, the set of equations (3.1) is solved for each time step.

### 3.1.2 Dynamics

According to the physics, input of heat and mass to the system might result in that phases disappear, and that new phases are formed. This means that the thermodynamic model needs inherent mechanisms to support these scenarios. In other words this means that the system should be able to change between different topologies. The model in this work is generated to support a system of two main phases, liquid and vapor, as illustrated in Figure 3.1. The model do not support solid precipitation. Then a maximum of four phases can exist in this system, as illustrated in section 3.1.1. Nevertheless, the model should be able to model that utility phases and any of the main phases disappear. Also the starting topology might differ from case to case. Figure 3.2 illustrates the different topologies that should be supported by the model.

From Figure 3.2 it is evident that the model should be able to change between six different topologies. A challenge was to generate mechanisms to get the model to change between these topologies, both to decide on a convenient criterion for throwing a phase away, and how to modify the equation set to fit the new topologies.

#### Virtual Phases

For each topology the equation set (3.1) was modified, so that each topology had its own set of equations. Even though the most obvious solution for this had been to take the disappearing phases out of the equation system, these phases remained in the system as virtual phases. The virtual phases were then solved for the equilibrium equations apart from the pressure equation, but excluded from the mass- and energy balances. Instead of the pressure equation the total mole amount of the virtual phases were set to equal unity. In this way the intensive quantities were calculated and updated for the virtual phases. The virtual phases could then serve as reference phases to reintroduce the real phases. For topology 6 (V1,L1,L2,V2) illustrated in Figure 3.2f, the equation system (3.1) is modified as evident from Equation (3.4). For topology 6, both utility phases serve as virtual phases. The variables for the virtual phases are colored red.

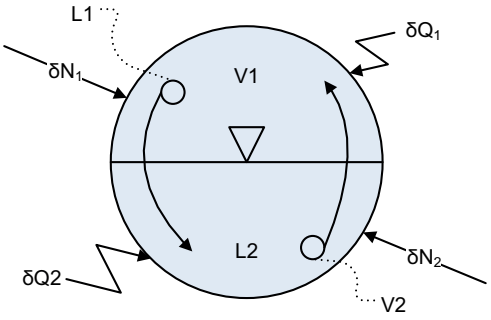


(a) Topology 1 (V1,L1,L2,V2). The original model. All phases are present

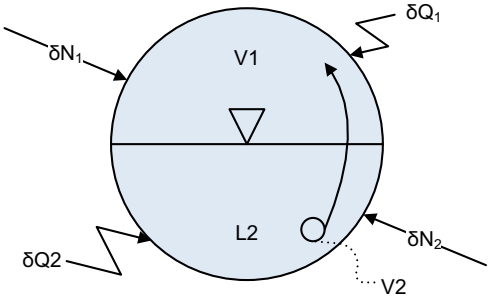


(b) Topology 2 (V1,L2,V2). The liquid phase (CV2) is exposed to heating, $\delta Q_2 > 0$. $\delta Q_1 = 0$ and no condense phase L1 is present

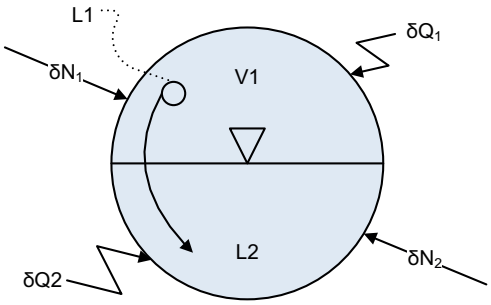


(c) Topology 3 (V1,L1,L2). May exist when the vapor phase (CV1) is exposed to cooling, $\delta Q_1 < 0$, and $\delta Q_2 = 0$. Then phase L2 may not evaporate, unless heated by L1

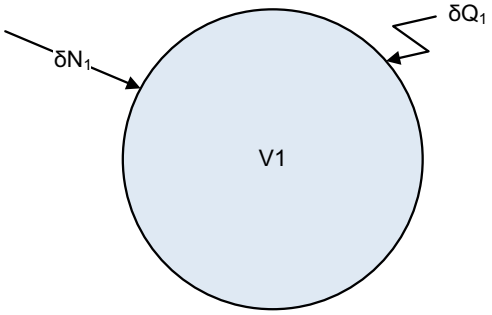


(d) Topology 4 (V1). Only the vapor phase (CV1) is present. The conditions for the system is in the vapor area.

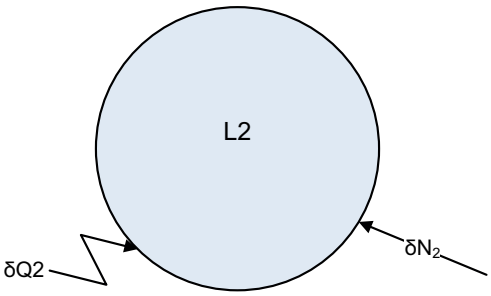


(e) Topology 5 (L2). Only the liquid phase is present. The conditions for the system is in the liquid area.

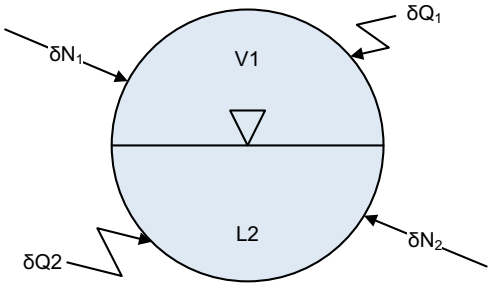


(f) Topology 6 (V1,L2). Both main phases are stable, and no adjustment of the containment in the different phases are needed. The system is at rest, no external forces (heat or mass) disturb the system.

Figure 3.2: The different topologies available to the thermodynamic model.

$$
\begin{pmatrix}
T^{V1} & -T^{L1} & & & \\
 & \mathbf{e}^T\mathbf{n}^{L1} & & & \\
\boldsymbol{\mu}^{V1} & -\boldsymbol{\mu}^{L1} & & & \\
 & & T^{L2} & -T^{V2} & \\
 & & & \mathbf{e}^T\mathbf{n}^{V2} & \\
 & & \boldsymbol{\mu}^{L2} & -\boldsymbol{\mu}^{V2} & \\
U^{V1} & & & & \\
V^{V1} & & +V^{L2} & & \\
\boldsymbol{n}^{V1} & & & & \\
 & & U^{L2} & & \\
p^{V1} & & -p^{L2} & & \\
 & & \boldsymbol{n}^{L2} & &
\end{pmatrix}^{k+1}
=
\begin{pmatrix}
0 \\ 1 \\ 0 \\ \\ 0 \\ 1 \\ 0 \\ \\ U^{V1}+\delta U^{V1} \\ V^{V1}+V^{L2} \\ \mathbf{n}^{V1}+\delta\mathbf{n}^{1} \\ \\ U^{L2}+\delta U^{L2} \\ 0 \\ \mathbf{n}^{L2}+\delta\mathbf{n}^{L2}
\end{pmatrix}^{k}
\tag{3.4}
$$

where $\mathbf{e}^T = [11\ldots1]$ with length equal to number of components in the system.

Nevertheless, only the utility phases can serve as virtual phases. If one of the main phases, V1 or L1, disappears, also their utility- or virtual phase have to be excluded from the system, then the equation system have to be reduced. Equation (3.5) gives an example of the reduced equation set. This equation set corresponds to topology 4 (V1,L1).

$$\begin{pmatrix} T^{V1} & -T^{L1} \\ & \mathbf{e}^T\mathbf{n}^{L1} \\ \boldsymbol{\mu}^{V1} & -\boldsymbol{\mu}^{L1} \\ \\ U^{V1} & \\ V^{V1} & \\ \mathbf{n}^{V1} & \end{pmatrix}^{k+1} = \begin{pmatrix} 0 \\ 1 \\ 0 \\ \\ U^{V1}+\delta U^{V1} \\ V^{V1} \\ \mathbf{n}^{V1}+\delta\mathbf{n}^{1} \end{pmatrix}^{k} \tag{3.5}$$

Similar equation systems yield for the other topologies as well. These equations are available in appendix A.1.

Nevertheless, not all topologies are directly reachable from another, without going via one of the other topologies. Table 3.1 demonstrates witch topologies that should be reachable from each other.

Table 3.1: Interaction scheme for the different topologies. The white cells represents the topology changes that should be possible from time step $k$ to time step $k+1$. The cells colored black represent the topology changes that are not possible without going through other topologies. The gray cells represent a topology going to the same topology, and is not a transformation.

| | | $k$ | | | | | |
|---|---|---|---|---|---|---|---|
| | | **V1 L1 L2 V2** | **V1 L1 L2 V2** | **V1 L1 L2 V2** | **V1 L1 L2 V2** | **V1 L1** | **L2 V2** |
| $k+1$ | **V1 L1 L2 V2** | | | | | | |
| | **V1 L1 L2 V2** | | | | | | |
| | **V1 L1 L2 V2** | | | | | | |
| | **V1 L1 L2 V2** | | | | | | |
| | **V1 L1** | | | | | | |
| | **L2 V2** | | | | | | |

Given the different topologies with their equation sets, as well as the knowledge of which topologies that should be reachable from a specific topology, the next challenge was to decide on how to change between the different topologies, and to implement the model into Matlab.

### 3.1.3 Changing between Topologies

To change between the topologies some control of the different phases needed to be established. Two main aspects had to be decided on, when to leave a phase behind, and when to introduce or

reintroduce a phase to the system. To be able to determine on whether a phase should be excluded from the system a norm control was established. For this purpose the state norm, $\sqrt{S^2 + V^2 + \mathbf{n}^T\mathbf{n}}$, was established. The following inequality was applied to each phase to decide on whether it should be excluded from the system:

$$\sqrt{\frac{S_i^2}{S_j^2} + \frac{V_i^2}{V_j^2} + \frac{(\mathbf{n}^T\mathbf{n})_i}{(\mathbf{n}^T\mathbf{n})_j}} < \epsilon \tag{3.6}$$

where $\epsilon$ is a small number defined by the user. $i$ denotes the phase to be tested, and $j$ denotes the phase it is tested relatively to. The utility phases are tested relatively to its main phase. Whilst the norms of the main phases are tested relatively to each other. When the value of the relative state norm are below a specified small number $\epsilon$ for a particular phase, the phase is considered to be absent from the system.

As explained in section 3.1.2, when a utility phase is left behind, it stays in the system as a virtual phase, and its intensive quantities are updated relative to its main phase. In this way the tangent plane test (3.7) could be applied to the virtual phase relatively to its main phase, to test for stability:

$$-(p - p^0)\delta V + (\mu - \mu^0)^T \delta N < 0 \tag{3.7}$$

where $p^0, \mu^0$ denotes the pressure and the chemical potential in the main phase and $p, \mu$ are the corresponding quantities in the virtual phase. If the inequality in equation (3.7) is true, the virtual phase should be reintroduced to the system. This mechanism for introducing phases are available both to a system existing of a single control volume, and to a system where both control volumes are present. When both control volume are present the utility phase is applied to the tangent plane test, to check if it should be reintroduced to the system. Then if the tangent plane check gives a negative value, the virtual phase are transformed to a real phase again, and it is included in the mass- and energy balances. The new phase are taken in as a fraction of its main phase, and the intenive quantities are adopted from the virtual phase.

The one-phase topologies, Topology 4 and Topology 5, exist of one real and one virtual phase. The purpose of the utility phases are to serve as transport mechanisms to transfer mass from one control volume to the other. Then when only one control volume exists there is no need for such a mechanism. Nevertheless, a negative value from the tangent plane test applied to this system, does mean that there exist a two-phase system with lower energy than the current configuration (Michelsen, 1982). In these circumstances this means that a main phase of the same type as the virtual phase (vapor or liquid) should be included in the system.

As the new phase can be viewed as a precipitation of the main phase, this phase is assumed to be in equilibrium with the other main phase, and a Newton-$U, V, n$ flash are applied to these phases to calculate the composition. As start estimates for these equilibrium calculations, the new phase adopt molar volume and fraction from the virtual phase. The amount of the new phase are scaled as a small fraction $\epsilon$ of the existing main phase. Equation (3.8)- (3.9) illustrate this procedure:

$$\mathbf{n}_{k+1}^{\beta_1} = \frac{\mathbf{n}_k^{\alpha_2}}{\mathbf{e}^T\mathbf{n}_k^{\alpha_2}} \epsilon \mathbf{n_k}^{\alpha_1} \tag{3.8}$$

$$V_{k+1}^{\beta_1} = \frac{V_k^{\alpha_2}}{\mathbf{e}^T\mathbf{n}_k} \epsilon \mathbf{n}_k^{\alpha_1} \tag{3.9}$$

where $\alpha$ denote the existing control volume, and $\beta$ represent the control volume to be introduced. The subscripts 1 and 2, denote the main phase and the utility phase respectively, and $e = [11\ldots1]$ deonotes the unit vector of length corresponding to the number of components in the system.

Then to keep the total amount of mole, as well as the total volume, in the system to a constant value, the amount and the volume of the existing phase are adjusted by subtracting the amount of the precipitation:

$$\mathbf{n}_{k+1}^{\alpha_1} = \mathbf{n}_k^{\alpha_1} - \mathbf{n}_{k+1}^{\beta_1} \tag{3.10}$$

$$V_{k+1}^{\alpha_1} = V_k^{\alpha} - V^{\beta_1} \tag{3.11}$$

In the way the $\beta$-phase are introduced based on evaporation or condensation in the $\alpha$-phase, it would be reasonable to believe that the $\alpha$-phase would continue to deposit the same amount during the next time step. Based on that assumption the utility phase $\alpha_2$ are introduced equivalent to the $\beta_1$-phase resulting from the $U,V,n$-flash.

The volume and amount of the other utility phase, $\beta_2$, are set to a small amount of $\alpha_1$, which represents the main phase of the same phase type as $\beta_2$. In the way a local equilibrium is decided to exist inside each control volume, the temperature of the utility phase $\beta_2$ is set equal its main phase $\beta_1$. This procedure has been given the name, "SetFeasible", and is also performed to initialize the utility phases when a two-phase system is available from the flow simulator. When phases are left behind, based on the norm criterion, their properties are no longer reliable, then to keep them in the system as virtual phases, these properties have to be adjusted. This is performed by the "Set Feasible" routine.

**Based** on the norm control to detect whether a phase should be excluded from the system, and the tangent plane, cooperating with the virtual phases to decide on the formation of phases, the model should be able to change between the 6 topologies illustrated in Figure 3.2, and in Table 3.1. Nevertheless, in the way both the stability checks and the initialization of the new phases are based on the virtual phases, the dynamics of this model to large extent rely on the existence of the virtual phases. Then problems arrive when the system are exposed to conditions where the virtual phases cease to be reliable. Since the utility phases are initialized based on the main phase from the other control volume, the same problems will be present whenever the system provided by VessFire, are in the one-phase area. Under these circumstances some external stability checks and initialization routines have to be performed.

### 3.1.4 Implementation Details

Founded on the model basics and the dynamics of the model outlined in section 3.1.1- 3.1.3, the model was implemented in Matlab. In Figure 3.3 this implementation is illustrated by a flow sheet.

The input to the model, which is the state of the different phases, is supplied by the flow simulator VessFire. Then a Peng-Robinson model is initialized to calculate the state of each of the main phases. Based on these main phases, the utility phases are introduced, as outlined in section 3.1.1. Then the system is solved for a given number of time steps as function of heat- and mass input from VessFire. Even though the system was developed to work with input from VessFire, it is also possible to type the input manually, which can be appropriate in some stages of the testing of the system. The system is solved due to the different topologies and the equation sets given in section 3.1.1.

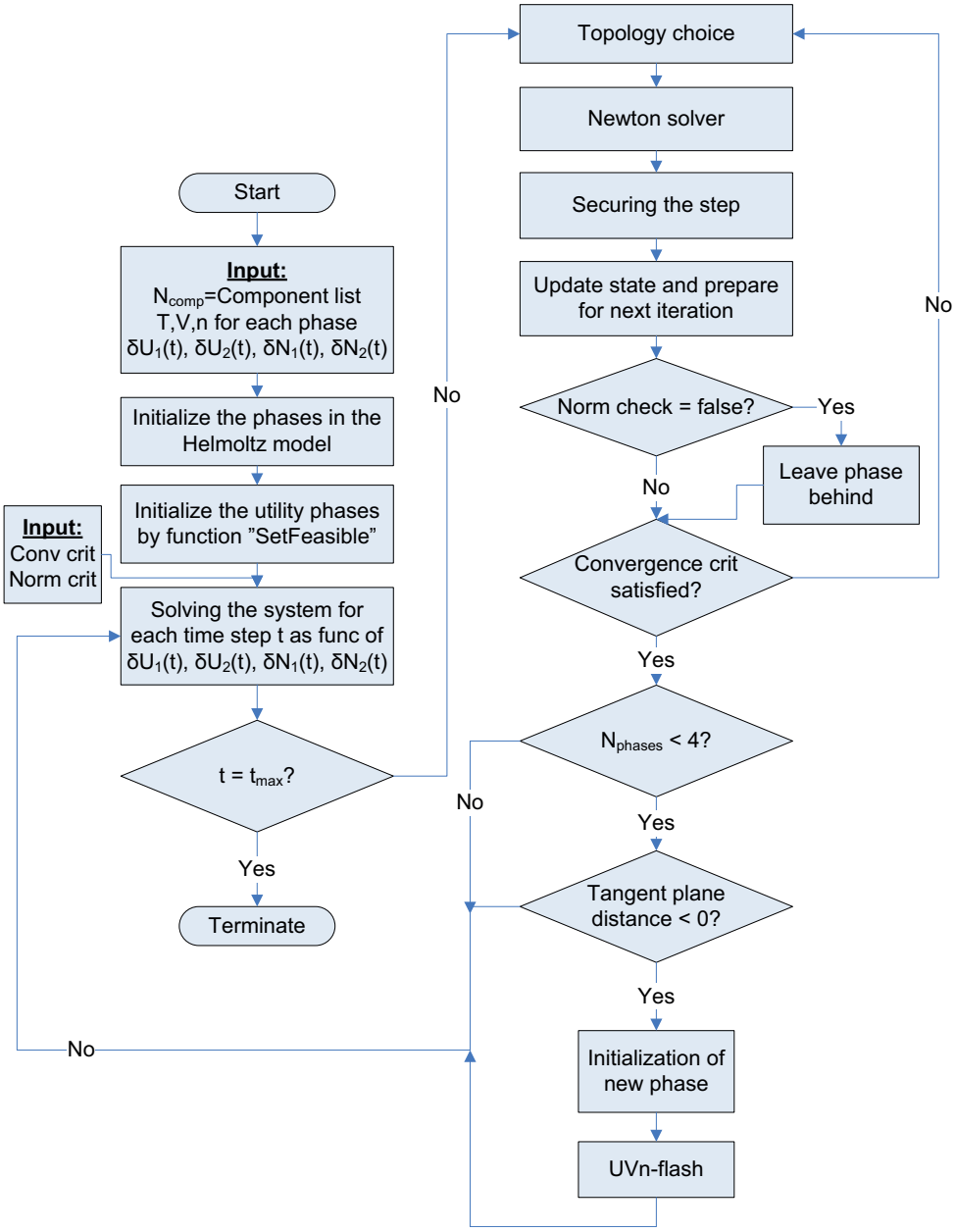


Figure 3.3: The implementation of the thermodynamic model in Matlab.

As a first step in the iteration loop, a topology choice based on the phases present in the system is performed. Based on this choice an equation set is solved by the Newton solver (3.2). The length of the Newton step is shortened as long as a call to the Helmholtz model returns a negative value or any of volume, total mole amount is negative. When these constraints are fulfilled, the step is accepted, the phase models are updated and prepared for the next step. To check whether a phase should be excluded from the system a norm control of the norm given in Equation (3.6) is done. A phase that due to the physics should not be in the system will not converge, and so it will create convergence problems for the system as a whole. Due to that fact, it is important to perform the norm check. It is important that the norm in use is able to detect the conditions where a phase should be left behind. Also a norm that throws away phases when it is not necessary, will create instability in the iteration.

Whenever the convergence criterion is not satisfied, a new iteration is performed. On the other hand, if the convergence criterion is fulfilled for the system, the next step is to check for phase stability. Nevertheless, the stability check is done only when less then 4 real phases are present. This means it

is not accomplished when Topology 1 is present. The stability check is performed by control of the tangent plane distance. When the system is applied to the tangent plane test, the system has fulfilled the convergence criterion. This means that its chemical potential, as well as the temperature are equal for the virtual phase and the main phase. Then the sign of the tangent plane distance is evident from the pressure differences between the virtual phase and the main phase. If the pressure in the virtual is above the pressure of the main phase, the tangent plane distance is negative, and a phase should be introduced to the system. The subsequent phase initialization is done as explained in section 3.1.3. After the new phase is included, the system is assumed to be solved for that time step. Whenever the tangent plane distance is negative or all phases are present in the system, the calculation sequence for that particular time step is terminated on earlier stages, as evident from Figure 3.3.

This calculation scheme is repeated until the given number of time step $t_{max}$ is reached.

To verify the model, as well as to detect its shortcomings, some test cases were applied to the implemented model. These tests are outlined in the next section.

## 3.2 Testing the Model

The main target for the testing was to verify the dynamics of the model, to check whether it was able to respond to external heat- and mass input, by changing between the different topologies. Then the objectives to test were the norm control criterion for leaving phases behind, as well as the initialization mechanisms based on the virtual phases and the tangent plane check. To be able to test these mechanisms, testing cases applied to the model should be constructed such that as many as possible of the topology changes should occur due to the physics. The different topology changes the model should support are illustrated in Table 3.1.

The test regime executed in this work consisted of three different test cases. Test Case I is a self constructed case, where the two component system ethane-n-butane is applied to input of heat. The aim of this test case is to verify the function of the norm criterion for throwing a phase away, as well as the initialization mechanisms, both for introducing an utility phase and to initialize a new control volume. In the second case the model is applied to actual simulation data from VessFire. Here both heat- and mass input are present. In this case too the two-component system consisting of ethane and n-butane is the system in question. The last testing case is on the a component system containing ethane. The purpose of this test is to illustrate some shortcomings of the model.

### 3.2.1 Experimental Details

The systems applied to the tests contained two different components, ethane and n-butane. In the context of phase equilibrium calculations the knowledge of critical points and bubble points are of considerable importance. For the components used in this work, these data are given in Table 3.2:

Table 3.2: Critical properties for the different components

| | $\mathbf{p_c}$[bar] | $\mathbf{T_c}$[K] | $\mathbf{T_{bp}}$[K] |
|---|---|---|---|
| **Ethane** | 48.8 | 305.4 | 185.15 |
| **n-butane** | 38.0 | 425.2 | 272.6 |

The convergence criterion used was equal in all cases, and this was true for the norm criterion as well. Otherwise the small number $\epsilon$, used to initialize the amount of the utility phases as fraction

of the main phases, as well as to initialize a main phase as a fraction of the other main phase, was identical in all cases. The values of these parameters are given in Table 3.3:

Table 3.3: Critical properties for the different components

| **Norm-criterion** | **Convergence criterion** | $\boldsymbol{\epsilon}$ |
|---|---|---|
| 1e-3 | 1e-6 | 1e-5 |

The convergence criterion was set on the delta norm of the iteration variables $T, V, n$. The value of this convergence criterion was set based on the numerical precision of the computer $\epsilon = 2.2204e-016$, and the rule of thumb that the calculations can only be considered as reliable to a precision of the square of the computer precision, which is equivalent to a precision of $1.4901e-008$. The state norm, used as the criterion to decide whether a phase should be left behind, was set due to trial and error. The small number $\epsilon$, used to set the amount of a new phase introduced to the system, was set relatively randomly, but with the thought in mind that the amount should reflect a precipitation of the main phase.

### 3.2.2 Two Component Case

The aim of this test case was to verify the model's functionalities for changing between the different topologies. These functionalities exist of three different mechanisms, the norm criterion for leaving a phase behind, as well as the initialization mechanisms both for introducing a utility phase and a for the formation of a new control volume to the system. These mechanisms are outlined in section 3.1.3.

Then the target was to construct a heat input case, in such a way that all of these mechanisms were to be needed. Also an objective was to do it as simple as possible. In that way only heat input, and no mass input, was used in this case. Then the total mole amount was constant during the time steps. The system was initialized in the two-phase area, with a total amount of 2 mol in the system. Firstly, the liquid phase were exposed to heating, aiming to evaporate the liquid. At a later stage the system was cooled. The objective was then to go from a four-phase (2 main phases and 2 utility phases) system, to a one-phase system, and then to introduce the lost phases again. In this way all three mechanisms should be applied to the system. The actual initialization variables, and the quantities of heat and mass per time step to the system, are given in Table 3.4 and Table 3.5 respectively.

Table 3.4: Initialization values for the main phases used in Test Case I.

| | $\mathbf{T}$ [K] | $\mathbf{V}$ [dm$^3$] | $\mathbf{n_{C_2H_6}}$ [mol] | $\mathbf{n_{C_2H_6}}$ [mol] |
|---|---|---|---|---|
| **V1** | 250 | 20.0 | 0.94 | 0.37 |
| **L2** | 250 | $5.87e-2$ | 0.06 | 0.63 |

Table 3.5: Heat- and mass input for Test Case I. The number of time step, $t_{max} = 150$.

| **t** | $\delta\mathbf{U^{V1}}$ [J] | $\delta\mathbf{U^{L2}}$[J] | $\delta\mathbf{N^{V1}}$ [mol] | $\delta\mathbf{N^{L2}}$[mol] |
|---|---|---|---|---|
| **1-49** | 0 | 500 | 0 | 0 |
| **50-150** | −500 | 0 | 0 | 0 |

### 3.2.3 VessFire Case

In this case the model is applied to actual simulation data from VessFire. The objective of this testing case was to see the behavior of the model when applied to both mass- and heat input. Due to the fact that these data are taken from a real case in the process industry, this test may verify the potential of the model for use in industrial simulations. This test case exists of a large number of time steps, and the external input is more random compared to the self-constructed cases, which was constructed for testing the mechanisms of the topology transitions. This enhance the possibility to obtain a wider range of the topology transformations, given in Table 3.1, which the model should support. Also the quantities of mass applied to the system is much larger in this case.

In the was this was a simulation case from VessFire, both the initialization of the phases as well as the input of heat- and mass were supplied from that simulator. The initialization values for the phases are given in Table 3.6. The heat- and mass inputs are given graphically in Figure 3.4.

Table 3.6: Initialization values for the main phases used in Test Case I.

| | **T** [K] | **V** [dm$^3$] | $\mathbf{n_{C_2H_6}}$ [mol] | $\mathbf{n_{C_4H_10}}$ [mol] |
|---|---|---|---|---|
| **V1** | 250 | 48078.63 | 1946.293 | 902.2466 |
| **L2** | 250 | 3588.25 | 2776.001 | 38793.34 |

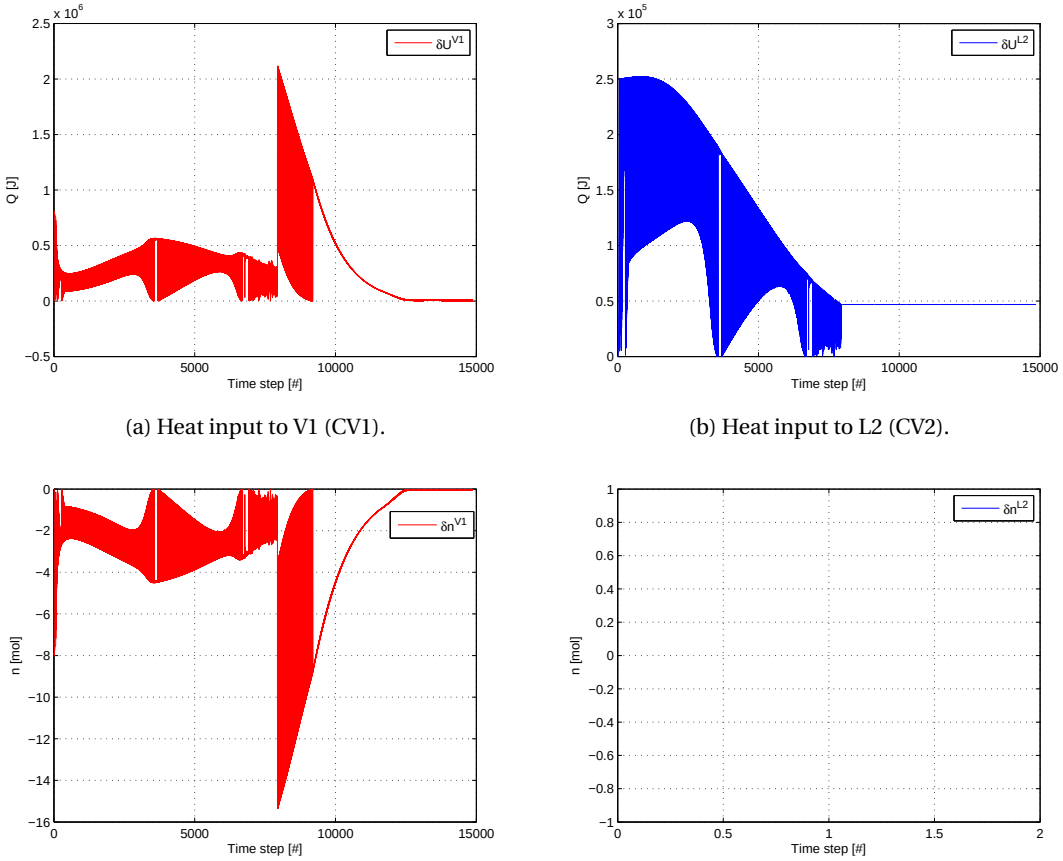


(a) Heat input to V1 (CV1).

(b) Heat input to L2 (CV2).

(c) Mass input to V1 (CV1).

(d) Mass input to L2 (CV2).

Figure 3.4: Profiles for heat- and mass input for the VessFire case.

From Figure 3.4a- 3.4b one can observe that the system is exposed to heating. From 3.4c it is evident that the system is discharged, in the way $\delta n \leq 0$. Figure 3.4d demonstrates that no mass is taken from,

or supplied to the liquid phase (CV2). The case exists of $t_{max}$ = 14858 time step.

### 3.2.4 One Component Case

In this case the model is applied to a one-component system existing of ethane. The objective of this case was to detect some shortcomings of the model. To eliminate the influence of the composition, a one component system was used. This test consists of two parts. In the first case the system is initialized in the two phase area, then the liquid phase is heated until it is totally vaporized. The heating is continued beyond this point, until a point where the virtual phase L1 has gone into the trivial solution. Then the system is cooled until a quite low temperature is obtained. Then if the model works properly, the liquid phase should be reintroduced.

The initialization data and the input data are given in Table 3.7- 3.8:

Table 3.7: Initialization values for the main phases used in Test Case I.

| | **T** [K] | **V** [dm$^3$] | $\mathbf{n_{C_2H_6}}$ [mol] |
|---|---|---|---|
| **V1** | 180 | 10.0 | 1 |
| **L2** | 180 | 0.05 | 1 |

Table 3.8: Heat- and mass input for Test Case I. The number of time step, $t_{max}$ = 150.

| **t** | $\delta\mathbf{U^{V1}}$ [J] | $\delta\mathbf{U^{L2}}$[J] | $\delta\mathbf{N^{V1}}$ [mol] | $\delta\mathbf{N^{L2}}$[mol] |
|---|---|---|---|---|
| **1-81** | 0 | 200 | 0 | 0 |
| **81-99** | 200 | 0 | 0 | 0 |
| **81-99** | −200 | 0 | 0 | 0 |

In the second part of the one comp test the system was initialized with a large liquid phase and a tiny vapor phase. The aim was to cool the vapor phase until it disappeared from the system. and then investigate the conditions for when the virtual phase V2 was no longer reliable.

The initialization values and the inputs to the model are given in Table 3.9 and 3.10:

Table 3.9: Initialization values for the main phases used in Test Case I.

| | **T** [K] | **V** [dm$^3$] | $\mathbf{n_{C_2H_6}}$ [mol] |
|---|---|---|---|
| **V1** | 180 | $1e-4$ | $1e-5$ |
| **L2** | 180 | 0.05 | 1 |

Table 3.10: Heat- and mass input for Test Case I. The number of time step, $t_{max}$ = 100.

| $\delta\mathbf{U^{V1}}$ [J] | $\delta\mathbf{U^{L2}}$[J] | $\delta\mathbf{N^{V1}}$ [mol] | $\delta\mathbf{N^{L2}}$[mol] |
|---|---|---|---|
| 0 | 0 | 0 | 0 |
| −100 | 0 | 0 | 0 |

## 3.3 Initialization

To be able to develop a thermodynamic model that are sufficiently robust and will perform well applied to a wide range of mass- and energy input, some kind of stability checks and initialization routines are needed. The initialization methods, as well as the stability check, used in the generated

model described in section 3.1, and tested in section 3.2 rely on the existence of the virtual phases. This seem to be a quite clever and efficient solution as long as the system is applied to moderate physical conditions. Nevertheless, as the state of the system approaches the critical state, the virtual phases will no longer be reliable. At this point the need for an external initialization routine is present. In this work the stochastic optimization routine Particle Swarm Optimization (PSO) is tested for this purpose. This routine is outlined in section 2.2.1. The implementation of this routine is given in the following section.

### 3.3.1 Implementation of the PSO algorithm

In this work the local dynamic PSO version, Dynamic Multi-Swarm Optimizer (DMS-PSO), given by Liang and Suganthan (2005) was tested for the four component system $N_2$, $CH_4$, $C_2H_6$, $C_3H_8$. This routine is outlined in section 2.2.1. The flowchart given in Figure 2.7 illustrates its implementation. The algorithm in this work was implemented according to this scheme. Nevertheless, the model need some user defined inputs, and also some specifications are needed to fit the routine into the context of equilibrium calculations. These are given in the following.

The user defined variables are listed in Table 3.11:

Table 3.11: User defined input variables used in the current implementation

| **m** | **n** | **R** | **MaxIter** |
|---|---|---|---|
| 5 | 4 | 5 | 400 |

where $m$ are the size of each subswarm, $n$ are the number of subswarms, and $MaxIter$ is the maximum number of iterations allowed, and are set to 400. Actually this serve as the convergence criterion in this implementation.

In addition some parameters are to be set directly to the solver, which illustrated by (2.9) at page 19. These are tuning variables that have been fitted in literature. In the current implementation, values given by Trelea (2003) are used for these parameters. These are given in Table 3.12.

Table 3.12: Tuning parameters used in the current implementation

| **a** | $\mathbf{b_1}$ | $\mathbf{b_2}$ |
|---|---|---|
| 0.6 | 1.7 | 1.7 |

Another issue related to the PSO-algorithm is to set lower- and upper bounds to the different variables, to define the feasible search space. Related to equilibrium calculations also an issue is to decide on which variables to optimize in the algorithm. Based on the initialization routine applied to reintroduce the virtual phases in the generated model (given in (3.8)- (3.9)), the PSO algorithm was used to search for fractions of the various components, as well as the total density for the new phase. Then the size of the new phase was estimated as a small fraction, $\epsilon$, of the existing phase, according to equation (3.8)- (3.9). Nevertheless, in the optimization routine, density was searched instead of molar volume due to a suspicion that the limits should be easier to obtain that way.

Figure 3.5 illustrates how the DMS-routine is applied to phase equilibrium calculations in this work. In the current implementation a Wilson flash was used in connection to set the upper and lower bounds on the fraction. The Wilson routine approximates the states based on the critical properties of the mixture, and then it uses a K-value method to estimate the phase fractions, as well as the component fractions in the phases. These component fraction estimates was used as a starting point for

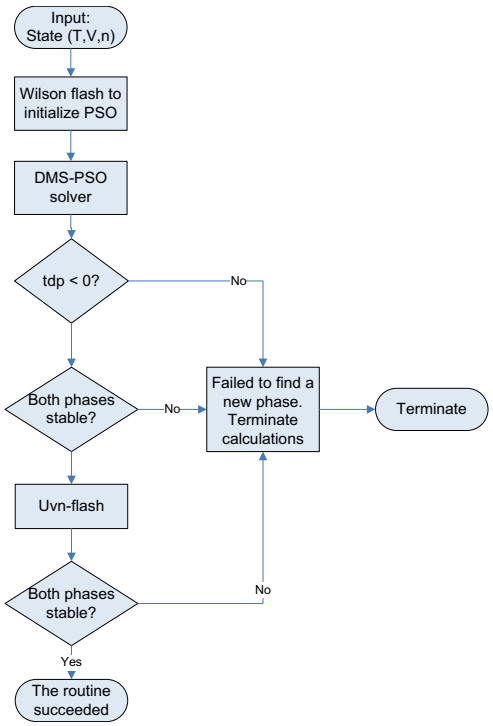


Figure 3.5: The implementation of the DMS-PSO used in this work.

the upper- and lower bounds of the component fractions in the new phase. The borders for the density was initially set to $\rho = [0, \frac{\mathbf{e}^T\mathbf{n}}{b}]$ both for the search of vapor phases and liquid phases. Later this was changed to $[0, \frac{\rho}{10}]$ in the search for a vapor phase, and to $[\frac{\mathbf{e}^T\mathbf{n}}{3b}, \frac{\mathbf{e}^T\mathbf{n}}{b}]$. This objective of this was to give the algorithm a clever guidance against the solution. The though behind the choice of liquid bounds was that the largest liquid volume for a given mixture under given conditions are the critical volume, for the der Waal equation of state this is $v_c = 3b$. Nevertheless $b$ depends on the composition, which means that this might not be a good choice of border. The bound for the search for the vapor phase was set more randomly, aiming to eliminate the liquid volumes.

Then the DMS-PSO solver is applied to the system, using the variables given in Table 3.11- 3.12 as input. As the objective with an initialization routine applied to equilibrium calculations is to detect whether a state with a lower energy are present at the energy surface, the tangent plane distance is used as the objective function. A negative value of this distance relatively to the current state, means that a state with lower energy is found for the system (Michael L. Michelsen, 2004). If the tangent plane is negative, the phases are applied to a stability check, before the composition of the phases are adjusted in a $UVn$-flash. Finally the resulting phases are tested for stability, if this stability test is positive, the initialization routine has succeed to find and introduce a new phase.

Nevertheless, to be able to start the test some initial state values for the system is needed. To obtain this information is to converge all points in a particular $xy$-grid for one-phase calculations. Here $xy$ denotes a pair of thermodynamic variables such that $Tp$, $Sp$, $UV$, $Hp$ and $pV$. This is outlined in the next section.

### 3.3.2 Preparing the States for PSO

The objective of an initialization routine applied to vapor—liquid phase equilibrium calculations, is that the routine should manages to find a two-phase solution when applied to an unstable or

metastable one-phase system. Then to be able to perform a proper test regime for a given system, feasible one-phase states is needed. Applied to phase equilibrium calculations also an important aspect is to know which states that will be convenient to test for. This means that some knowledge about the properties of the system is a benefit.

In this work feasible one-phase states were obtained by converging the rectangular $Hp$-diagram for one-phase calculations. The objective was to converge all the points in the physical range for these coordinates in the one-phase area, and mark the locations where the stability conditions would not be fulfilled. At these location the one-phase solution will not correspond to a feasible state. The physical range of enthalpy and pressure was defined from a $Hp$-phase envelope for the current system, generated by Olaf Trygve Berglihn at SINTEF.

Due to the fact that $Tp$, $Sp$ and $UV$, as well as $Hp$, constitute standard approaches in chemical processes, stability plots to obtain one-phase states were generated in all of these coordinates. Also the $pV$–plot, which represent a common description of a thermodynamic system, was generated. The procedures were similar in each case, Figure 3.6 illustrates this procedure in a flow diagram.

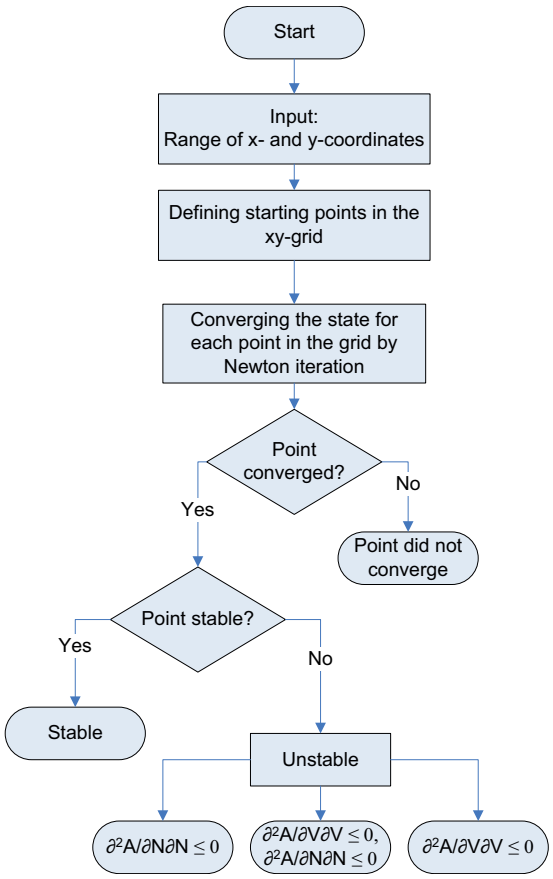


Figure 3.6: The procedure used for generating stability plots. Each point are categorized according to the stability conditions of the converged state. Not convergence is also an possibility. According to this scheme the points are divided into 5 different categories.

According to Figure 3.6 the states for each point in the $xy$-grid was calculated by converging the states for the specified variables by the Newton-Raphson scheme. This method is outlined in section 2.3.2. The calculation of each point in the grid was initialized from the same starting point. Subsequent to the convergence routine, each point was categorized according to its convergence properties. The convergence criterion in these iterations was set on the delta norm of the iteration variables, and was set to a small number $\epsilon = 1e-5$. If a point did not converge in 200 iterations, the point was categorized

as not convergent. After a point was converged a stability check was applied to the calculated state. Then the given state was categorized as stable, or unstable. Given that the state was unstable, it was noted whether the mechanical stability condition, $(\frac{\partial^2 A}{\partial V \partial V})_{T,N} > 0$, or the diffusive stability condition $(\frac{\partial^2 A}{\partial N \partial N})_{T,V} > 0$ that was violated. Then a total of 5 stability categories were noted. These were marked with different colors in the plots.

As a starting point plots were generated both for $UV$, $Tp$ and $pV$-coordinates. In a single plot, each point was initialized from the same state.

## 3.4 Testing of PSO

In this work the local and dynamic PSO version, Dynamic Multi Swarm PSO (DMS-PSO), developed by Liang and Suganthan (2005), was implemented and tested for the four component system, $N_2$, $CH_4$, $C_2$, $C_3$. A system of 4 components was chosen due to the fact that higher dimensional problems are expected to be more complex and more difficult to solve than problems of fewer dimensions. Also little testing of phase equilibrium calculations for multicomponent systems are evident from the literature.

The starting point for the testing was a $Hp$-grid that was converged for one-phase together with a phase envelope generated by Olaf Trygve Berglihn at SINTEF. The converged one-phase grid supplied the initialization routine with feasible states, whilst the phase envelope served as a reference for the location of the two-phase domain of the system. In figure 3.7 the converged one phase states are plotted together with the phase envelope.

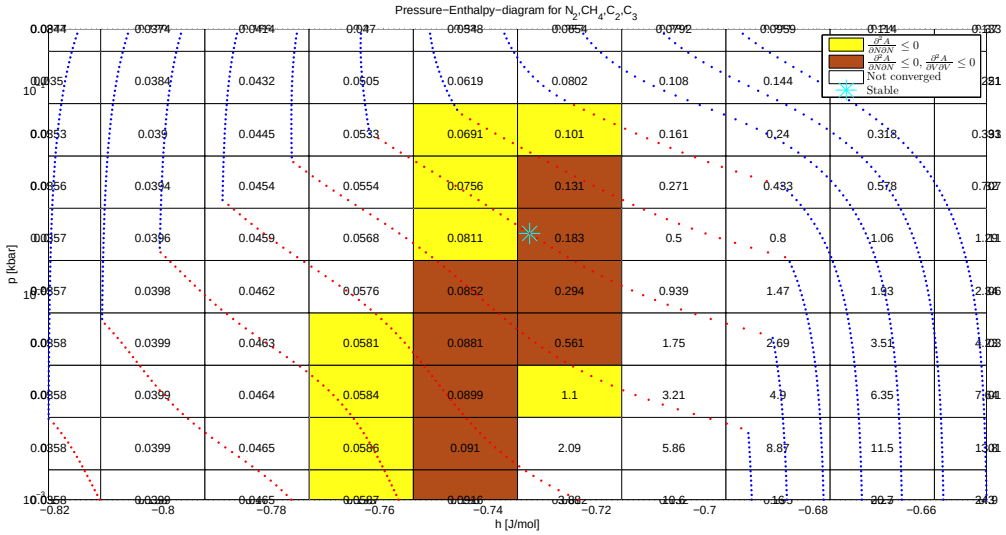


Figure 3.7: Enthalpy-pressure envelope for the system $N_2$, $CH_4$, $C_2$, $C_3$, generated by Olaf Trygve Berglihn at SINTEF, revised in this work. The calculated one-phase volumes is given in each patch in the grid. The colored patches represents unstable locations.

The implementation of the DMS-PSO is given in section 3.3.1.

Nevertheless, the differences between this plot and Figure 3.7 will represent the metastable area. A main objective of the the initialization routine is that it is capable of finding solutions in the metastable area.

# Chapter 4

# Results

## 4.1 Testing the Model

In this part of the result chapter the results from the testing of the generated thermodynamic model are given. The test regime consisted of three different test cases, hence this section is divided into three subsections. The first subsection gives the results from the Test Case I which is a self-constructed case. The results from the real scenario case from VessFire are given next. Finally the third part presents the results from the one component case.

### 4.1.1 Two Component Case

This case was constructed aiming to verify the mechanism generated for leaving out phases, and the corresponding mechanisms for adding utility phases, as well as main phases to the system. Starting with a four-phase system the aim was to vaporize the liquid phase, until an one-phase system was present. Then the system was cooled such that the liquid phase should be reintroduced. In that way, both the function of the norm control criterion, the stability check, as well as the initialization routine should be tested.

The results from this test case are given in Figure 4.1a- 4.2a. Figure 4.1 gives the temperature profile of the different phases, as well as the pressure development in the vapor phase during the test. According to the modeling basics, outlined in section 3.1.1, the pressure are set to be equal in both control volumes.

From the Figure 4.1 one can observe that the temperatures in both phases are elevated, until the liquid phase disappears at time step 36. During this time period the liquid phase is heated. This heating will lead to evaporation of liquid, and mass are transported from the liquid phase to the vapor phase. The evaporation mechanisms are modeled by the utility phases. This mass exchange is illustrated by the mass profiles of the different control volumes in Figure 4.2a. In the way the liquid phase and the vapor phase were initialized at the same temperatures, the mass evaporating from the liquid phase will elevate the temperature in the vapor phase. This is evident from the temperature profiles in 4.1a.

From time step 1-49, external heating was applied only to the liquid phase. In that way no precipitation should be present in the vapor phase, and so no utility phase was needed for the vapor phase at this time. Then the system converged to Topology 2 (V1,, L1,L2,V2) during the first time step.

From Figure 4.1a as well as Figure 4.2a one can observe that the liquid phase are totally evaporated at time step 36. At this point the system is exposed to a topology change. The signal for this trans-

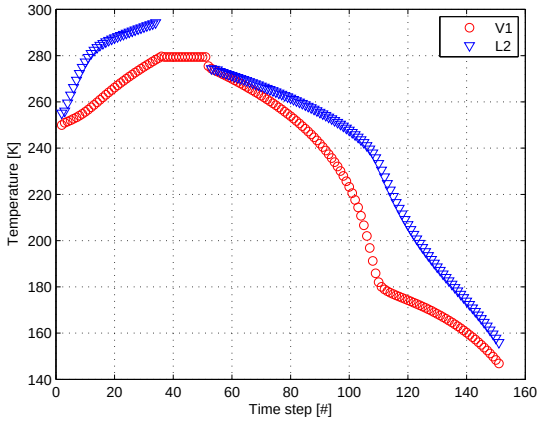


(a) The development of the temperature in CV1 (V1) and CV2 (L2), applied to heat input according to test case 1.

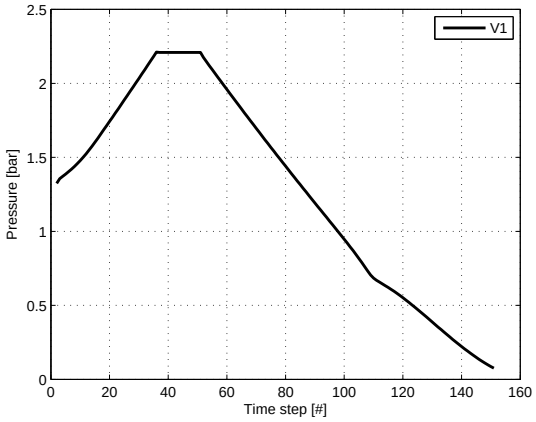


(b) Pressure developement in the system.

Figure 4.1: Temperature ans pressure profiles from Testing Case I.

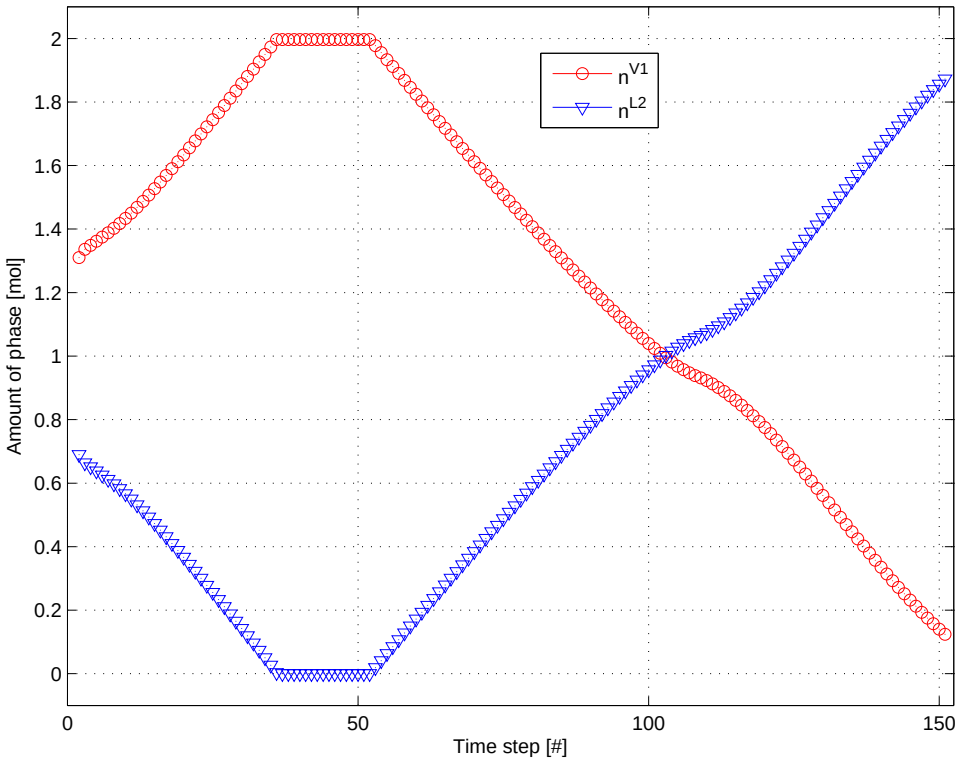


(a) The developement of the mole amount in CV1 applied to test case 1.

| | **Top 1** | **Top 2** | **Top 3** | **Top 4** | **Top 5** | **Top 6** |
|---|---|---|---|---|---|---|
| **Converged to top** | 98 | 35 | 1 | 16 | 0 | 0 |

(b) Distribution of topologies present during the Test Case. Only converged states are considered, which means the sum of the topologies in the table equals the number of time step.

Figure 4.2: Simulation results from Testing Case I.

formation is given by the norm check (see Equation (3.6)). The mechanisms of the topology change

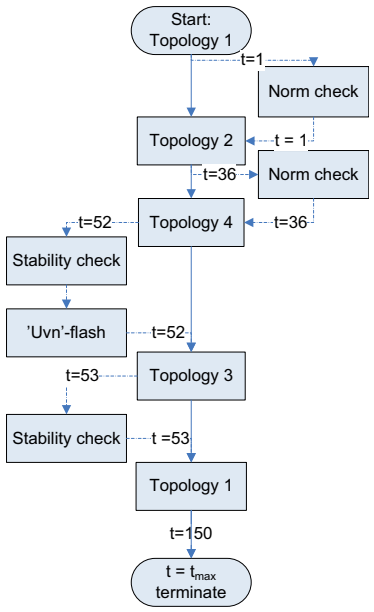


Figure 4.3: The topology track of the model during the simulation

is illustrated in Figure 4.3, which gives the topology track during the test case. At the point where the liquid phase is gone, the temperature in the vapor phase stays at a constant value. This because the system is no longer exposed to the heat that were applied to the liquid phase.

From time step 50 and for the rest of the time period for the test, external cooling is applied to the vapor phase. After a couple of time steps this results in condensation of the vapor phase, and the liquid phase are reintroduced. (This is evident both from the plot of the mass in Figure 4.2, and from the temperature plot in Figure 4.1a.) This topology transition involves both the tangent plane check and the $UVn$-flash. The tangent plane check (3.7) applied to V1 and its virtual phase L1 signals that a liquid phase should be introduced. Then a liquid phase is initialized based on V1 and L1. At this point the reintroduced liquid phase L2 are assumed to be in equilibrium with the vapor phase V1, and the equilibrium state is calculated from a Newton $UVn$-flash. This procedure is outlined in section 3.1.3.

Continued cooling is applied to the vapor phase. This reduces the pressure in the system, and the liquid phase tends to evaporate. Then Topology 1 is applied to the system at time step 53. After this point no further topology transformations is applied to the system. Nevertheless both Figure 4.1a and Figure 4.2a show a break in the curves around time step 110. At this point the pressure $p = 0.68$ bar, and the temperature in V2 is $T^{V2} = 182.0$K, which makes it likely to believe that this breaks are associated with the boiling point for ethane.

Summarized Test Case I indicates that the mechanisms generated to perform initialization and expulsion of phases in a properly manner for a two-component system applied to moderate heat input. Under these condition the topology changes seem to work satisfactory. During the time period spanned by the case, the system converges to four different topologies. Table 4.2b gives the number of time steps the system converged to the different topologies.

### 4.1.2 VessFire Case

In this case the model is applied to actual simulation data from VessFire. The objective of this testing case was to see the behavior of the model when applied to both mass- and heat input. Due to the fact that these data are taken from a real case in the process industry, this test may verify the potential of the model for use in industrial simulations. The results from this simulation follows in this section.

In this case the system was discharged. This is illustrated in Figure 4.4a, where a profile of the development of the total amount in the system is given.

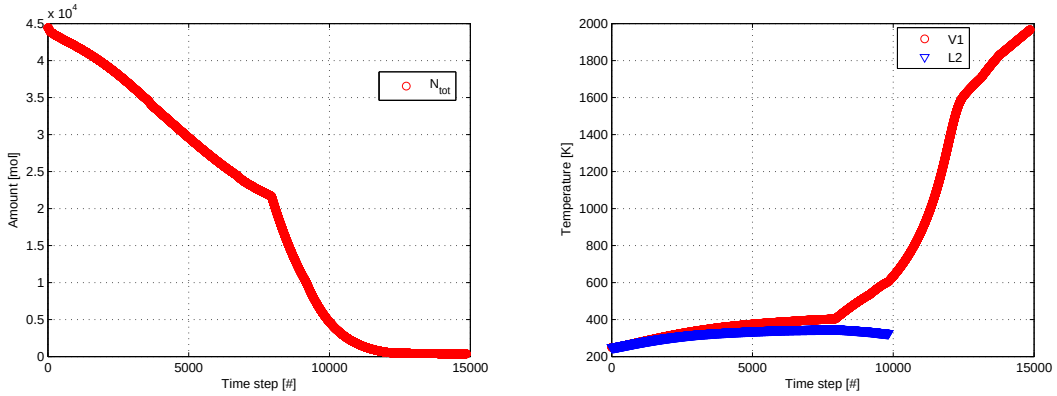


(a) Development of total mole in the system as function of time for the VessFire testing case.

(b) The development of the temperature in CV1 (V1) and CV2 (L2), applied to heat input according to test case 1.

Figure 4.4: Results from the simulation case with initialization values and heat- and mass inputs from VessFire.

The temperature profiles for the different phases are given in Figure 4.4b. From this figure one can observe that the system is exposed to considerable amount of heat, as the temperature in the vapor phase raises to a about 2000 K. Under such conditions the vapor phase will be supercritical as the state is far above the critical point. The liquid phase ceases to exist after 10000 time steps. This is also observable from Figure 4.5, which illustrates the development of the total mole amount in the different phases.

From Figure 4.5 it is observable that the vapor amount are elevated markedly in the beginning, even though the total amount in the system is reduced. This is due to the considerable heat that is applied to the to the liquid phase during the first part of the case (see Figure 3.4). Nevertheless, at a point around 8000 time steps, the discharging rate of the system is elevated, then also the amount of the vapor phase is reduced considerably.

During this case five different topologies are applied to the system. The topology track is available in Table 4.5c. In the very beginning the system alternates between Topology 3 (V1,L1,L2,V2) and Topology 6 (V1,L1,L2,V2). This indicates that at that point, vapor is condensed to the liquid phase. This is also indicated from the very first part of Figure 4.5a. Nevertheless, due to the extreme heating of the system, most of the time the system is applied to Topology 2 (9777 time steps), and turns to Topology 4 (5026 time steps) when the liquid phase is gone. In the way that this system are applied to extremely high temperatures $\approx$ 2000 K, which is far beyond the two-phase area, no physical liquid phase can be found. This means that at some point the virtual liquid phase (L1) must have ceased to be reliable and the trivial solution has been attained. Based on this knowledge the density of the virtual phase L1 was investigated. It was found that the trivial solution was obtained for L1 after 2362 time steps, at this point the temperature in the system equals $T^{V1} = 322$ K. Figure 4.6a illustrates the

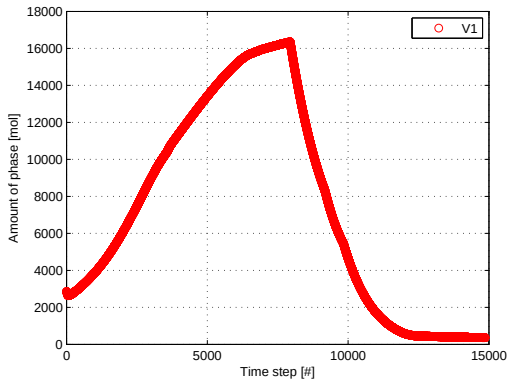


(a) The developement of the mole amount in CV1 applied to test case 1.

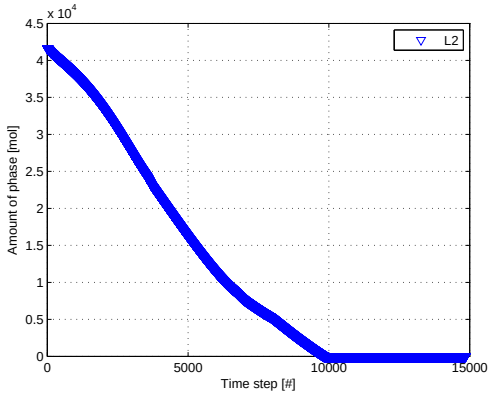


(b) The developement of the mole amount in CV2 applied to test case 1.

| Time step | Topology | Time step | Topology | Time step | Topology |
|---|---|---|---|---|---|
| **1** | Top 3 | **9** | Top 3 | **58-65** | Top 2 |
| **2** | Top 6 | **10** | Top 6 | **66** | Top 6 |
| **3** | Top 3 | **11** | Top 3 | **67-68** | Top 3 |
| **4** | Top 6 | **12** | Top 6 | **69** | Top 1 |
| **5** | Top 3 | **13-31** | Top 3 | **71-** | Top 2 |
| **6** | Top 6 | **32** | Top 1 | **9835** | |
| **7** | Top 3 | **33-38** | Top 2 | **9836-** | Top 4 |
| **8** | Top 6 | **39-57** | Top 1 | **14858** | |

(c) Transition track of topologies present during the VessFire test case. Only converged states are considered.

Figure 4.5: Results from the simulation case with initialization values and heat- and mass inputs from VessFire.

path of the state of the virtual phase L1 in $pV$-isotherm plot as the trivial solution is approached for L1.

The virtual phase is solved for the temperature and the chemical potential as in equilibrium with its main phase. Also the total mol amount is set to be constant. Then the pressure (or volume) is the degree of freedom left. From Figure 4.6a one can observe that at the point where the minimum of a given $pV$-isotherm is reached, the virtual phase will approach the trivial solution whenever the external input to the system continues in the same direction . At this point a liquid volume satisfying the applied constraints will no longer exist.

Nevertheless, for the given case, no problems were associated with the trivial solution of the virtual phase L1. Summarized the results show that the model respond well to external inputs both in mass and heat. During the time period of this case, 7 of the 13 different topology transitions that the model should support, were present (Table 4.8b). Even though, initialization problems had obviously entered into the picture if the system were cooled sufficiently at a point were the trivial solution was attained for L1. To get a better feeling with the shortcomings of the model, a one component system was applied to some extreme conditions.

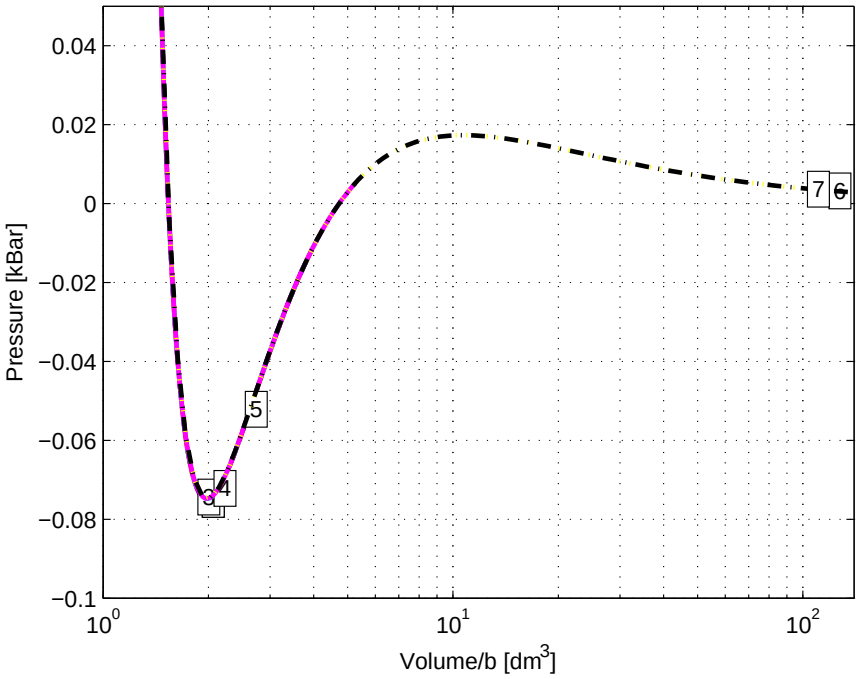


(a) Approaching trivial solution for phase L1. The numbering 1-7 in the figure are relative to the time steps in Table 4.8b, which means that 1 = 2357, 2 = 2358, etc.

| **Time step** | $T^{V1}$ | $\rho^{\mathbf{V1}}$ | $\rho^{L1}$ | $(\frac{\partial \mathbf{p}}{\partial \mathbf{V}})_{\mathbf{T,n}}$ | $(\frac{\partial^2 \mathbf{A}}{\partial \mathbf{N} \partial \mathbf{N}})_{\mathbf{T,V}} > 0$ |
|---|---|---|---|---|---|
| **2357** | 321.9 | 7.46e-010 | 4.458e-008 | -0.43089 | $true$ |
| **2358** | 321.9 | 7.4642e-010 | 4.5929e-008 | -0.95482 | $true$ |
| **2359** | 322.0 | 7.4684e-010 | 4.1198e-008 | 0.39258 | $false$ |
| **2360** | 322.0 | 7.4726e-010 | 3.3284e-008 | 0.84066 | $false$ |
| **2361** | 322.0 | 7.4748e-010 | 6.5775e-010 | -0.00037742 | $true$ |
| **2362** | 322.1 | 7.4789e-010 | 7.4789e-010 | -0.00049298 | $true$ |

(b) Comparing densities for V1 and L1. $\rho_{L1} = \rho_{V1}$ at $t = 2362$. The stability parameters $(\frac{\partial p}{\partial V})_{T,n}$ and $(\frac{\partial^2 A}{\partial N \partial N})_{T,V}$ are given

Figure 4.6: The main experiment.

### 4.1.3 One Component Case

In this case a one component system is tested. This test was constructed to illustrate some shortcomings of the model. Then the aim was to expose the system to conditions that probably would make trouble for the model. The results from the VessFire case showed that the trivial solution was obtained for the virtual phase as the system was heated sufficiently beyond the point where the liquid phase ceased to exist. Nevertheless, as no cooling was applied to the system after this point no problems entered into the picture. Then this case is constructed to illustrate the problems the model would meet under such circumstances. The results are given in the following.

The temperature profile as well as the mol amount in the different phases during the time period for this testing case are given in Figure 4.9.

From Figure 4.9 one can observe that the temperature for both phases is elevated until the liquid phase L2 disappears at time step 80. Nevertheless the heating of the system is continued until the temperature $T \approx 260$, which is relatively far below the critical temperature for the system. Then the

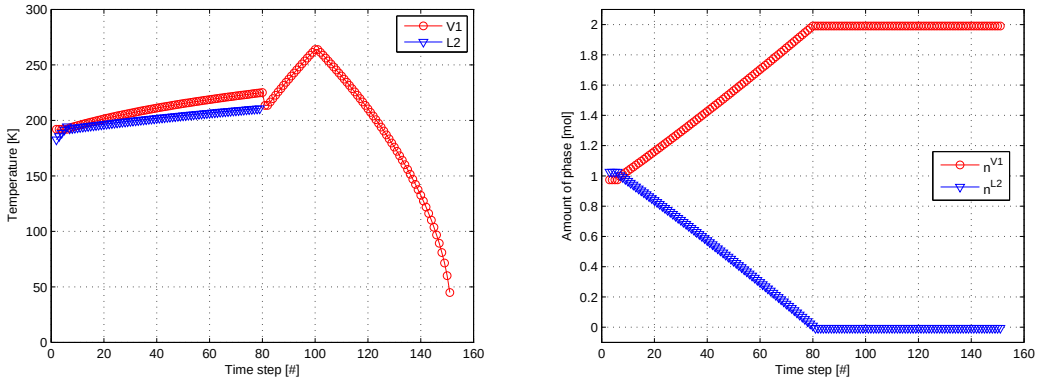


(a) The temperature profile in V1 (CV1) and L2 (CV2) applied to Test Case III.

(b) The developement of the mole amount in CV1 applied to test case III

Figure 4.7: Simulation results from Tesing Case III.

system is cooled until a temperature of $T \approx 260$ is reached. From both Figure 4.7b and Figure 4.7a is is evident that even at this low temperature no liquid phase are modeled to condense from the vapor phase V2.

To investigate why the system did not manage to introduce the liquid phase, the densities of V1 and L1 were compared and the $pV$-isotherm plot was generated. The results from these are given in Figure 4.8. From this figure it is evident that the trivial solution is obtained for the virtual phase L1 during time step $t = 96$.

The second part of the one-component case was to cool a system, initialized as Topology 1, mainly as liquid, but with tiny vapor fraction. The aim was to get rid of the vapor phase and obtain a transition from topology 3 (V1,L1,L2,V2). The results are given in Figure 4.9.

From Table 4.9c one can observe that no topology changes was present in this case. This means that the cooling applied to the vapor phase V1 did not lead to disappearance of this phase, even though its fraction is very low. From the temperature profiles in Figure 4.9 it is evident that the cooling of the vapor phase leads to cooling of the liquid phase to the same extent. As the temperature is reduced, also a pressure drop is present in the system. The system did not manage to converge for the 75 th time step. At this point the conditioning of the Jacobian matrix is very poor. And finally the iteration sequence was interrupted due to a negative volume in the liquid phase L1 in Figure 4.10 illustrates the convergence properties at the time step 74.

### 4.1.4 Summary

All things considered the results from the testing of the model indicated that the model responded well to both mass- and heat inputs. Applied to external heat and mass the model was able to change between the different topologies in a satisfactory manner. From Table 4.1.4 one can observe that there are four transitions that not has been accomplished by these test cases. These transitions are occasions where the vapor phase (CV1) is excluded from the system. Due to the density differences between the gas and the liquid phase, the norm criteria is not susceptible to leave the vapor phase behind unless liquid is added to the system. This is not the case in the testing performed in this work. Nevertheless, since the same mechanisms (see section 3.1.3) apply to both cases, introducing the vapor phase control volume (CV1) should be no harder then the introduction of the liquid phase control volume (CV2).

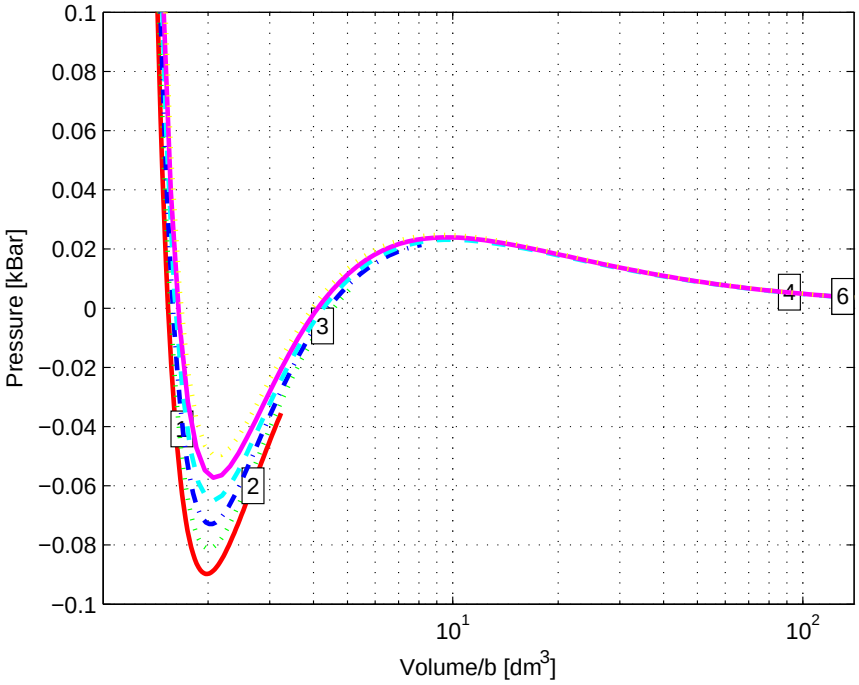


(a) Approaching trivial solution for phase L1. The numbering 1-6 in the figure are relative to the time steps in Table 4.8b, which means that 1 = 92, 2 = 93, etc.

| **Time step** | $T^{V1}$ | $\rho^{\mathbf{V1}}$ | $\rho^{L1}$ | $(\frac{\partial \mathbf{p}}{\partial \mathbf{V}})_{\mathbf{T,n}}$ | $(\frac{\partial^2 \mathbf{A}}{\partial \mathbf{N} \partial \mathbf{N}})_{\mathbf{T,V}}$ |
|---|---|---|---|---|---|
| **92** | 242.7 | 5.9561e-010 | 4.5974e-008 | -9.786 | 0.041864 |
| **93** | 245.5 | 5.9561e-010 | 2.8844e-008 | 1.2065 | -0.013112 |
| **94** | 248.2 | 5.9561e-010 | 1.8252e-008 | 0.4817 | -0.013074 |
| **95** | 250.9 | 5.9561e-010 | 8.4589e-010 | -0.0014025 | 0.017723 |
| **96** | 253.5 | 5.9561e-010 | 5.9561e-010 | -0.00073996 | 0.01886 |
| **97** | 256.1 | 5.9561e-010 | 5.9561e-010 | -0.00074913 | 0.019094 |

(b) Comparing densities for V1 and L1. $\rho_{L1} = \rho_{V1}$ at $t = 2362$. The stability parameters $(\frac{\partial p}{\partial V})_{T,n}$ and $(\frac{\partial^2 A}{\partial N \partial N})_{T,V}$ are given

Figure 4.8: The utility phase L1 approaches the trivial solution.

Nevertheless, the Test Case III revealed that there is a shortcoming with the model whenever the virtual phase for a one-phase system ceases to be reliable. Under such circumstances the initialization mechanisms for this model that are based on the virtual phases can no longer be applied to initialize a phase. Then an external initialization method is needed.

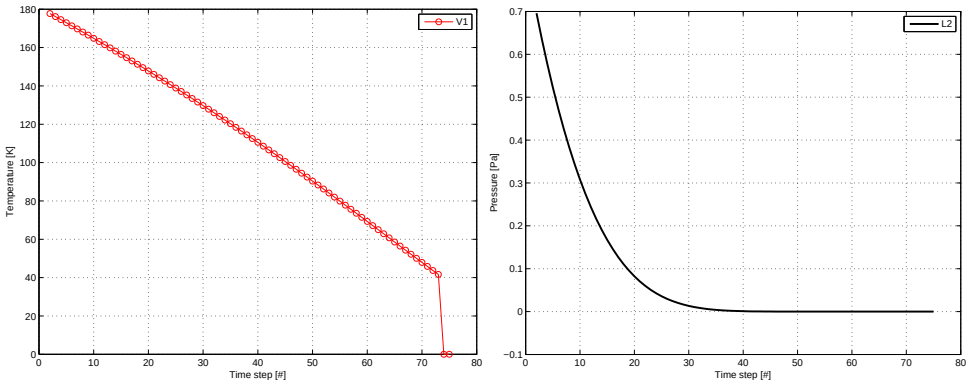


(a) The temperature profile in V1 (CV1) and L2 (CV2) applied to Test Case III, part 2.

(b) The pressure profile in CV2 applied to test case III, part 2.

| | Top 1 | Top 2 | Top 3 | Top 4 | Top 5 | Top 6 |
|---|---|---|---|---|---|---|
| **Converged to top** | 74 | 0 | 0 | 0 | 0 | 0 |

(c) Distribution of topologies present during the Test Case. Only converged states are considered, which means the sum of the topologies in the table equals the number of time step.

Figure 4.9: Simulation results from Tesing Case III, part 2.

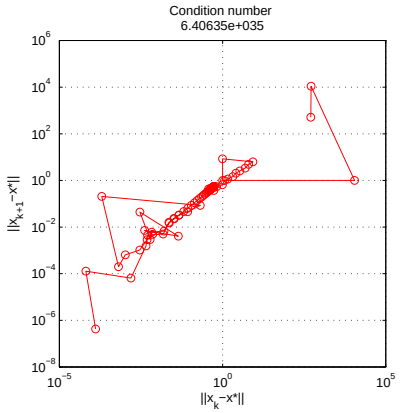


Figure 4.10: Norm norm plot for the error norm of the delta norm of the iteration variables at the 74 time step. This mean that $|\delta x|_2$, where $x = (T, V, n)$ and $x* = \epsilon$, which is the convergence criterion. At this point 140 iterations were needed to obtain convergence.

| $k+1$ \ $k$ | V1 L1 L2 V2 | V1 L1 L2 V2 | V1 L1 L2 V2 | V1 L1 L2 V2 | V1 L1 | L2 V2 |
|---|---|---|---|---|---|---|
| V1 L1 L2 V2 | | VessFire | VessFire TestCaseI | | | |
| V1 L1 L2 V2 | VessFire | | | | | |
| V1 L1 L2 V2 | | | | VessFire | TestCaseI | |
| V1 L1 L2 V2 | | VessFire | VessFire | | | |
| V1 L1 | | VessFire TestCaseI | | | | |
| L2 V2 | | | | | | |

## 4.2 Preparing the states for PSO

The testing of an initialization routine for a vapor—liquid phase equilibrium system, requires feasible one-phase states for the system to start the searches. To be able to perform a systematic and efficient test regime, also some knowledge about the properties of the system is needed. In this connection it is of considerable importance to obtain a knowledge about the stability conditions for the system. To obtain this information the starting point should be a pair of thermodynamic variables.

$Tp$, $Hp$, $Sp$ and $UV$ constitute standard approaches in chemical processes, and applies for initialization, irreversible stationary-, reversible stationary- and dynamic energy balances. $pV$ represents the quantity that can be deduced directly from an the equation of state. To be able to calculate on these constraints it is necessary to converge the system in these coordinates. Then an element to obtain knowledge about is the ease of the convergence for each of these grids.

In this work a starting point was to generate plots in the different variables $Tp$, $Hp$, $UV$ and $pV$ and mark each point due to the stability properties of the current state.

To obtain a deeper understanding of the energy surfaces, the calculations scheme for the stability plots were started from other starting points as well. Nevertheless, all points in a single grid was initialized from the same state. The objective was to see whether the same states were obtained. Table 4.1 gives an overview of relative placement of these starting points in the grid.

Table 4.1: Different starting points used to converge the physical space. Calculations performed in this work are shaded. The dark shaded cells denote the main foci this work.

| | $Tp$ | $Hp$ | $UV$ | $pV$ |
|---|---|---|---|---|
| **C** | | | | |
| **LL** | | | | |
| **UL** | | | | |
| **UR** | | | | |
| **LR** | | | | |

The main focus of this work was on the schemes initialized from the center point, which represent a point in the two-phase area.

The resulting states were categorized into 5 different categories, according to stability conditions and convergence. This is outlined in Section 3.3.2. Figure 4.11 illustrates resulting plots for the center starting state. The different coordinates in the figure are set to span the same physical area. For all points in a single grid, all points were initialized from the same starting state.

From Figure 4.11 it is evident that whenever the mechanical stability criterion, $(\frac{\partial^2 A}{\partial V \partial V})_{T,\mathbf{n}}$ is violated, the diffusive stability criterion, $(\frac{\partial^2 A}{\partial N \partial N})_{T,V}$, are broken as well. This is in accordance with fundamental theory (Radzyminski and Whiting, 1987). Furthermore the figure indicates that the propagation of the unstable points, as well as the convergence properties, differs between the different frameworks.

For the $pV$- and $Tp$-coordinates, sub-figure 4.11c and sub-figure 4.11d reveal the calculations resulted in a large fraction of unstable points. For most of these points, both the mechanical stability constraint $(\frac{\partial^2 A}{\partial V \partial V})_{T,\mathbf{n}} > 0$ and the diffusive stability constraint $(\frac{\partial^2 A}{\partial N \partial N})_{T,\mathbf{n}}$ were violated. Nevertheless, none of the points in the $pV$-framework failed to converge.

On the other hand, sub-figure 4.11b illustrates that a large fraction of the points in the $UV$-plot did not converge for these coordinates. For the non convergent points in the $UV$-grid, the temperature became very low, regardless of strictness of the constraint on the temperature step.

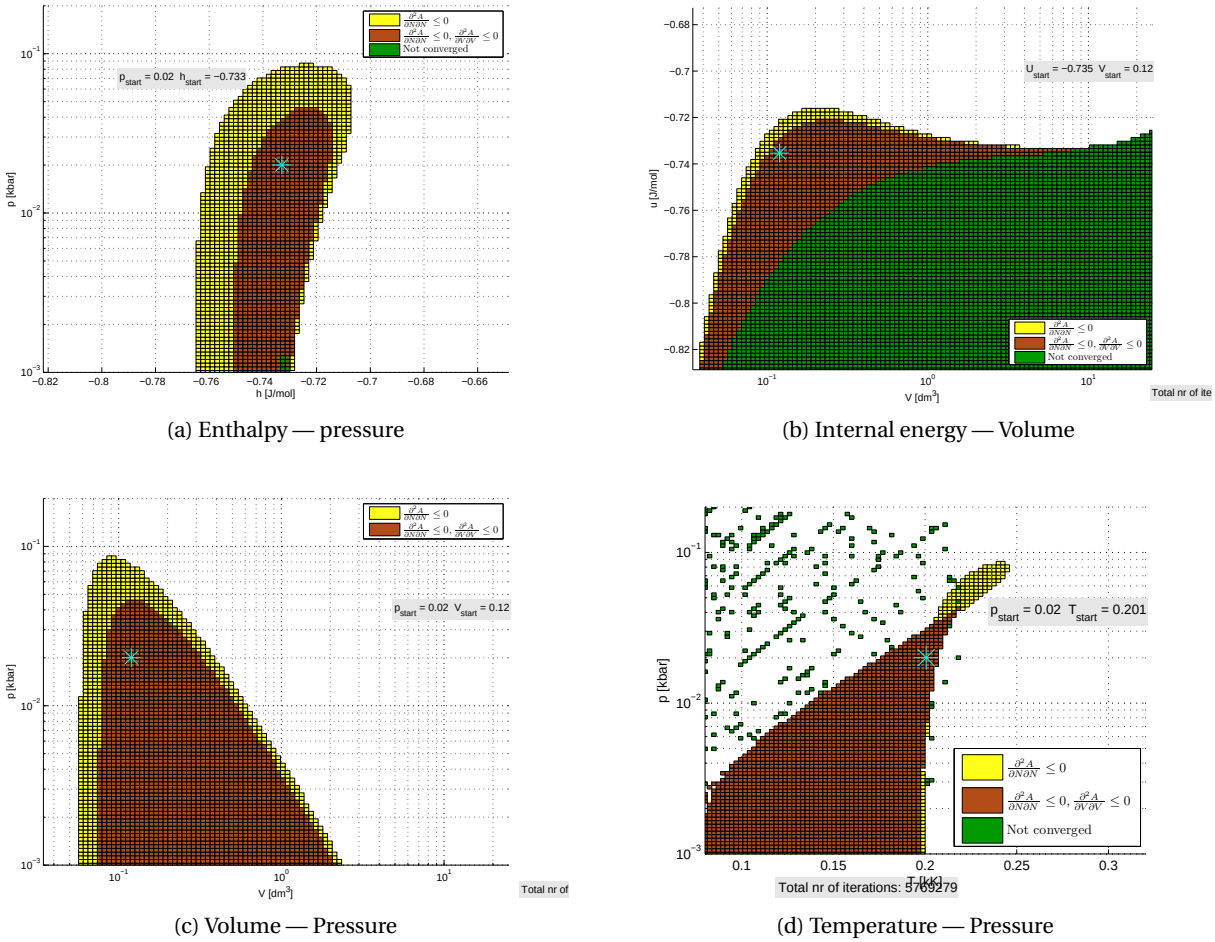


(a) Enthalpy — pressure

(b) Internal energy — Volume

(c) Volume — Pressure

(d) Temperature — Pressure

Figure 4.11: Stability plot in different coordinates for $N_2, CH_4, C_2, C_3$. The uncolored areas in the figure represents the locations where the calculations converged to physical stable points in the one-phase area. All grid are initialized from exactly the same state in the two-phase area..

An observation from Figure 4.11 is that the $Tp$-calculations fail to converge for some seemingly random points in the diagram. In any case, these points spread, and a non convergent point are surrounded by convergent points. This is not the case for the plot in any of the other coordinates. This was an interesting point owing to the fact that $Tp$ represents the most used approach in teaching of chemical engineering. On the other hand, the convergence properties in the $Hp$-scheme seems to be good. Also the $Hp$-scheme seem to find stable states at a larger area compared to $Tp$. Then an interesting point was to investigate why the $Hp$-framework seem to behave so well, whilst the $Tp$-framework did not. In the rest of this work, the focus is directed to $Hp$- and $Tp$-coordinates.

### 4.2.1 The Step Functions

To solve the iteration problem the Newton-Raphson method was used. This method is outlined in section 2.3.2. Then, to improve the understanding of the mechanism that influence the iteration sequence, the step function (Jacobian inverse) was expressed in terms of thermodynamical variables. The equation for the step in the iteration variables T,V becomes as shown in 4.1 below:

$$\delta \begin{pmatrix} T \\ V \end{pmatrix} = \left( J^{xy}_{T,V} \right)^{-1} \begin{pmatrix} x_{spec} - x \\ y_{spec} - y \end{pmatrix} \tag{4.1}$$

As the iteration sequence approaches the solution, the search direction will stabilize. From equation (4.1), it is evident that when the inverse of the Jacobian changes sign, the search direction will change by somewhere around 180 degrees. When such situation apply two subsequent search will be in opposite directions, which in most cases will not be advantageous for approaching the solution.

Applied to $Hp$ the expression in (4.1) become as expressed by (4.2).

$$\delta\begin{pmatrix}T\\V\end{pmatrix} = \frac{1}{det(J^{Hp}_{T,V})}\begin{pmatrix}(\frac{\partial p}{\partial V})_{T,n} & -T(\frac{\partial p}{\partial T})_{V,n} - V(\frac{\partial p}{\partial V})_{T,n}\\ -(\frac{\partial p}{\partial T})_{V,n} & C_V + V(\frac{\partial p}{\partial V})_{T,n}\end{pmatrix}\begin{pmatrix}h_{spec}-h\\p_{spec}-p\end{pmatrix} \tag{4.2}$$

In these equations the following are true for the thermodynamical variables,

$$\left(\frac{\partial p}{\partial T}\right)_{V,n} > 0 \quad \left(\frac{\partial p}{\partial V}\right) < 0 \quad \vee \quad \left(\frac{\partial p}{\partial V}\right) > 0$$

Intuitively also $T > 0$ and $V > 0$ for a physical valid state.

From Equation (4.2) it is evident that as the sign of the determinant is changed, the search direction will change as well. From the expression of the determinant in equation 4.2 one can deduce that the determinant will be negative if the following inequality is true:

$$\left(T(\frac{\partial p}{\partial T})_{V,n} + V(\frac{\partial p}{\partial V})\right)_{T,n}\left(\frac{\partial p}{\partial T}\right)_{V,n} > \left(C_V + V(\frac{\partial p}{\partial V})_{T,n}\right)\left(\frac{\partial p}{\partial V}\right)_{T,n} \tag{4.3}$$

Intuitively the inequality in equation 4.3 has the potential to fail for to obvious evidents. If the temperature turns very low in the physical area, such that $T(\frac{\partial p}{\partial T})_{V,n} < V(\frac{\partial p}{\partial V})$. Another occurrence is when $(\frac{\partial p}{\partial V})$ turns positive in the unphysical area where. This leads to a positive left side of equation 4.3. Further on, in the physical area, the proportions between $T(\frac{\partial p}{\partial T})$ and $V(\frac{\partial p}{\partial V})$, and between $C_V$ and $V(\frac{\partial p}{\partial V})$, as well as the ratio $\frac{\partial p}{\partial V}$ to $\frac{\partial p}{\partial T}$ decide on the sign of the determinant.

Equation (4.4)- (4.5) gives the corresponding expression in $Tp$-coordinates.

$$\delta\begin{pmatrix}T\\V\end{pmatrix} = \left(\frac{\partial p}{\partial V}\right)_{T,\mathbf{n}}\begin{pmatrix}(\frac{\partial p}{\partial V})_{T,n} & 0\\ -(\frac{\partial p}{\partial T})_{V,n} & 1\end{pmatrix}\begin{pmatrix}T_{spec}-T\\p_{spec}-p\end{pmatrix} \tag{4.4}$$

After some iterations the temperature will be set, then $T_{spec} - T = 0$ and a simpler expression will be valid for the equation for Newton direction:

$$\delta\begin{pmatrix}T\\V\end{pmatrix} = \left(\frac{\partial p}{\partial V}\right)^{-1}_{T,n}\begin{pmatrix}0\\p_{spec}-p\end{pmatrix} \tag{4.5}$$

From equation (4.5) it is evident that the only variable that decides on the direction of the step is $(\frac{\partial p}{\partial V})_{T,n}$, as well as which side of the specified pressure the given pressure of the system is. The next subsection gives an evaluation of the iteration sequences for some of the points in the stability plots in $Tp$-coordinates shown in Figure 4.16.

In the next sections an iteration sequence from the $Tp$-calculations are compared with a corresponding iteration sequence calculated in $Hp$-coordinates.

### 4.2.2 Comparison between Hp and Tp

As a starting point for the investigation of the $Hp$– and $Tp$-calculation schemes, a single point in each of the grids were chosen to calculate on. The feature of these point was that both $Hp$- and $Tp$-coordinates had the same pressure specification, and they ended up at the same temperature. The starting point for the calculation was also the same in both cases. Nevertheless, an important difference, and the objective of investigation, was that the iteration sequences ended up at two different volumes, representing a stable and an unstable state for $Hp$ and $Tp$ respectively. Hence a target was to have a closer look at the path of each of these sequences.

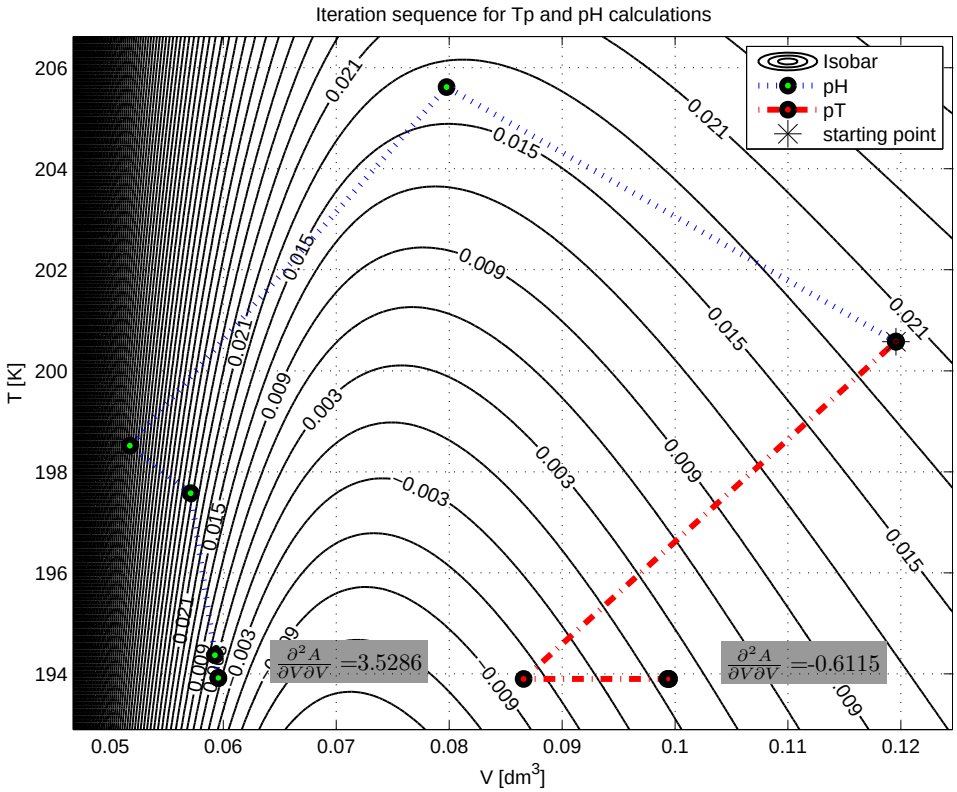


Figure 4.12: Comparision of the iteration paths for Hp and Tp calculations aiming for the same pressure

From sub-figure 4.12 one can observe how the $Tp$ – iteration- and the $Hp$ – iteration sequences, starting from the same starting point, aiming for the same pressure and converging to the same temperature, follows different paths. The sequence for the $Tp$ – iteration converges to the target temperature during the first iteration, then the iteration sequence follows this isotherm until a volume solution that corresponds to the target pressure is reached. For this particular case the solution volumes turns out to correspond to an unphysical state. Figure 4.13a on page 58 illustrates the development of the placement of the iteration sequence relative to the isotherms in a pV plot. From this figure it is evident that iteration sequence converges to an unphysical point where $(\frac{\partial p}{\partial V})_{T,\mathbf{n}} > 0$.

Unlike the $Tp$-sequence, the Hp-iteration has no specifications on the temperature. In fact, for the Hp calculation none of the model variables $T, V, n$, have specifications. Then this iteration scheme has more degrees of freedom. For finding a stable state in this particular case this seemed to be an advantage.

During the first iteration, the system has an almost isobaric compression, and the temperature raises.

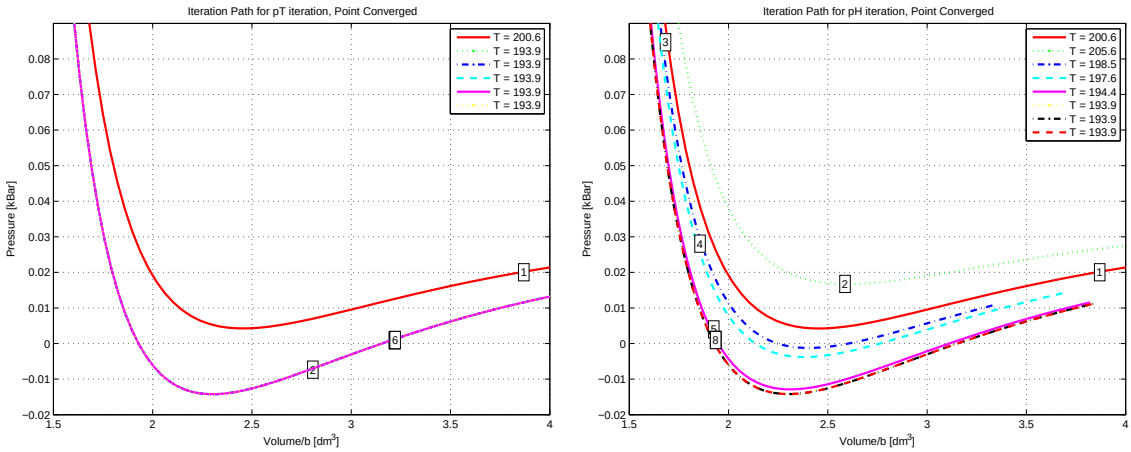


(a) Tp iteration to unstable state.

(b) Hp iteration to stable state.

Figure 4.13: Iteration path for Hp iteration sequence. The starting point was $V_{start}$ = 0.12 dm$^3$, $T_{start}$ = 200.6 K, and the pressure spesification was $p_{spec}$ = 1 bar.

This stands in opposition to the corresponding $Tp$-path. A feature of the $Hp$-path in that in Figure 4.12 is however that the path to some extent seem to follow the isobars.

Figure 4.13 on page 58 pictures the movement of the iteration sequence on several isotherms in a $pV$ – plot. From this figure one can observe that the $Hp$-sequence converges to a volume at the liquid side of the $pV$—isotherm. For the same temperature and pressure the $Tp$ – iteration converged to an unphysical solution.

### Euler integration of the Newton Step

The discovery presented in the former section, revealed that the $Hp$-calculations manage to find a path that allowed the sequence to get past the unstable region, while the correlating calculations for $Tp$ ended up in the unstable area. One reasonable cause of this occurrence could be the length of the Newton step. To investigate whether this could be the case, an effort was done to integrate the Newton direction (with $\delta T = 0.01$). If the foregoing theory was true, the sequence was susceptive to meet problems as the step became sufficiently small. Figure 4.14 compares the iteration path for the integrated sequence, to the original sequence.

From Figure 4.14 it becomes evident that the integrated Newton direction path, ends up at the same solution as the original sequence. Unlike the non integrated sequence, the pressure do not raise during the iteration. The starting point for these iterations are in the unstable area.

The results from the integration of the Newton direction indicate that the integration continues to be in the unstable area, goes into the stable area and continues to find a stable liquid solution. From Figure 4.14 one can observe that the integrated sequence finds a solution that are nearly identical to the solution found by the original sequence.

An investigation of the development of the determinant as the iteration proceed, reveals that the determinant stays positive during the whole iteration. This indicate that the search direction do not turn, or do sudden direction changes. This is also evident from Figure 4.14, the sequence path have a steady curvature. During its journey aiming for the solution, the iteration sequence continues from the starting point in the unstable area, crosses the the minimum of the $pV$ – isotherm, and converges to a stable liquid state.

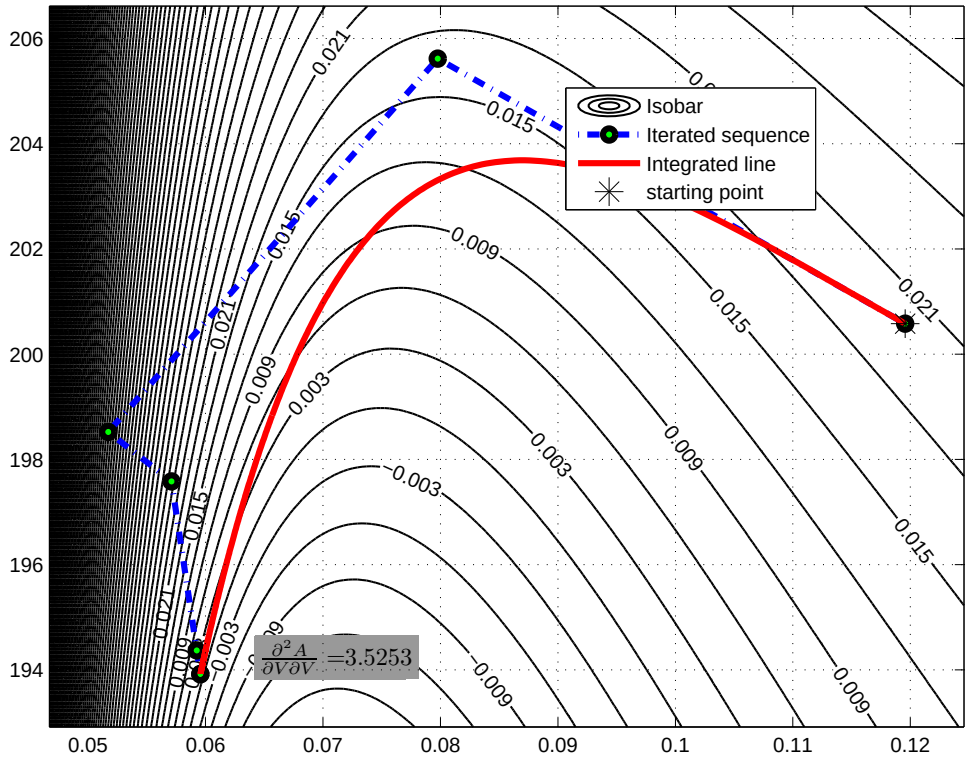


Figure 4.14: Iteration paths for Hp iteration sequence. The original iteration path, compared with the Euler integration. Convergence to a physical state.

Integration of the Newton direction was also performed for the $Tp$–sequence. The result are present in Figure 4.15.

From Figure 4.15 it is evident that the integration line ends up at the same point as the iterated sequence. A main difference for the integrated line compared to the iterated sequence is that for the former, the temperature specification is not reached before the solution point. This mean that the line do not follow the isotherm. Nevertheless, the resulting state are the same. Both paths stays in the the unstable area during the calculations.

An observation from Figure 4.14 is that the integrated line to a larger extent follows the isobar compared to the iterated $Hp$-sequence. This might indicate that if the calculations are initialized at specified pressure, the iterations will follow the isobar during its journey to obtain the solution. To do a further consideration of this feature, the step function in Equation (4.2) can be investigated:

As the specified pressure is reached, the Equation (4.2) obtain the following form:

$$\delta \begin{pmatrix} T \\ V \end{pmatrix} = \frac{1}{det(J^{Hp}_{T,V})} \begin{pmatrix} (\frac{\partial p}{\partial V})_{T,\mathbf{n}}(h_{spec}-h) \\ -(\frac{\partial p}{\partial T})_{V,\mathbf{n}}(h_{spec}-h) \end{pmatrix} \tag{4.6}$$

This implies that $\delta T$ and $\delta V$ are proportional to $(\frac{\partial p}{\partial V})_{T,\mathbf{n}}$ and $(\frac{\partial p}{\partial T})_{V,\mathbf{n}}$ respectively:

$$\delta T \propto \left(\frac{\partial p}{\partial V}\right)_{T,\mathbf{n}} \quad \delta V \propto \left(\frac{\partial p}{\partial T}\right)_{V,\mathbf{n}} \tag{4.7}$$

The pressure $p$ is a function of $T, V$, a preturbation in $\delta p$ in pressure can be expressed as follows:

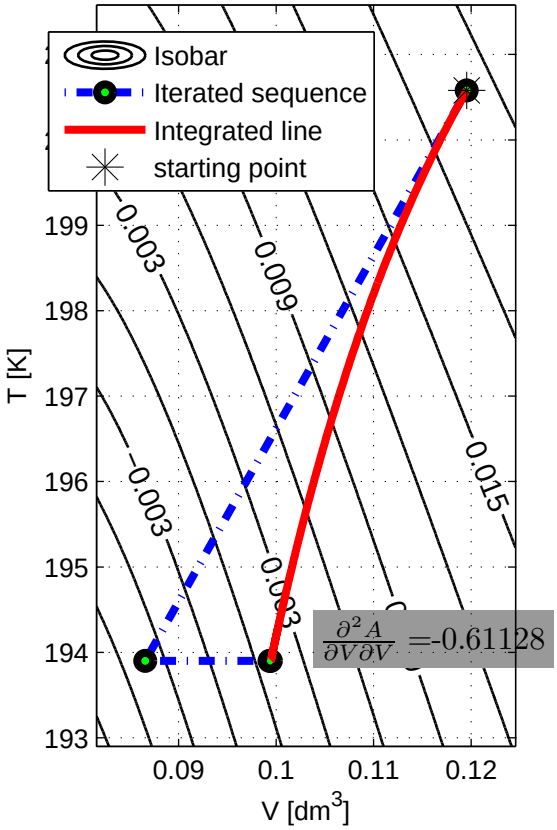


Figure 4.15: Iteration paths for $Tp$ – iteration sequence. The original iteration path, compared with the integrated path. Convergens to a physical state.

$$\delta p(T,V)_{\mathbf{n}} = \left(\frac{\partial p}{\partial T}\right)_{V,\mathbf{n}} \delta T + \left(\frac{\partial p}{\partial V}\right)_{T,\mathbf{n}} \delta V \tag{4.8}$$

Then (4.7) can be inserted to (4.8) and the following expression is obtained for the alteration in the pressure:

$$\delta p = -\delta V \delta T + \delta T \delta V = 0 \tag{4.9}$$

Equation (4.9) shows that as the iteration sequence reaches the specified pressure, the asymptotic behavior is that the search direction follows the isobar.

Then for this specific test case the $Tp$-sequence converged to an unstable solution by following the isotherm. The $Hp$-sequence converged to a stable solution by tending to follow the isobars. Then an interesting point would be to find out whether the same pattern would be present starting the calculation from other starting states as well. To get a feeling of this, $Tp$- as well as the the $Hp$-scheme was calculated from other starting points. The results from this part is given in the following sections.

### 4.2.3 Calculation with other Starting Points

The former section revealed that searching a state with specified $T, p$, an iteration sequence in $Tp$-variables converged to a volume in the unstable area, whilst a $Hp$-sequence, aiming for the same

pressure converged to a stable state. Based on the knowledge of the $pV$–isotherm (see Figure 2.3), it is known that the for given $T$ and $p$, three different volume will exist, as long as the physical conditions are below the critical. Under the circumstances given in the case above, the $Tp$ sequence obviously found the solution in the unphysical part of the given isotherm. Based on the knowledge of the curvature of the $pV$–isotherm, an interesting point would be to see whether the situation would change, when changing the starting point for the calculations. As a starting point for this investigation, the $Tp$-grid from sub-figure 4.11a in Figure 4.11, was generated starting from 4 other states in the grid. Table 4.1 outlines the relative placements of these starting points in the grid.

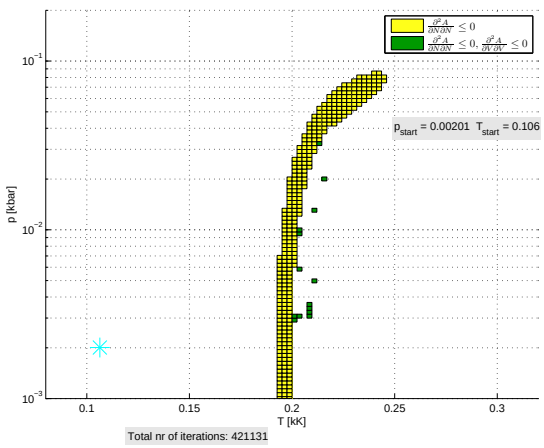


(a) Start point located at the lower left of the figure.

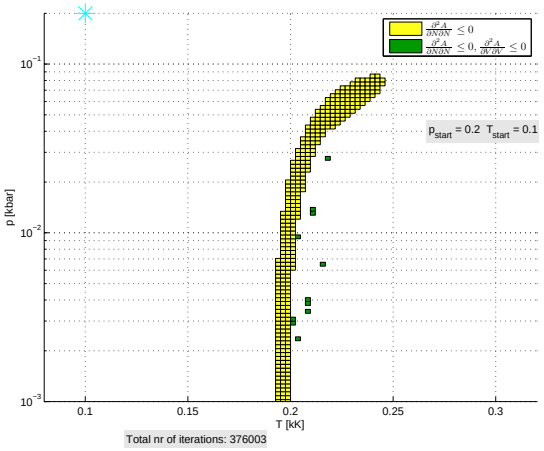


(b) Start point located at the upper left.

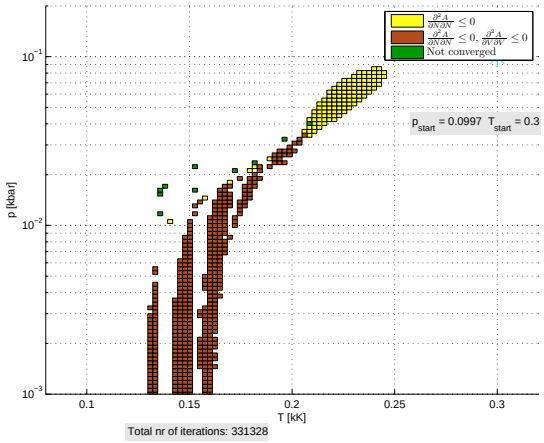


(c) Start point locates upper right in the figure.

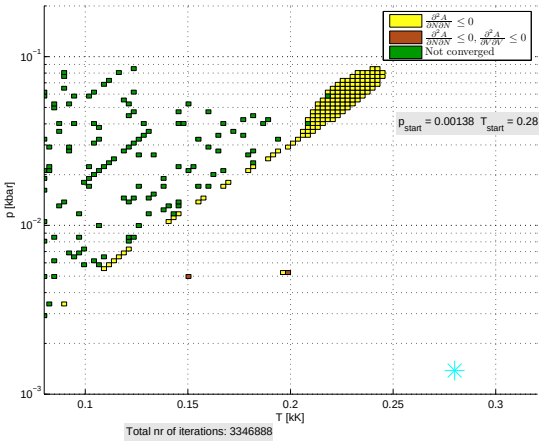


(d) Start point 5. Located lower right in the figure.

Figure 4.16: Stability plot in Temperature—Pressure coordinates for $N_2, CH_4, C_2, C_3$. The uncolored areas in the figure represents the locations where the calculations converged to physical stable points in the one-phase area.

From Figure 4.16 at page 61 one can observe that the stability properties for a given point in the grid, to a great extend depends on the starting point used for the calculation. When the calculations are started at low temperature, most of the points converges to stable states. This is evident from sub-figure 4.16a and sub-figure 4.16b. None of the points in these figures converges to states where the mechanical stability criterion is broken. Nevertheless some of the points converged to states where the diffusive stability condition, $(\frac{\partial^2 A}{\partial N \partial N})_{T,V}$, did not hold. Worth noting is that for these grid, only a small fraction of the points do not converge, and they are all located relatively close to the unstable area.

For the last starting point a larger fraction of the points do not converge. These points are relatively spread and distributed in locations to the upper left in the figure. For this starting point also some points are present where both stability conditions are violated.

The resulting volumes from the calculations of the different grids reveals that for the locations in the grid, that in sub-figure 4.11d converged to unstable states, converges to different volumes, dependent on whether the calculations were initialized as liquid states or vapor states. To investigate on this behavior the iteration sequences are plotted at their $pV$—isotherms. This is illustrated in Figure 4.17. The temperature- and pressure specifications are equivalent for all points, which means they represent the same point in the $Tp$–grid.

Sub-figure 4.17b illustrates an iteration sequence that is initialized from the center point in Table 4.1. In the same way as the iteration sequence that was compared with a $Hp$-sequence, this sequence converges to an unstable point. On the other hand, the sequences in sub-figure 4.17b and sub-figure 4.17c, which both are initiated at the liquid side of the isotherm, converge to a stable liquid volume. Sub-figure 4.17d in Figure 4.17 pictures the iteration sequence for the calculations initialized at a temperature beyond the critical temperature. Also this iteration sequence converge to a stable state at the liquid side.

The last iteration sequence is also initialized as a supercritical fluid (beyond the critical point). Compared to the previous case, this starting point has a larger volume. Hence it corresponds to a state to the right of the maximum of the $pV$—isotherm, and the iteration sequence converges to a point in the vapor side of the isotherm.

Summarized, the results in Figure 4.16 and Figure 4.17 illustrates that the resulting volumes, as well as the stability conditions become quite different depending on the state the calculations are initialized from. The volumes from the calculated states in Figure 4.16 also reveals that whenever the calculations are initialized in the two phase area, an unstable state is found, as long as such a state is available at the specified pressure. Correspondingly, if the calculations are started from the vapor side, the calculations converge to stable vapor volume, and likewise to liquid volumes if a liquid the initial state is a liquid.

To see if a similar pattern applies to the $Hp$-coordinates, the 4 new $Hp$-grid was calculated, each scheme differs from the other scheme by the starting point for the calculations. The different schemes were initialized from the same states as for the $Tp$–grids shown in Figure 4.16. The calculated $Hp$-grids are shown in 4.18 at page 4.18.

Figure 4.18 reveals that the locations where the iteration sequence converged to unstable points, are the same independent of the starting point used. This is in contrast to the corresponding $Tp$-calculations. Also the resulting volumes calculated in a specific location in the grid were identical in each grid whenever the calculations converged.

For the starting point given in sub-figure 4.18d, there exist an area where the iteration sequences did not converge. Nevertheless, the unstable area seems to be similar also in this plot. This particular starting point are located at low pressure and high enthalpy, which corresponds to a large vapor volume. The area where the calculations did not converge belongs to the liquid area. This means that the volume differences between these to points are large, and so the starting values for the Newton iteration is not satisfactory to calculate these points.

Nevertheless, when a stricter constraint was set on the temperature step from one iteration to the other the plot became equal to rest of the $Hp$-plot. However this increased the number of iterations needed, which made the equation scheme slower. Therefore, the criterion for the maximum temperature step was set to $\delta T = 0.15$, which resulted in a non convergent area when the calculations was started lower right in the $Hp$–grid.

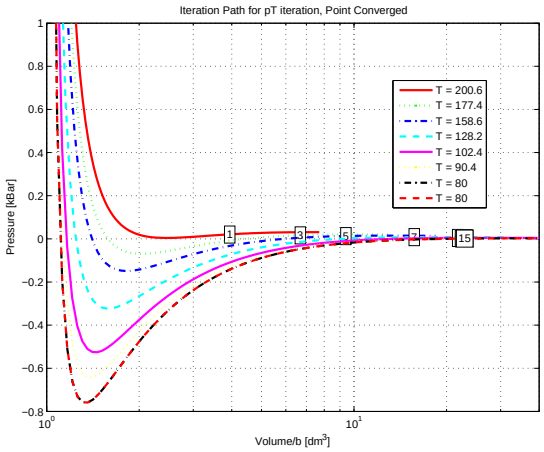


(a) Starting point marked with a blue star in the middle of the figure.

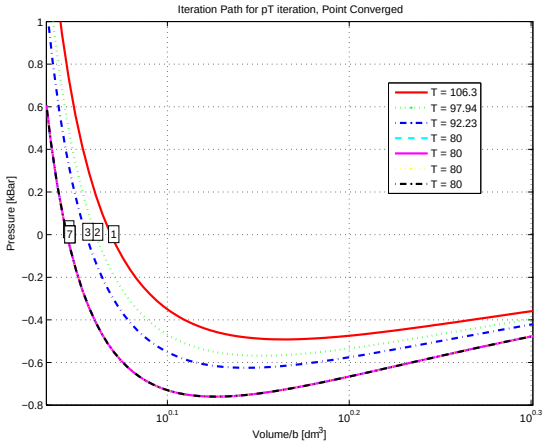


(b) Start point located at the lower left of the figure.

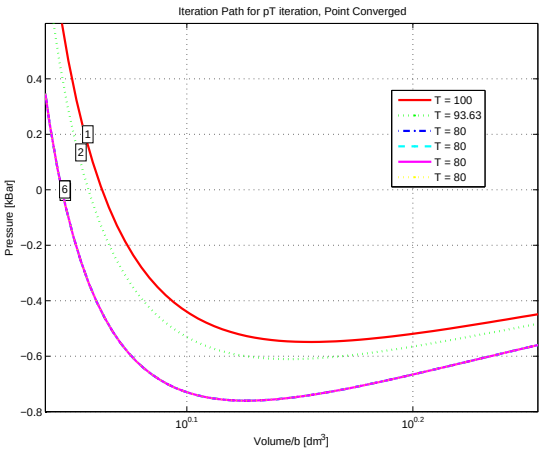


(c) Start point located at the upper left.

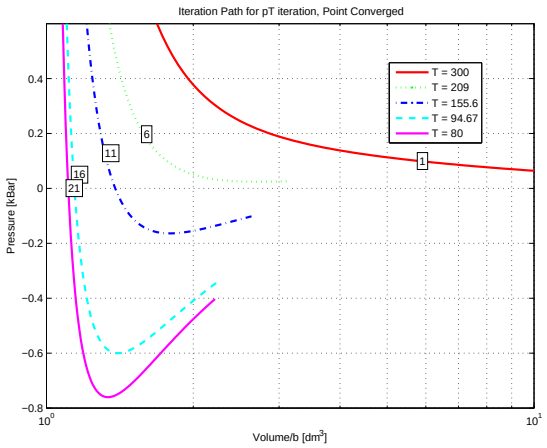


(d) Start point locates upper right in the figure.

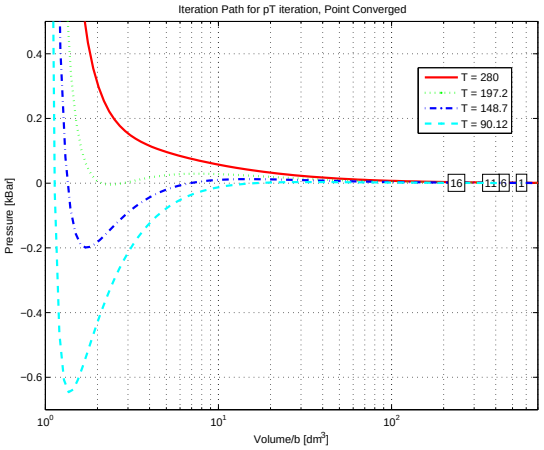


(e) Start point located lower right in the figure.

Figure 4.17: Developement of the placement at the pV-isotherm as the iteration sequence proceed for the different starting points. Trying to converge the point $p_{spec} = 0.001$bar, $T_{spec} = 80$K

The same trick could not be applied to get rid of the non convergent point in the $Tp$-framework. Nevertheless, to detect why some random points upper left in the $Tp$-grid, when initialized from the two-phase area, did not converge, an analysis of one such point was performed. This is outlined in

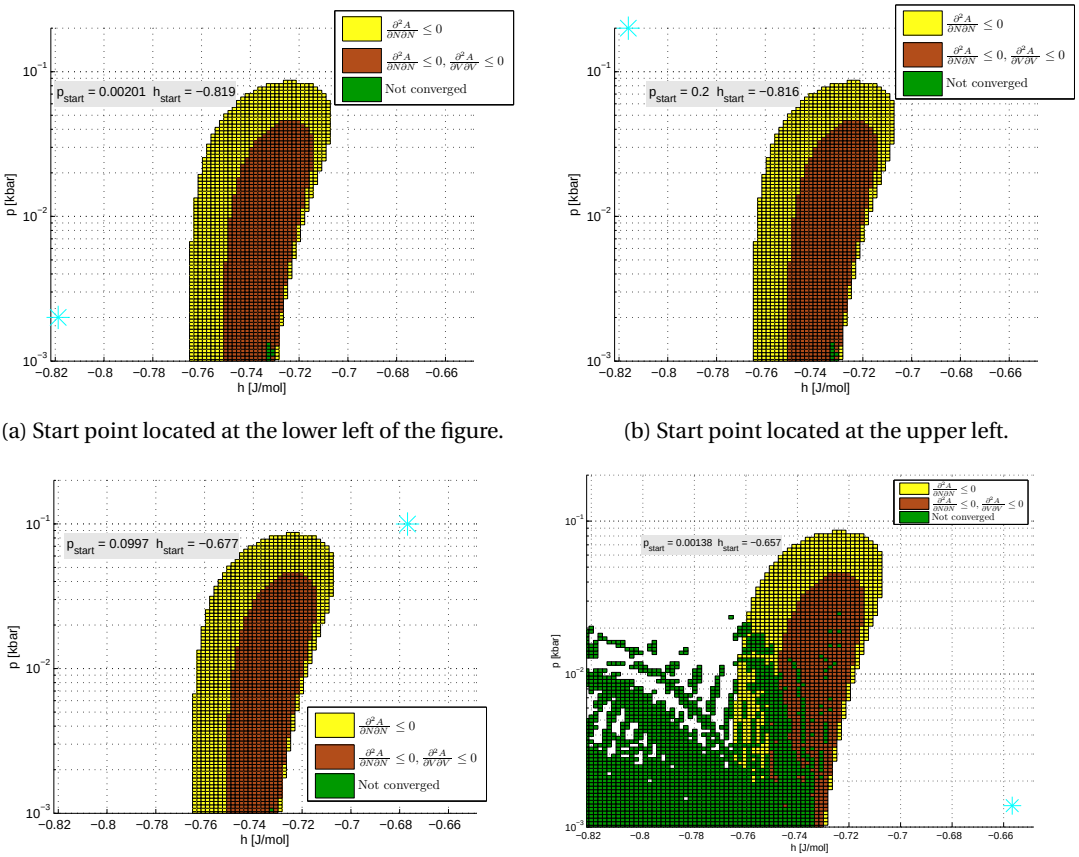


(a) Start point located at the lower left of the figure.

(b) Start point located at the upper left.

(c) Start point locates upper right in the figure.

(d) Start point located lower right in the figure.

Figure 4.18: Stability plot in Enthalpy—Pressure coordinates for $N_2, CH_4, C_2, C_3$. The uncolored areas in the figure represents the locations where the calculations converged to physical stable points in the one-phase area.

the next section.

### 4.2.4 Investigation of a non convergent Tp-points

Figure 4.16 demonstrate that the locations where the calculations did not converge, are quite unordered. Some points that did not converge are surrounded by points that did converge. This is evident from all the sub-figures in Figure 4.16 at page 61. In this section the iteration sequence for a non convergent point are evaluated and compared to a convergent neighboor point.

From equation (4.5) it is evident that the only variables that decide on the direction is $(\frac{\partial p}{\partial V})_{T,n}$, as well as the sign of $p_{spec} - p$. As long as the specified temperature is below the critical temperature for the mixture, there will be three solutions for a given volume, one at the liquid side, one at the gas side, and one in the unphysical area. From the knowledge of curvature(path/slope) of the $pV$—isotherm illustrated in section 2.1.2, it is known that in a single isotherm there are two locations where the sign of the quantity $(\frac{\partial p}{\partial V})_{T,n}$ will change. These locations are at the bottom and at top of the isotherm. Based on this one should believe that convergence problems should enter into the picture if the iteration sequence get stuck into either of these locations.

Figure 4.19 shows two different kind of occasions where the iteration sequence do not converge.

From Figure 4.19 one can observe that the iteration sequence in sub-figure 4.19a fails to pass the

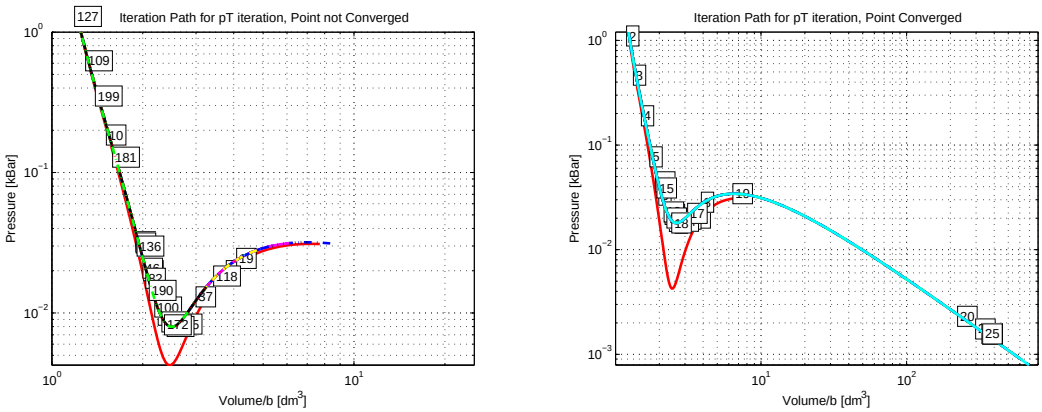


(a) Non convergent seq, every 19'th iteration is shown. (b) Convergent sequence, every iteration is displayed.

Figure 4.19: Developement of the placement at the pV-isotherm as the iteration proceed. $p_{spec} = 0.001$(both) $T_{spec} = 202$(left) $T_{spec} = 206$(right). The starting point is the same for both sequences.

maximum point of the $pV$–isotherm, whilst the sequence in sub-sequence 4.19b manage to find a gas volume. A closer look at the sequences reveals that as the curvature of the $pV$–isotherm changes direction, the direction of the step changes by nearly 180 degrees.

Examining sub-figure 4.19a it is evident that as long as the slope the $pV$–isotherm is in the same direction for to subsequent points, the sequence proceed in the same direction along the isotherm. As the sequence approaches the bottom point, the step becomes smaller, and two subsequent iteration points becomes closer. This is also evident from Table 4.2, where some key values from the last iterations in each of the sequences are given.

From the sub-figure 4.19b one can observe that at the nineteen'th iteration the sequence settles just to the right of the maximum of the $pV$—isotherm. Hence the sign of $(\frac{\partial p}{\partial V})_{T,n}$ did not change from the previous iteration point. Then the search direction did not turn by 180 degrees, but continued to be in the same quadrant. In this case the search direction continues in direction of a larger volume. After 25 iterations the sequence has converged to a volume at the gas side of the isotherm.

The data for the thermodynamic variables in Table 4.2 enforce the given interpretation of the iteration sequences in Figure 4.19. The results from this table indicate that $(\frac{\partial p}{\partial V})_{T,n}$, which for the $Tp$-calculations is the determinant, reaches a smaller value before it crosses the minimum of the isotherm, for the convergent sequence than for the sequence that did not converge. This difference seems to be the margin that makes one of the sequences to find a point just to the right of the maximum of the isotherm, and then continue to find a gas volume, whilst the other sequence finds a point just to the left of the maximum, which leads the sequence to a liquid volume. As long as there do not exist a volume for the given pressure at the liquid side of the isotherm, the sequence will never be able to find a solution if it do not manage to cross the maximum.

Table 4.2: Comparision of some key values from the 10 last iteration of one convergent and one non convergent iteration sequence for the Tp calculations. $p_{spec}$ = 0.001 for both sequences. $T_{spec}$ = 202(non convergent) $T_{spec}$ = 206(convergent)

| **Convergent sequence** | | | | | | | |
|---|---|---|---|---|---|---|---|
| **Iter** | $\det \mathbf{J}^{\mathbf{Tp}}_{\mathbf{T,V}}$ | $\|\|J_{Tp}^{-1}\|\|$ | $(\frac{\partial p}{\partial V})_{T,n}$ | $(\frac{\partial p}{\partial T})_{V,n}$ | $\|\|\delta \begin{pmatrix} T \\ V \end{pmatrix}\|\|$ | $T_{spec} - T$ | $p_{spec} - p$ |
| **14** | -3.51 | 1.47 | -3.51 | 4.56 | 0.923 | 0 | -0.0373 |
| **15** | -0.655 | 4.62 | -0.655 | 4.56 | 0.171 | 0 | -0.0185 |
| **16** | 0.293 | 6.62 | 0.293 | 4.56 | 0.388 | 0 | -0.0207 |
| **17** | -0.128 | 20.7 | -0.128 | 4.56 | 0.697 | 0 | -0.0164 |
| **18** | -0.00465 | 251 | -0.00465 | 4.56 | 1.63 | 0 | -0.0327 |
| **19** | -0.000312 | 3.21e+003 | -0.000312 | 4.56 | 34 | 0 | -0.000745 |
| **20** | -0.000178 | 5.61e+003 | -0.000178 | 4.56 | 0.33 | 0 | -0.000181 |
| **21** | -0.000146 | 6.83e+003 | -0.000146 | 4.56 | 0.106 | 0 | -1.7e-005 |
| **22** | -0.000143 | 6.98e+003 | -0.000143 | 4.56 | 0.0109 | 0 | -1.81e-007 |
| **23** | -0.000143 | 6.98e+003 | -0.000143 | 4.56 | 0.000118 | 0 | -2.1e-011 |
| **24** | -0.000143 | 6.98e+003 | -0.000143 | 4.56 | 1.36e-008 | 0 | -4.34e-019 |
| **Not Convergent sequence** | | | | | | | |
| **Iter** | $\det \mathbf{J}^{\mathbf{Tp}}_{\mathbf{T,V}}$ | $\|\|J_{Tp}^{-1}\|\|$ | $(\frac{\partial p}{\partial V})_{T,n}$ | $(\frac{\partial p}{\partial T})_{V,n}$ | $\|\|\delta \begin{pmatrix} T \\ V \end{pmatrix}\|\|$ | $T_{spec} - T$ | $p_{spec} - p$ |
| **190** | -0.197 | 14.5 | -0.197 | 2.68 | 0.125 | 0 | -0.00664 |
| **191** | 0.36 | 5.05 | 0.36 | 1.49 | 0.45 | 0 | -0.0167 |
| **192** | -3.18 | 1.57 | -3.18 | 3.76 | 0.428 | 0 | -0.0231 |
| **193** | -0.925 | 3.61 | -0.925 | 3.06 | 0.117 | 0 | -0.0095 |
| **194** | 0.123 | 21.3 | 0.123 | 2.42 | 0.148 | 0 | -0.00655 |
| **195** | -2.92 | 1.64 | -2.92 | 3.69 | 0.67 | 0 | -0.0214 |
| **196** | -0.813 | 4.02 | -0.813 | 3.02 | 0.117 | 0 | -0.00895 |
| **197** | 0.183 | 14 | 0.183 | 2.35 | 0.158 | 0 | -0.00676 |
| **198** | -60.9 | 1.01 | -60.9 | 8.33 | 0.456 | 0 | -0.349 |
| **199** | -21.2 | 1.04 | -21.2 | 6 | 0.13 | 0 | -0.138 |
| **200** | -7.6 | 1.17 | -7.6 | 4.56 | 0.13 | 0 | -0.0522 |

## 4.3 Testing PSO-implentation

The implementation of the local dynamic multi swarm PSO version was tested for the four component system, $N_2$, $CH_4$, $C_2H_6$, $C_3H_8$. The test regime was performed based on calculated one-phase states for the physical area of the system. From these calculations the unstable one-phase area became evident. As a reference for the locations of the two-phase area, a phase envelope generated by SINTEF was used.

Based on this background information, testing of the algorithm was applied to the metastable area of the one-phase calculation scheme. The results from this testing is given in Figure 4.20- 4.21 and Table 4.3.

From Figure 4.20 one can observe that the initialization routine was able to detect negative tangent plane values at locations close to the phase envelope. This was true both when the search was executed from a liquid phase, searching for a vapor phase, and when the objective was to find a liquid phase. Nevertheless, the liquid phases introduced to the vapor phases did not manage to converge applied to the $UVn$-flash.

A well known outcome of a search after a new phase to be introduced in a system are the obtainment of the trivial solution. In that way an important aspect of the evaluation of the results is to detect whether the trivial solution is obtained. In Table 4.3 densities for the two phases in the obtained two-

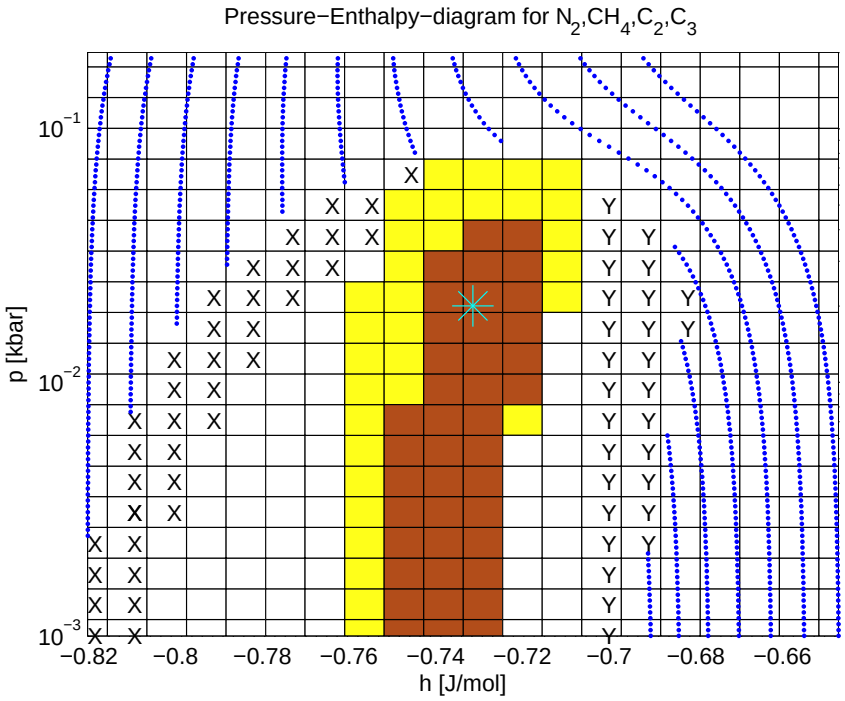


Figure 4.20: Results from tesing of DMS-PSO applied to phase equilibrium calculations of the a 4-component system. $X$ denotes the locations where a stable two phase equilibrium where obtained. $Y$ denotes locations where the tangent plane where negative, both phases stable, but $UVn$-flash failed to converge.

Table 4.3: Some resulting densities from the optimization. The densities, $\rho^{\beta}$, are for the new phases. Note that the trivial solution is not obtained.

| **Searching liquid phase** | | **Searching vapor phase** | |
|---|---|---|---|
| $\rho^{\beta}$ | $\rho^{\alpha}$ | $\rho^{\beta}$ | $\rho^{\alpha}$ |
| 6.4102e-008 | 1.9943e-010 | 7.179e-010 | 6.4738e-008 |
| 6.2786e-008 | 2.5829e-010 | 1.7741e-009 | 6.2068e-008 |
| 6.299e-008 | 3.4118e-010 | 7.5453e-010 | 6.4622e-008 |
| 6.2775e-008 | 3.4118e-010 | 1.8862e-009 | 6.1837e-008 |

phase systems. The trivial solution do not seem to be obtained for any of these cases. The densities are compared for the rest of the states where a negative tangent plane distance where present in appendix B.

The movements of the PSO-particles are influenced by its own best position as well as the best obtained position for the entire swarm. Dependent on the surface of the energy surface, the movement of the best position for the swarm might bubble around before it approaches the minima. Figure 4.21 illustrates the trajectory for the second point from the left at the lowest pressure in Figure 4.20. This point is also given in the second row, third column in Table 4.3.

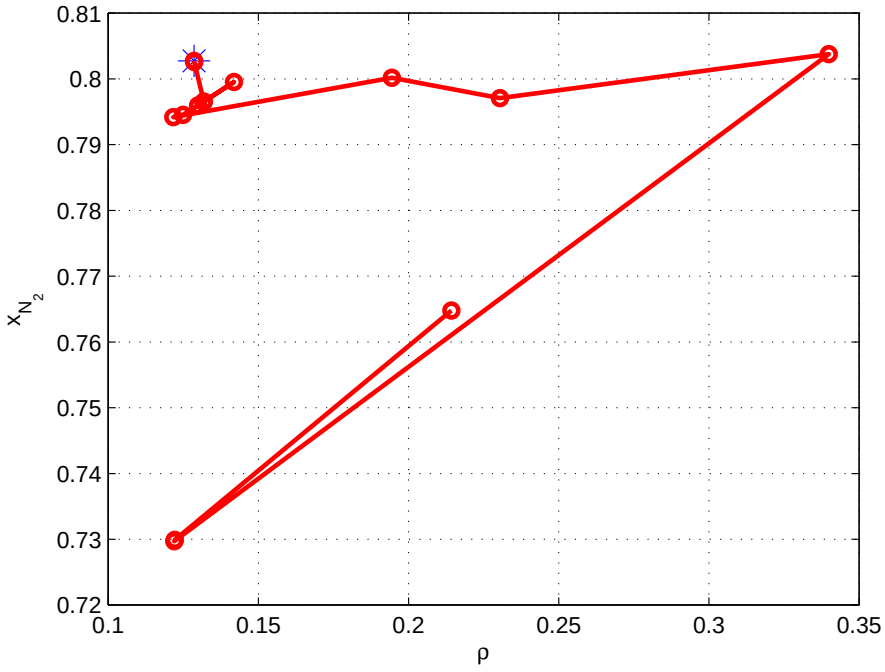


Figure 4.21: The movement of the best position for the swarm might bubble around before it approaches the minima

# Chapter 5

# Discussion

## 5.1 The VessFire Model

The objective of testing the VessFire model was to examine its performance when applied to variable heat- and mass input. The aim was to verify that the mechanisms for taking in, and leaving out phases function satisfactory. Detecting possible shortcomings of the model was also an important perspective of the testing regime. Due to the fact that the initialization routines in this model was based on relative quantities within the system, at some point an expected shortcomings would be related to initialization of phases.

The results from the two component case and VessFire case demonstrate that the model respond well to the heat- and mass inputs applied to the system in these cases. For all time steps in these cases the system converge to the expected topologies in a relatively small number (5-10) of iterations.

The norm criterion for vanishing phases are formulated in a way such that phases are excluded from the system based on their extensive quantities entropy, volume and moles. If the normed value of these quantities, relative to the size of the system, is below a defined small number, the phase should be excluded from the calculations. As a vaporizing or condensing phase becomes very small in a multicomponent mixture, at one point some of the components will become absent from that phase, which leads to an infinite chemical potential, at this point the Jacobian matrix will be singular (Trangenstein, 1987). The purpose of the norm criterion is to eliminate phases that otherwise would introduce singularities to the Jacobian matrix. In the way the model manage to converge the system for all time steps within a few iterations (5-10) for these test cases, the norm criterion seemed to perform well in this cases.

In the one component case, the vapor phase did not vanish from the system, even though extensive cooling was applied to it. A reason for this was probably that the pressure was reduced concurrently with the temperature. Then, also the boiling point is reduced. As a result, both evaporation and condensation are present in the system at all time steps. To achieve transition to the one-phase liquid topology, mass must be added to the system, in order to keep the pressure up. Nevertheless, because of the big differences in density between liquid and vapor, the vapor phase will expand to large volumes, even though its mass is small relative to the liquid phase. Then, unless mass is added to the system, the vapor phase is not expected to be excluded. In the present case where the system is cooled with no mass added, and an unphysical low temperature (40 K) is obtained for the system, the Jacobian matrix is badly conditioned and the iteration sequence start to wiggle around without making progress. Finally, the step size in the solver obtains a too small value, and the iteration sequence is interrupted. The step size is shortened to avoid a negative volume for the liquid phase L1, which

represent the condense from V1.

The initialization routines applied to the model were tested both in the two component case and in the VessFire case. In the two component case both the initialization of a new main phase, and the initialization of a utility phase were achieved. In the VessFire Case only initialization of utility phases was needed.

Independent of whether a main phase or a utility phase are to be formed in the system, the signal to initialize a phase are given by the tangent plane check (2.6). A negative value of this check, proves that the energy in the system would be reduced by adding a new phase to the system (Michael L. Michelsen, 2004). Then the initialization of the new phase is based on the virtual phase and one of the main phases. The initialization routines are somewhat different dependent on whether a main phase or a utility phase should be included, this is described in section 3.1.3. Owing to the fact that no problems were present for the model as these initialization routines were applied to it, the initialization both for introducing a new main phase and a utility phase proved to perform well in these cases.

Nevertheless, as the system, both in the VessFire Case and in the one-component case, were heated sufficiently beyond the point where the liquid phase can exist, a trivial solution was obtained for the virtual liquid phase. This means that the state found by the virtual phase, is exactly the same state as the state of the main phase. At the point where the critical point is reached for the system, only one minima will exist on the energy surface, and the trivial solution is the only solution (Callen, 1985). Nevertheless the trivial solution is obtained for L1 before the critical temperature is reached. This can be observed from Figure 2.4a. For a virtual phase the chemical potential as well as the temperature are constricted to be equal its main phase.

$$\mu^{\alpha_1} = \mu^{\alpha_2} \quad T^{\alpha_1} = T^{\alpha_2}$$

and the pressure is a function of these:

$$p = p(T, \mu)$$

As the temperature is raised further away from the two-phase area the constraints for $T$ and $\mu$ are fulfilled by reducing the pressure in the virtual phase. At the point where it is no longer possible to find a physical liquid solution for a given isotherm, the virtual phase enters the unstable area of the $pV$-isotherm and then of the energy surface, to satisfy the given constraints. At this point the results from the tangent plane check will no longer be reliable.

The trivial solution for L1 was obtained both for the VessFire case and for the one-component case. For the VessFire case this fact caused no problems. This is due to the fact that the system was not cooled after the trivial solution was obtained for the virtual phase L1. Nevertheless, in the one-component case, cooling was applied to the system after the trivial solution was obtained for L1. As illustrated in Figure 4.9 no liquid phase was formed even though the system is exposed to extensive cooling. Partly, this behavior can be explained due to the fact that the pressure is reduced with the temperature. Then the dew point for the vapor is reduced. Nevertheless, the fact that the trivial solution is obtained for the virtual phase, means that the virtual phase are the very same phase as its vapor phase. Then there is no way that the tangent plane check will be negative, in fact it will always be equal to zero, since the pressure and the chemical potential will not differ within the same phase.

Then as the virtual phase converges to the trivial solution, the stability check done by the tangent plane check has no meaning anymore. The initialization routines applied to the model also base their values on the virtual phases, and when these phases are no longer reliable, global initialization

routines have to be performed. Global initialization routines are also needed to initialize the virtual phases whenever the starting point for the calculations are in the one-phase area. To develop routines that overcome these shortcomings of the model was the focus of the second half of this master work.

## 5.2 Preparing the states for PSO

The objective of this part of the work was to generate one-phase states to be used in the Dynamic Multi Swarm—Particle Swarm Optimization (DMS-PSO) routine (Liang and Suganthan, 2005). This was done by converging one-phase calculations in $Hp$, $UV$, $Tp$, and $pV$-coordinates. $Tp$, $Hp$, $Sp$ and $UV$ constitute standard approaches in the chemical processes industry, and applies for initialization, irreversible stationary-, reversible stationary- and dynamic energy balances. $pV$ represents the quantity that can be deduced directly from the equation of state. To be able to calculate these constraints it is necessary to converge the system in these coordinates. Even though convergence of the grid in one coordinate would have been sufficient to create starting states for the testing of DMS-PSO, converged grid for multiple variable pairs were generated. This was done to obtain knowledge about the convergence properties of each grid.

The main aim of this part of the work was to generate feasible states for the initialization routine, a secondary goal was to investigate which coordinates that would be most appropriate to converge the states for. Owing to the fact that $Hp$, $Tp$, $UV$ and $pV$ are different thermodynamic variables, it is not expected that the all have the same convergence properties.

The resulting (stability) plots for the different coordinate pairs, demonstrates that the fraction of the unstable points, as well as the convergence properties, differs between the different frameworks. For instance a lot of points in the $UV$–grid did not converge. For these points, the iteration sequences approach a temperature near 0 K, even with constraints on the temperature step down to $\delta T_{max} = 1e-5$. This might indicate that the state is not physically defined for these locations in the grid. A reason for this is that the range for the axes in the different grid were based on the maximum and minimum values for the different variables obtained from the calculations of the $Hp$-diagram.

This means that the grid in the $Hp$-coordinates constitute the rectangular grid. The other grids are then mapped from the rectangular $Hp$-grid into their own coordinates. The physical defined domain in the transformed plot might not be rectangular. Then it might be the case that not all coordinates within a grid other then $Hp$ should be defined due to the physics. This might be the case for the $UV$-grid. Here the calculations resulted in a large fraction of points that did not converge. To get an answer to this, the corner point in the diagram could have been calculated, then it could have been possible to make it clear whether these points represent physical locations.

Another feature of the stability properties of the plots where that the mechanical stability constraint, $(\frac{\partial^2 A}{\partial V \partial V})_{T,\mathbf{n}}$, never was violated unless the diffusive stability constraint, $(\frac{\partial^2 A}{\partial N \partial N})_{T,V}$, was violated as well. This is in accordance with theory (Radzyminski and Whiting, 1987).

Owing to the fact that $Tp$-calculations represents the most used approach in teaching of chemical engineering, an interesting point was that the $Tp$-calculations seem to overestimate the unstable domain in the grid. A wide range of points converged to unstable points where both the mechanical-, and the diffusive stability condition were violated. Also the calculations in this grid failed to converge for some seemingly random points in the diagram.

It was found that for a $Hp$- and a $Tp$-sequence that with the same pressure specification that started from the same starting point, and ended at the same temperature, the $Hp$-calculations converged to a stable state, whilst the iteration sequence for $Tp$ ended up at an unstable point. An investigation of these sequences revealed that whilst the $Tp$–sequence went directly to the specified isotherm, the

$Hp$–sequence tend to follow the isobars. In this way the $Hp$–sequence manages to find a stable or metastable liquid point, whilst the $Tp$-sequence end up at a unstable location. In the way $T, V, \mathbf{n}$ represent the variables to be set in the in the model used to serve the calculations with thermodynamic variables, a $Hp$-framework will have one more degree of freedom than a corresponding framework in $Tp$. The current results indicates that, in some situation, this can be an advantage. Nevertheless, it is hard to tell whether the $Hp$-sequence illustrated in the presented example converged to a stable- or metastable state.

The results discussed above were obtained when the calculations were initialized in the two-phase domain. When the very same $Tp$-grid was generated starting from various points in the one-phase area, the resulting stability plot became very different. For three of the four additional starting points tested, the whole grid, apart from a small fraction of points in the middle of the grid converged to stable states. Nevertheless, the calculated volumes for the converged states revealed that these became very different dependent on whether the initialization was from the liquid side or the gas side. An interesting aspect was that the very same locations in the grid that, according to the first starting point was categorized as unstable, converged to liquid points when initialized from a liquid volume, and to a gas state when initialized from a gas volume.

These results indicate that the calculations initialized on the liquid side converge to liquid states as long as a liquid volume exist for the given pressure along the particular $pV$–isotherm. Correspondingly, the calculations initialized in the two-phase area converge to unstable points along the $pV$–isotherm as long as the pressure are between $p_R$ and $p_B$ in Figure 5.1, which shows the metastable areas as discussed in section 2.1. The inflection point of this curve, $p_D$, denotes the border between stability and metastability on the vapor side. Points on the isotherm above this pressure are metastable. Correspondingly, at the liquid side, points below this pressure, $p_D$, is metastable. It is evident from the curve of the $pV$-isotherm that for these metastable locations the mechanical stability condition will not be broken for these cases. The results from this work shows that the iteration sequence converges to the closest of the three alternative solutions. The resulting states will differ according to this.

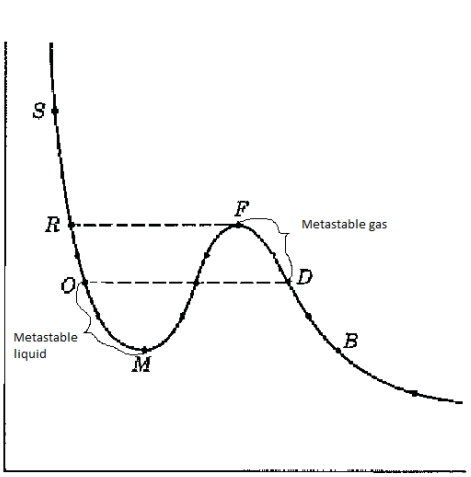


Figure 5.1: The general $pV$–isotherms for a cubic equation, marked for metastable locations.

Whilst the results from the $Tp$-calculation was very dependent on the state they were initialized from, the pH-diagram converged to exactly the same states for each point in the grid, regardless of choice of starting point. Then a likely conclusion is that the $S(h, p, n)$-surface is without folders.

Another feature with the $Tp$-diagram initialized in the two phase area, was that the calculations failed to converge for some seemingly random points in the diagram. An investigation was done of two points in this domain, one non convergent point and a convergent neighbor point. The objective of this investigation was to detect the reason behind this phenomena. The result illustrates that the sequence that did not converge, got stuck in the curvature of the $pV$-isotherm. As the iteration sequence proceed, both sequences approaches the minimum of the $pV$–isotherm. The difference between the two sequences is that for the convergent sequence, the variable, $(\frac{\partial p}{\partial V})_{T,n}$, which for the $Tp$-calculations is the determinant, reaches a smaller value before it crosses the minimum of the

isotherm. This difference seems to be the margin that makes one of the sequences to find a point just to the right of the maximum of the isotherm, and then continue to find a gas volume, whilst the other sequence finds a point just to the left of the maximum, which leads the sequence to a liquid volume. As long as there do not exist a volume for the given pressure at the liquid side of the isotherm, the sequence will never be able to find a solution if it do not manage to cross the maximum.

Nevertheless, the main objective of this part of the work was to investigate the convergence properties and stability properties of the different grids, and to obtain feasible states for the initialization routine. According to this, some information was obtained from the $Hp$– as well as the $Tp$-grid.

The results from $Tp$ demonstrated that when the calculations are initialized sufficiently far away from the two-phase area, most of the points in the $Tp$-grid will converge to stable- and metastable states. For an initialization routine that needs a feasible one-phase state as a starting point, this will be an advantage. On the other hand, that the $Tp$-grid converges to stable states over most of the physical domain, means that many of this states are metastable. Whether a state is unstable can easily be revealed by checking the mechanical- and diffusive stability criterion, $(\frac{\partial^2 A}{\partial V \partial V})_{T,\mathbf{n}} > 0$ and $(\frac{\partial^2 A}{\partial N \partial N})_{T,V} > 0$. The distinction between metastable and stable mixtures is more difficult in the way the mentioned stability criterion not will be reflected for these cases (Stateva and Tsvetkov, 1991). Then to check whether a state is unstable require a global search.

In the way a global search is demanding, it would be preferable that a particular point was unstable whenever the state belonged to the two-phase area. Nevertheless, the case for the $Tp$–calculations, when initialized in the two-phase area, are that they converge to unstable states, also at locations where stable states exist. This will introduce unnecessary problems for the reliability of the calculation.

On the other hand the $Hp$-scheme gave unique defined states for every points in the diagram, then the locations in the grid that should belong to the stable one-phase area, are denoted as stable in all cases. This is a benefit in the way no initialization efforts are needed for a stable phase (or system). Nevertheless, the $Hp$-calculation converged to a stable state for a point that converged to an unstable point for the $Tp$, then the $Hp$–sequence has converged to a stable or a metastable point. If the point in question is metastable, the point should belong to the two-phase area. This condition is more easily detected by the $Tp$-sequence that converged to an unstable state, owing to the fact that the stability checks is more easily performed in the unstable area.

Nevertheless, the results for the $Tp$–calculations showed that $Tp$ (initialized from two-phase) finds unstable points as long as such points are present along a given isotherm, then the same path would be present whether the $Hp$-point is stable or metastable. When the point found by the $Hp$–sequence really are stable, this solution is preferable compared to the unstable solution found by the $Tp$–sequence. This is because no initialization efforts are needed for a stable phase (or system).

## 5.3 PSO

In this work the local and dynamic PSO version, Dynamic Multi Swarm PSO (DMS-PSO), developed by Liang and Suganthan (2005), was implemented and tested for the four component system, $N_2$, $CH_4$, $C_2$, $C_3$. The starting point for the testing was a rectangular enthalpy—pressure diagram, where each state were converged for one-phase. In this way one-phase states were available, and testing could be performed. A $Hp$–envelope generated by SINTEF was used as a reference for where the stable one-phase should be present.

The results from the testing revealed that the implemented routine was able to obtain a negative tangent plane distance at locations near the phase envelope. This was true both on the vapor- and the liq-

uid side of the unstable area. A negative tangent plane distance denotes that the system would reduce its energy by introducing the trial phase that is found by the search mechanism (Michelsen, 1982). All trial phases that were found to give a negative tangent plane distance, passed the mechanical- and diffusive stability test.

Then the next step was to adjust the composition in the two phases, and they were applied to an $UVn$-flash. For all trial phases introduced to liquid systems, the equilibrium calculations converged to non trivial solutions. And for all cases the resulting phases was proved to be stable due to the local stability conditions, $(\frac{\partial^2 A}{\partial X \partial X})_{X \neq T}$. The same was not true at the vapor side. Here the routine was able to find stable phases that gave negative values for the tangent plane distance, but the $UVn$–flash failed to converge for all cases. That the $UVn$-flash did not converge for the introduction of the liquid phase, might have something to do with the size estimate of the phase. The size of the state is estimated as a small fraction of the main phase.

Even though the results indicates that the current routine was able to find stable phases at locations relatively close to the phase envelope, it fails to find such phases close to the unstable area. Intuitively at these locations the tangent plane distance should be even more negative. This give rise to concern.

Furthermore the reliability of the calculations may be limited due to the boundaries set on the variables to estimate, as well as the choice of variables to estimate. In this approach the fraction of each component in the new phase, as well as the density, represents the variables to be found in the optimization. The upper- and lower bounds for the fractions of the different components are set based on a Wilson approximation succeed by K-value equilibrium calculations. In this way a relatively large computational load is placed on the PSO-routine, which will constitute a large disadvantage for a computer program.

An alternative, and probably better, solution could have been to use the mol amounts to be estimated by the PSO, and then set the corresponding boundaries based on the hard core volume of each component, as well as the critical volume for that component, when a liquid phase should be introduced. And correspondingly, the upper and lower bounds on the vapor side could be set based on ideal gas.

The borders for the density was initially set to $\rho = [0, \frac{\mathbf{e}^T\mathbf{n}}{b}]$ both for the search of vapor phases and liquid phases. Later this was changed to $[0, \frac{\mathbf{e}^T\mathbf{n}}{10b}]$ in the search for a vapor phase, and to $[\frac{\mathbf{e}^T\mathbf{n}}{3b}, \frac{\mathbf{e}^T\mathbf{n}}{b}]$. The objective of this was to give the algorithm a clever guidance against the solution. The though behind the upper bound for the liquid volume was the critical volume for a van der Waal fluid, $v_c = 3b$. The critical volume of a mixture under given conditions will represent the largest possible liquid volume for that mixture. Nevertheless, the calculations performed in this work is based on the Peng-Robinson equation of state, which mean that the expression for the critical volume will not be the same. On the other hand, the Peng-Robinson equation of state do in the same way as the van der Waal equation of state, constitute a cubic equation of state, and a similar expression for the critical volume will exist.

The choice of the lower bound for the liquid was based on the fact that smallest possible volume will be equal to the hard core volume. Nevertheless $b$ depends on the composition, which means that this might not be a good choice of border. The lower bound for the search for the vapor phase was set more randomly, aiming to eliminate liquid volumes in the search for a vapor phase.

Although the implemented routine was able to find trial phases with negative tangent plane distance for more than half of the metastable points, the current implementation of the routine has some considerable drawbacks. Better solutions could have been found regarding to decide on the boundaries, as well as to the choice of parameters to estimate.

# Chapter 6

# Conclusion

## 6.1 The VessFire model

The results from the two component case and VessFire case demonstrate that the model respond well to the heat- and mass inputs applied to the system in these cases. For all time steps in these cases the system converge to the expected topologies in a relatively small number (5-10) of iterations. Also in these cases the system was exposed to 8 of the 13 topology transformations that should be available for the system. Both the norm criterion for excluding phases and the initialization routine based on the tangent plane criterion, was proved to work.

Nevertheless, the test on the one component system reveals that as the virtual phase converges to a trivial solution, the stability check done by the tangent plane check has no meaning anymore. The initialization routines applied to the model base their values on the virtual phases, and when these phases are no longer reliable, global initialization routines have to be performed. Global initialization routines are also needed to initialize the virtual phases whenever the starting point for the calculations are in the one-phase area.

## 6.2 Preparation of feasible States

The main discovery of the investigation of the convergence- and stability properties for the different grids, were that the calculated state for a single point in the $Tp$-grid became very different depending on the initialization of the calculations. The results from this work shows that the iteration sequence converges to the closest of the three alternative solutions available on the $pV$-isotherm. The resulting states will differ according to this. Then when the initial state belongs to the two-phase domain the $Tp$-calculations seem to overestimate the unstable domain of the grid. Correspondingly the calculations initialized on the liquid or vapor side will converge to liquid– or vapor states respectively, as long as a such states exist for the given pressure along the particular $pV$–isotherm. This behavior was not present for the $Hp$-scheme. Here the calculations converge to unique defined states regardless of the initialization point.

To test the initialization routine, the behavior of $Tp$, where almost the whole grid converged to stable- and metastable points, could be preferable, due to the fact that feasible one-phase states is needed. Nevertheless, a global search routine is needed to detect whether a phase is stable or metastable. On the other hand, whether a phase is unstable are easily detected by the mechanical- and the diffusive stability condition. In the way a global search is demanding, it would be preferable that a particular

point was unstable whenever the state belonged to the two-phase area. Nevertheless, the case for the $Tp$–calculations, when initialized in the two-phase area, are that they converge to unstable states, also at locations where stable states exist. This will introduce unnecessary problems for the reliability of the calculation.

## 6.3 PSO

The results from the testing of the local and dynamic PSO version, Dynamic Multi Swarm PSO (DMS-PSO) for a four component system revealed that the implemented routine was able to obtain a negative tangent plane distance at locations near the phase envelope. This was true both on the vapor- and the liquid side of the unstable area. All trial phases that gave a negative tangent plane distance, passed the mechanical- and diffusive stability test. To include the trial phases to the system, an $UVn$-flash was applied to calculate the equilibrium composition. For all trial phases introduced to liquid systems, the equilibrium calculations converged to non trivial solutions. Nevertheless, for all trial phases included to vapor system, the equilibrium calculations failed to converge.

Although the implemented routine was able to find trial phases with negative tangent plane distance for more than half of the metastable points, the current implementation of the routine has some considerable drawbacks. Better solutions could have been found regarding to decide on the boundaries, as well as to the choice of parameters to estimate.

# Bibliography


M. N. Ammar and H. Renon. The isothermal flash problem: New methods for phase split calculations. *AIChE Journal*, 33(6):926–939, 1987. ISSN 1547-5905. doi: 10.1002/aic.690330606. URL http://dx.doi.org/10.1002/aic.690330606.

Paul T. Boggs, Richard H. Byrd, and Robert B. Schnabel, editors. *Numerical Optimization 1984*. SIAM, 1985.

Adrián Bonilla-Petriciolet and Juan Gabriel Segovia-Hernández. A comparative study of particle swarm optimization and its variants for phase stability and equilibrium calculations in multicomponent reactive and non-reactive systems. *Fluid Phase Equilibria*, 289(2):110 – 121, 2010. ISSN 0378-3812. doi: DOI:10.1016/j.fluid.2009.11.008. URL http://www.sciencedirect.com/science/article/pii/S037838120900452X.

Herbert B. Callen. *Thermodynamics and an introduction to thermostatistics*. Wiley, New York, 2 edition, 1985.

Jarbas C. Ferrari, Gabriel Nagatani, Fernanda C. Corazza, J. Vladimir Oliveira, and Marcos L. Corazza. Application of stochastic algorithms for parameter estimation in the liquid-liquid phase equilibrium modeling. *Fluid Phase Equilibria*, 280(1-2):110 – 119, 2009. ISSN 0378-3812. doi: DOI:10.1016/j.fluid.2009.03.015. URL http://www.sciencedirect.com/science/article/pii/S0378381209001046.

Mark S. Ghiorso. Algorithms for the estimation of phase stability in heterogeneous thermodynamic systems. *Geochimica et Cosmochimica Acta*, 58(24):5489 – 5501, 1994. ISSN 0016-7037. doi: DOI:10.1016/0016-7037(94)90245-3. URL http://www.sciencedirect.com/science/article/pii/0016703794902453.

K.M. Hangos and I.T. Cameron. *Process modelling and model analysis*, volume 4. San Diego : Academic Press, c2001.

Tore Haug-Warberg. *Den termodynamiske arbeidsboken*. Kolofon Forlag AS, 2006.

James Z. Hua, Joan F. Brennecke, and Mark A. Stadtherr. Reliable computation of phase stability using interval analysis: Cubic equation of state models. *Computers & Chemical Engineering*, 22(9):1207 – 1214, 1998. ISSN 0098-1354. doi: DOI:10.1016/S0098-1354(98)00024-6. URL http://www.sciencedirect.com/science/article/pii/S0098135498000246.

Yan Jiang, Tiesong Hu, ChongChao Huang, and Xianing Wu. An improved particle swarm optimization algorithm. *Applied Mathematics and Computation*, 193(1):231 – 239, 2007. ISSN 0096-3003. doi: DOI:10.1016/j.amc.2007.03.047. URL http://www.sciencedirect.com/science/article/pii/S009630030700392X.

J. Kennedy and R. Eberhart. Particle swarm optimization. In *Neural Networks, 1995. Proceedings., IEEE International Conference on*, volume 4, pages 1942 –1948 vol.4, nov/dec 1995. doi: 10.1109/ICNN.1995.488968.

Lixiang Li, Yixian Yang, and Haipeng Peng. Computation of multiple global optima through chaotic ant swarm. *Chaos, Solitons & Fractals*, 40(3):1399 – 1407, 2009. ISSN 0960-0779. doi: DOI: 10.1016/j.chaos.2007.09.024. URL http://www.sciencedirect.com/science/article/pii/S096007790700759X.

J.J. Liang and P.N. Suganthan. Dynamic multi-swarm particle swarm optimizer. In *Swarm Intelligence Symposium, 2005. SIS 2005. Proceedings 2005 IEEE*, pages 124 – 129, june 2005. doi: 10.1109/SIS.2005.1501611.

Bjorn Tore Lovfall. Computer realization of thermodynamic models using algebraic objects. Doctor of philosophy thesis, NTNU, 2008. URL http://www.nt.ntnu.no/users/haugwarb/PhDtheses/bjorn_tore_lovfall.pdf.

Jørgen M. Mollerup Michael L. Michelsen. *Thermodynamic models: fundamentals & computational aspects*. Holte: Tie-Line Publications, 2004. ISBN 87-989961-1-8, h.

Michael L. Michelsen. The isothermal flash problem. part i. stability. *Fluid Phase Equilibria*, 9 (1):1 – 19, 1982. ISSN 0378-3812. doi: DOI:10.1016/0378-3812(82)85001-2. URL http://www.sciencedirect.com/science/article/pii/0378381282850012.

D.V. Nichita, S. Gomez, and E. Luna-Ortiz. Multiphase equilibrium calculation by direct minimization of gibbs free energy using the tunneling global optimization method. *Journal of Canadian Petroleum Technology*, 43(5), 2004.

NIST. Homepage nist, July 2011. URL http://www.nist.gov/index.html.

Jorge Nocedal and Stephen J. Wright. *Numerical Optimization*. Springer Science+Business Media, LLC, New York, 2 edition, 2006.

O. Orbach and C. M. Crowe. Convergence promotion in the simulation of chemical processes with recycle — the dominante eigenvalue method. *The Canadian Journal of Chemical Engineering*, 49: 528–533, 1975.

Ding-Yu Peng and Donald B. Robinson. A new two-constant equation of state. *Industrial & Engineering Chemistry Fundamentals*, 15(1):59–64, 1976. doi: 10.1021/i160057a011. URL http://pubs.acs.org/doi/abs/10.1021/i160057a011.

petrell.no. Homepage petrell, June 2011. URL http://petrell.no/2010/07/06/about-petrell/.

Riccardo Poli, James Kennedy, and Tim Blackwell. Particle swarm optimization. *Swarm Intelligence*, 1:33–57, 2007. ISSN 1935-3812. URL http://dx.doi.org/10.1007/s11721-007-0002-0. 10.1007/s11721-007-0002-0.

Irene F. Radzyminski and Wallace B. Whiting. Fluid phase stability and equations of state. *Fluid Phase Equilibria*, 34(1):101 – 110, 1987. ISSN 0378-3812. doi: DOI:10.1016/0378-3812(87)85053-7. URL http://www.sciencedirect.com/science/article/pii/0378381287850537.

Imran Rahman, Anwesh Kr. Das, Raju B. Mankar, and B.D. Kulkarni. Evaluation of repulsive particle swarm method for phase equilibrium and phase stability problems. *Fluid Phase Equilibria*, 282(2):65 – 67, 2009. ISSN 0378-3812. doi: DOI:10.1016/j.fluid.2009.04.014. URL http://www.sciencedirect.com/science/article/pii/S0378381209001514.

Mekapati Srinivas and G. P. Rangaiah. Differential evolution with tabu list for global optimization and its application to phase equilibrium and parameter estimation problems. *Industrial & Engineering Chemistry Research*, 46(10):3410–3421, 2007. doi: 10.1021/ie0612459. URL http://pubs.acs.org/doi/abs/10.1021/ie0612459.

Roumiana P. Stateva and Stefan G. Tsvetkov. A new method for thermodynamic stability analysis of multicomponent systems. *Hungarian Journal of Industrial Chemistry Veszprèm*, 19:170 – 188, 1991.

John A. Trangenstein. Customized minimization techniques for phase equilibrium computations in reservoir simulation. *Chemical Engineering Science*, 42(12):2847 – 2863, 1987. ISSN 0009-2509. doi: DOI:10.1016/0009-2509(87)87051-3. URL http://www.sciencedirect.com/science/article/pii/0009250987870513.

Ioan Cristian Trelea. The particle swarm optimization algorithm: convergence analysis and parameter selection. *Information Processing Letters*, 85(6):317 – 325, 2003. ISSN 0020-0190. doi: DOI:10.1016/S0020-0190(02)00447-7. URL http://www.sciencedirect.com/science/article/pii/S0020019002004477.

# Appendix A

# Derivations

## A.1 Equation set for the different topologies

To each topologies available for the thermodynamic model, there exist a corresponding set of equations. The equation sets for Topology 1, Topologi 4, and Topology 6 are available in chapter 3. The equation set for the remaining topologies are given in equation (A.1), (A.2), and (A.3), for Topologi 2, Topology 3, and Topology 5 respectively. Topology 2 (V1,L1,L2,V2) has the following configuration:

$$\begin{pmatrix} T^{V1} & -T^{L1} & & & \\ & \sum_{i=1}^{\mathbf{n}} \mathbf{n}_i^{L1} & & & \\ \boldsymbol{\mu}^{V1} & -\boldsymbol{\mu}^{L1} & & & \\ & & T^{L2} & -T^{V2} & \\ & & p^{L2} & -p^{V2} & \\ & & \boldsymbol{\mu}^{L2} & -\boldsymbol{\mu}^{V2} & \\ U^{V1} & & & -H^{V2} & \\ V^{V1} & & +V^{L2} & & \\ \boldsymbol{n}^{V1} & & & -\boldsymbol{n}^{V2} & \\ & & U^{L2} & +H^{V2} & \\ p^{V1} & & -p^{L2} & & \\ & & \boldsymbol{n}^{L2} & +\boldsymbol{n}^{V2} & \end{pmatrix}^{k+1} = \begin{pmatrix} 0 \\ 1 \\ 0 \\ \\ 0 \\ 0 \\ 0 \\ \\ U^{V1} + \delta U^{V1} \\ V^{V1} + V^{L2} \\ \mathbf{n}^{V1} + \delta \mathbf{n}^{1} \\ \\ U^{L2} + \delta U^{L2} \\ 0 \\ \mathbf{n}^{L2} + \delta \mathbf{n}^{L2} \end{pmatrix}^{k} \tag{A.1}$$

In Topology 3 (V1,L1,L2,V2) the utility phase V2 has become a virtual phase:

$$\begin{pmatrix} T^{V1} & -T^{L1} & & \\ p^{V1} & -p^{L1} & & \\ \boldsymbol{\mu}^{V1} & -\boldsymbol{\mu}^{L1} & & \\ & & T^{L2} & -T^{V2} \\ & & & \sum_{i=1}^{\mathbf{n}} \mathbf{n}_i^{V2} \\ & & \boldsymbol{\mu}^{L2} & -\boldsymbol{\mu}^{V2} \\ U^{V1} & +H^{L1} & & \\ V^{V1} & + & +V^{L2} & \\ \boldsymbol{n}^{V1} & +\boldsymbol{n}^{L1} & & \\ & -H^{L1} & +U^{L2} & \\ p^{V1} & & -p^{L2} & \\ & -\boldsymbol{n}^{L1} & +\boldsymbol{n}^{L2} & \end{pmatrix}^{k+1} = \begin{pmatrix} 0 \\ 0 \\ 0 \\ 0 \\ 1 \\ 0 \\ U^{V1}+\delta U^{V1} \\ V^{V1}+V^{L2} \\ \mathbf{n}^{V1}+\delta \mathbf{n}^{1} \\ U^{L2}+\delta U^{L2} \\ 0 \\ \mathbf{n}^{L2}+\delta \mathbf{n}^{L2} \end{pmatrix}^{k} \tag{A.2}$$

Topology 5 represents the one-phase liquid system (L2,V2), modeled with the corresponding virtual phase V2:

$$\begin{pmatrix} T^{L2} & -T^{V2} \\ & \sum_{i=1}^{\mathbf{n}} \mathbf{n}_i^{V2} \\ \boldsymbol{\mu}^{L2} & -\boldsymbol{\mu}^{V2} \\ U^{L2} & \\ V^{L2} & \\ \boldsymbol{n}^{L2} & \end{pmatrix}^{k+1} = \begin{pmatrix} 0 \\ 1 \\ 0 \\ U^{L2}+\delta U^{L2} \\ V^{L2} \\ \mathbf{n}^{L2}+\delta \mathbf{n}^{L2} \end{pmatrix}^{k} \tag{A.3}$$

## A.2 Deviation of mass- and energy balances

The mass and energy balances over the different control volumes are deduced from the general mass- and energy balances, given in. The general mass balance for a non-reacting system are given by (A.4) and (A.5):

$$\begin{pmatrix} \textit{Rate of accumulation} \\ \textit{in the system} \end{pmatrix} = \begin{pmatrix} \textit{Rate of flow} \\ \textit{into the system} \end{pmatrix} - \begin{pmatrix} \textit{Rate of flow out} \\ \textit{of the system} \end{pmatrix} \tag{A.4}$$

$$\left(\frac{d\mathbf{N}_{CV}}{dt}\right) = \hat{\mathbf{n}}_{in} - \hat{\mathbf{n}}_{out} \tag{A.5}$$

For a discrete framework the left hand side of (A.5) can be expressed as $\frac{d\mathbf{N}_{CV}}{dt} = \mathbf{n}_{k+1} - \mathbf{n}_k$ between to subsequent time steps. Based on (A.5), the balance over the vapor phase is given by Equation (A.6):

$$\mathbf{n}_{k+1}^{V1} - \mathbf{n}_k^{V1} = \mathbf{n}_{k+1}^{V2} - \mathbf{n}_{k+1}^{L1} + \delta \mathbf{n}_k^{V2} \tag{A.6}$$

where $\delta \mathbf{n}^{V2}$ is external mass input. $k$ refer to the time step. $\mathbf{n}_{k+1}^{V2}$ denotes the mass that evaporates from L1 (CV1) to V2 (CV2) at time step $k+1$, and $\mathbf{n}_{k+1}^{L1}$ represent condensate from V1 (CV1) to L2 (CV2) in the same time step. Then collecting the terms by time step, implies (A.16):

$$\mathbf{n}_{k+1}^{V1} - \mathbf{n}_{k+1}^{V2} + \mathbf{n}_{k+1}^{L1} = \mathbf{n}_{k}^{V1} + \delta\mathbf{n}_{k}^{V2} \tag{A.7}$$

where the expression on the right hand side will be constant within each time step. The corresponding energy balance are deduced based on the general energy balance (A.8)- (A.9):

$$\begin{pmatrix} \textit{Rate of} \\ \textit{accumulation} \\ \textit{of energy} \\ \textit{within} \\ \textit{the system} \end{pmatrix} = \begin{pmatrix} \textit{Rate of energy} \\ \textit{added to the} \\ \textit{system by mass} \\ \textit{flow into the} \\ \textit{system} \end{pmatrix} - \begin{pmatrix} \textit{Rate of} \\ \textit{energy leaving} \\ \textit{the system by} \\ \textit{mass flow out} \\ \textit{of the system} \end{pmatrix} + \begin{pmatrix} \textit{Rate of flow} \\ \textit{of heat to the} \\ \textit{system from the} \\ \textit{surroundings} \end{pmatrix} - \begin{pmatrix} \textit{Rate of work} \\ \textit{done by the} \\ \textit{system on the} \\ \textit{surroundings} \end{pmatrix} \tag{A.8}$$

$$\frac{dE_{CV}}{dt} = \dot{E}_{inn} - \dot{E}_{out} + \dot{Q} - \dot{W} \tag{A.9}$$

where $E = U + E_k + E_p$, $\dot{W}$ represent the work term, and $\dot{Q}$ denotes the heat input to the system. Neglecting kinetic- and potential energy:

$$E \approx U \tag{A.10}$$

The work term can be expressed by:

$$\dot{W} = -p\dot{V}_{in} + p\dot{V}_{out} + \dot{W}_s \tag{A.11}$$

where $\dot{W}_s$ are referred to as shaft work, and the pV terms denotes the flow work. Inserting (A.10)-(A.11) into (A.9):

$$\frac{dU_{CV}}{dt} = \dot{U}_{in} + p\dot{V}_{in} - \dot{U}_{out} - p\dot{V}_{out} - \dot{W}_s + \dot{Q} \tag{A.12}$$

Internal energy can be expressed in terms of enthalpy through the following expression (A.13):

$$H = U + pV \tag{A.13}$$

Applying (A.13) to (A.12), as well as neglecting the shaft work gives as follows:

$$\frac{dU_{CV}}{dt} = \dot{H}_{inn} - \dot{H}_{out} + \dot{Q} \tag{A.14}$$

For a discrete framework the left hand side of (A.14) can be expressed as $\frac{dU_{CV}}{dt} = U_{k+1} - U_k$ between to subsequent time steps. Applied to the Petrell control volume, CV1, the the following expression will emerge for V1:

$$U_{k+1}^{V1} - U_{k}^{V1} = H_{k+1}^{V2} - H_{k+1}^{L1} + \delta U_{k}^{V2} \tag{A.15}$$

collecting the terms for the same time step on each side of the equality gives (A.16):

$$U_{k+1}^{V1} - H_{k+1}^{V2} + H_{k+1}^{L1} = U_k^{V1} + \delta U_k^{V2} \tag{A.16}$$

where $\delta U_k^{V2}$ represent the external heat input. Similar expressions can be deduced for the liquid control volume (CV2).

# Appendix B

# Data from PSO

## B.1 PSO-tables

| Stable | Q(pressure level) | q(temperature level) | $\rho^{\beta}$ | $\rho^{\alpha}$ |
|---|---|---|---|---|
| stab:1 | Q: 1 | q: 1 | 7.179e-010 | 6.4738e-008 |
| stab:1 | Q: 1 | q: 2 | 1.7741e-009 | 6.2068e-008 |
| stab:1 | Q: 2 | q: 1 | 7.5453e-010 | 6.4622e-008 |
| stab:1 | Q: 2 | q: 2 | 1.8862e-009 | 6.1837e-008 |
| stab:1 | Q: 3 | q: 1 | 7.4294e-010 | 6.4659e-008 |
| stab:1 | Q: 3 | q: 2 | 1.9927e-009 | 6.1623e-008 |
| stab:1 | Q: 4 | q: 1 | 7.9222e-010 | 6.4506e-008 |
| stab:1 | Q: 4 | q: 2 | 1.9933e-009 | 6.1622e-008 |
| stab:1 | Q: 5 | q: 1 | 1.9989e-009 | 6.1611e-008 |
| stab:1 | Q: 5 | q: 2 | 3.8176e-009 | 5.8373e-008 |
| stab:1 | Q: 6 | q: 1 | 2.0602e-009 | 6.149e-008 |
| stab:1 | Q: 6 | q: 2 | 3.8599e-009 | 5.8307e-008 |
| stab:1 | Q: 7 | q: 1 | 2.0198e-009 | 6.157e-008 |
| stab:1 | Q: 7 | q: 2 | 3.836e-009 | 5.8345e-008 |
| stab:1 | Q: 8 | q: 1 | 2.0599e-009 | 6.1491e-008 |
| stab:1 | Q: 8 | q: 2 | 3.8413e-009 | 5.8338e-008 |
| stab:1 | Q: 8 | q: 3 | 6.063e-009 | 5.4917e-008 |
| stab:1 | Q: 9 | q: 1 | 3.8502e-009 | 5.8325e-008 |
| stab:1 | Q: 9 | q: 2 | 6.0629e-009 | 5.4921e-008 |
| stab:1 | Q: 10 | q: 1 | 3.835e-009 | 5.8351e-008 |
| stab:1 | Q: 10 | q: 2 | 6.0473e-009 | 5.4947e-008 |
| stab:1 | Q: 10 | q: 3 | 8.4857e-009 | 5.1326e-008 |
| stab:1 | Q: 11 | q: 1 | 6.0134e-009 | 5.5001e-008 |
| stab:1 | Q: 11 | q: 2 | 8.4596e-009 | 5.1375e-008 |
| stab:1 | Q: 12 | q: 1 | 5.97e-009 | 5.507e-008 |
| stab:1 | Q: 12 | q: 2 | 8.4124e-009 | 5.1456e-008 |
| stab:1 | Q: 12 | q: 3 | 1.086e-008 | 4.7675e-008 |
| stab:1 | Q: 13 | q: 1 | 8.3492e-009 | 5.1563e-008 |
| stab:1 | Q: 13 | q: 2 | 1.081e-008 | 4.7786e-008 |
| stab:1 | Q: 13 | q: 3 | 1.3097e-008 | 4.3914e-008 |
| stab:1 | Q: 14 | q: 1 | 1.0731e-008 | 4.7946e-008 |
| stab:1 | Q: 14 | q: 2 | 1.3062e-008 | 4.4063e-008 |
| stab:1 | Q: 14 | q: 3 | 1.5087e-008 | 4.0234e-008 |
| stab:1 | Q: 15 | q: 1 | 1.3002e-008 | 4.4266e-008 |
| stab:1 | Q: 15 | q: 2 | 1.5148e-008 | 4.0355e-008 |

Table B.2: Density values from the iteration. These densities are the densities obtain after the $UVn$-flash

| **Stable** | **Q(pressure level)** | **q(temperature level)** | $\rho^{\beta}$ | $\rho^{\alpha}$ |
|---|---|---|---|---|
| stab:1 | Q: 3 | q: 1 | 6.4102e-008 | 1.9943e-010 |
| stab:1 | Q: 3 | q: 2 | 6.2786e-008 | 2.5829e-010 |
| stab:1 | Q: 3 | q: 3 | 6.299e-008 | 3.4118e-010 |
| stab:1 | Q: 3 | q: 4 | 6.2775e-008 | 3.4118e-010 |
| stab:1 | Q: 3 | q: 5 | 6.2134e-008 | 5.9841e-010 |
| stab:1 | Q: 3 | q: 6 | 6.189e-008 | 7.93e-010 |
| stab:1 | Q: 3 | q: 7 | 6.1005e-008 | 7.93e-010 |
| stab:1 | Q: 3 | q: 8 | 6.0959e-008 | 7.93e-010 |
| stab:1 | Q: 3 | q: 9 | 6.0262e-008 | 7.93e-010 |
| stab:1 | Q: 3 | q: 10 | 6.029e-008 | 7.93e-010 |
| stab:1 | Q: 3 | q: 11 | 6.0019e-008 | 7.93e-010 |
| stab:1 | Q: 3 | q: 12 | 6.2275e-008 | 7.93e-010 |
| stab:1 | Q: 3 | q: 13 | 5.9159e-008 | 7.93e-010 |
| stab:1 | Q: 3 | q: 14 | 5.7856e-008 | 7.93e-010 |
| stab:1 | Q: 3 | q: 15 | 6.0644e-008 | 7.93e-010 |
| stab:1 | Q: 4 | q: 1 | 6.096e-008 | 7.93e-010 |
| stab:1 | Q: 4 | q: 2 | 6.0358e-008 | 7.93e-010 |
| stab:1 | Q: 4 | q: 3 | 6.2073e-008 | 7.93e-010 |
| stab:1 | Q: 4 | q: 4 | 6.025e-008 | 7.93e-010 |
| stab:1 | Q: 4 | q: 5 | 5.8216e-008 | 7.93e-010 |
| stab:1 | Q: 4 | q: 6 | 5.8096e-008 | 7.93e-010 |
| stab:1 | Q: 4 | q: 7 | 5.9914e-008 | 7.93e-010 |
| stab:1 | Q: 4 | q: 8 | 5.9742e-008 | 7.93e-010 |
| stab:1 | Q: 4 | q: 9 | 5.9692e-008 | 7.93e-010 |
| stab:1 | Q: 4 | q: 10 | 5.9893e-008 | 7.93e-010 |
| stab:1 | Q: 4 | q: 11 | 6.0475e-008 | 7.93e-010 |
| stab:1 | Q: 5 | q: 1 | 5.9453e-008 | 7.93e-010 |
| stab:1 | Q: 5 | q: 2 | 5.8878e-008 | 7.93e-010 |

Table B.4: Density values from the iteration. Here the a liquid phase are searched. The values are before the $UVn-flash$